DEVELOPMENT OF HIGH-SENSITIVITY ATMOSPHERIC PRESSURE (AP) MATRIX-ASSISTED LASER DESORPTION/IONIZATION (MALDI) AND OPEN AIR IONIZATION TECHNIQUES FOR THE ANALYSIS OF BIOMOLECULES BY MASS SPECTROMETRY

A Dissertation
Presented to
The Academic Faculty

by

Arti T. Navare

In Partial Fulfillment
of the Requirements for the Degree
Doctor of Philosophy in the
School of Chemistry & Biochemistry

Georgia Institute of Technology

May, 2010

DEVELOPMENT OF HIGH-SENSITIVITY ATMOSPHERIC PRESSURE MATRIX-ASSISTED LASER DESORPTION/IONIZATION AND OPEN AIR IONIZATION TECHNIQUES FOR THE ANALYSIS OF BIOMOLECULE BY MASS SPECTROMETRY

Approved by:

Dr. Facundo M. Fernández, Advisor
School of Chemistry & Biochemistry
Georgia Institute of Technology

Dr. Alfred H. Merrill, Jr.
School of Biology
Georgia Institute of Technology

Dr. Ken R. Brown
School of Chemistry & Biochemistry
Georgia Institute of Technology

Dr. Thomas M. Orlando
School of Chemistry & Biochemistry
Georgia Institute of Technology

Dr. Fernando G. Noriega
Department of Biological Sciences
Florida International University

Date Approved: March 15th, 2010

This is dedicated to…

my mother, Anjali Risbud, father, Balwant Risbud, my brother Milind, my husband Tonmoy, my wonderful baby boy Neel, and my in-laws Gunesh and Hema Navare for their enormous help, support, and unconditional love. Thank you!

ACKNOWLEDGEMENTS

I am grateful to be in this position to thank all the people who have influenced my life and career, and have helped me become a better person. First and foremost, I would like to thank my mother for inculcating a dream-big attitude in me and for showing me how to be strong-willed and determined, in the face of adversity. She has always been a beacon of encouragement and a reminder of the importance of balancing career and family, by setting the right priorities.. I would like to thank my father for being supportive and for teaching me how to be pragmatic in my choices. He always reminds me of a quote by Walter Elliot, '*Perseverance is not a long race; it is many short races one after another*'. I am yet to meet a more positive and patient person than my father….Thanks Dad!! My brother, Milind has never stopped being a mentor and a confidante when it mattered most. I cannot thank my husband Tonmoy enough for being there during every challenging phase in my pursuits. While giving me time and help, he unknowingly gave me strength and a strong will. I cannot thank my parents-in-law enough for being there 24/7 and helping me take care of our infant son during my dissertation phase.

My gratitude for my advisor Dr. Facundo M. Fernández cannot be easily expressed in an acknowledgement section of a dissertation. Right from the point of accepting me in his research group till date, he has been an outstanding advisor, an inspiring mentor and a gracious human being. His eruditeness and high expectations, slowly but surely bolstered my research discipline. Some of my key accomplishments occurred just a few steps away from the point of giving up; with Dr. Fernández pushing

for excellence, attention to detail and persistence. I want to thank him especially for accommodating a work-life balance, when it mattered most. Dr. Fernádez, you have truly enriched my academic life, and I am sure our professional association will continue to grow.

My fellow graduate students in the group deserve a fair share in my success for making me smile on a bad day. Our past group members, Dr. Christina Y. Hampton and Dr. Leonard Nyadong, who are currently pursuing their post-doctorates have set the bar high for all of us. I am grateful to both of them for being wonderful colleagues and special friends during our journey in the doctoral program together. Christina, would often wait for me late into the night while I finished my never-ending experiments to make sure that I reached home safely. I consider myself immensely lucky to have had such a loving, caring and intelligent friend and colleague.. I thank our post-doctoral fellows Dr. Asiri Galhena, and Dr. Manshui Zhou, for their timely advice and help around the lab. I would also like to thank Mark Kwasnik, Courtney Phillips, Dana Hostetler, Glenn Harris, Jose Perez, Carrie Pierce and our undergraduate students Joe Caramore and David Rizzo for creating all those wonderful memories, full of fun and laughter without which this journey would not have been so enjoyable.

I wish to thank Dr. Thomas Orlando, Dr. Bridgette Barry, Dr. Alfred Merrill Jr., and Dr. Ken Brown for serving on my Ph.D. committee. I am grateful to Dr. Fernando Noriega for being on my committee and for his invaluable research collaboration. I appreciate Dr. Salvador Hernandez, Dr. Marcela Nouzova, and Dr. Jaime Mayoral for their enormous help and timely advice throughout our collaboration. It was a privilege to have worked with such a great team of scholars over the past five years. Many thanks to

Dr. Cameron Sullards, and David Bostwick at the Georgia Tech mass spectrometry facility for accommodating my instrument requests upon short notices. I want to extend my thanks to Sam Mize of the College of Science machine shop for his excellent help in machining needs and to Richard Berdell and José Fonts in the electronics shop in the School of Chemistry and Biochemistry for their assistance. These three individuals are the often unsung heroes, whose help is of tremendous value to doctoral students.

Many thanks to Dr. Leigh Bottomley, Dr. Toby Block, Dr. Robert Braga, and Dr. Mary Peek, for making my graduate student experience at Georgia Tech so smooth. I would also like to thank Dr. Camron Tyson, graduate co-coordinator of the Chemistry Department, Selina Tinsely, and Kourtnie Robin for their prompt guidance in various administrative matters.

I have no doubt, left out many other people who made a difference to me. I consider myself honored and also lucky, to have been surrounded with such amazing people at Georgia Tech.

Lastly, I would like to acknowledge my 1 year old son, Neel, who probably understood during the past few months that his mother was busy pursuing something he'll be proud of some day..

TABLE OF CONTENTS

LIST OF TABLES

LIST OF FIGURES

LIST OF SYMBOLS

2^3S_1	Helium metastable atom excited to the triplet state
He^*	Helium metastable atom
m/z	mass-to-charge ratio
pI	Isoelectric point
S/N	Signal-to-noise ratio

LIST OF ABBREVIATIONS

ACN	Acetonitrile
AGC	Automatic Gain Control
AP	Atmospheric Pressure
API	Atmospheric Pressure Interface
AP-MALDI	Atmospheric Pressure Matrix-Assisted Laser Desorption/Ionization
AS-C	Allatostatin-C
AT	Allatotropins
CI	Chemical Ionization
CID	Collision Induced Dissociation
CZE	Capillary Zone electrophoresis
DART	Direct Analysis in Real Time
DESI	Desorption Electrospray Ionization
DIOS	Desorption/Ionization on Silicon
DOE	Design of Experiment
EI	Electron Ionization
ESI	Electrospray Ionization
FD	Field Desorption
FT-ICR	Fourier Transform- Ion Cyclotron Resonance
GC	Gas Chromatography
HPLC	High Performance Liquid Chromatography
HV	High Voltage
IMAC	Immobilized Metal Affinity Chromatrography

IT	Ion Trap
IR	Infrared
LC	Liquid Chromatography
LDI	Laser Desorption Ionization
LOD	limit of Detection
MALDESI	Matrix-Assisted Laser Desorption Electrospray Ionization
MALDI	Matrix-Assisted Laser Desorption/Ionization
MCP	Micro-Channel Plate
MS	Mass Spectrometry
MS/MS	Tandem Mass Spectrometry
NIST	National Institute of Standards and Technology
NMR	Nuclear Magnetic Resonance
PDF	Pulsed Dynamic Focusing
PEG	Polyethylene glycol
PA-AP-MALDI	Pneumatically-Assisted-AP-MALDI
Q-TOF	Quadrupole Time-of-Flight
RMME	Reverse Micellar Micro-Extraction
RSM	Response Surface Method
SALDI	Surface-Assisted Laser Desorption/ioization
SAM	Self-Assembled Monolayer
SELDI	Surface-Enhanced Laser Desorption/Ionization
SAX	Strong Anion Exhange
SNR	Signal-to-Noise Ratio

SPE	Solid-Phase Extraction
SRM	Selected Reaction Monitoring
TFA	Trifluoroacetic Acid
TIC	Total Ion Chronogram
TOF	Time-of-Flight
UFMP	Ulta Fine Metal Powder
UV	Ultraviolet
WCX	Weak Cation Exhange

LIST OF PUBLICATIONS

CHAPTER 2

Navare AT, Nouzova M, Noriega FG, Hernandez-Martinez S, Menzel C, Fernández FM, "On-chip Solid-phase Extraction Pre-concentration/Focusing Substrates Coupled to Atmospheric pressure Matrix-assisted Laser Desorption Ionization Ion Trap Mass Spectrometry for High Sensitivity Biomolecule Analysis", *Rapid Commun. Mass Spectrom.*, **2009**, 23, 477-486.

Li Y, Hernandez-Martinez S, Fernández FM, Mayoral JG, Topalis P, Priestap H, Perez M, Navare AT, Noriega FG, "Biochemical molecular and functional characterization of PISCF-alltostatin, a regulatory juvenile hormone biosynthesis in the mosquito *Aedes aegypti*", *J. Biol. Chem*., **2006**, 281, 34048-34055.

CHAPTER 3

Navare AT, Fernández FM, **"**In-Line Pneumatically-assisted Atmospheric Pressure Matrix-assisted Laser Desorption/Ionization", *JMS,* **2010,** *Accepted*.

CHAPTER 4

Navare AT, Nouzova M, Mayoral JG, Fernández FM, "Optimization of Direct Analysis in Real Time for Rapid Analysis of Juvenile Hormone (III) and Terpene Precursors", *manuscript in preparation,* **2010**.

Mayoral JG, Nouzova M, Navare AT, Noriega FG, "NADP-Dependent Farnesol Dehydrogenase, A *Corpora Allata* Enzyme Involved In Juvenile Hormone Synthesis", *PNAS*, **2009**, 106, 21091-21096

CHAPTER 5

Navare AT, Zhou M, Mcdonald J, Noriega FG, Sullards CM, Fernández FM, "Serum Biomarkers Profiling by Solid-phase Extraction with Particle Embedded Micro Tips and Matrix-assisted Laser Desorption/Ionization Mass Spectrometry", *Rapid Commun. Mass Spectrom.,* **2008**, 22, 997-1008.

Fernández FM, Hampton CY, Nyadong L, Navare AT, Kwasnik M, "Liquid Chromatography and Ambient Ionization Time-of-flight Mass Spectrometry for the Analysis of Genuine and Counterfeit Pharmaceuticals", in **LC/TOF-MS for Accurate Mass Analysis: Principles and Applications**, ed. by I. Ferrer and E.M. Thurman, Wiley: **2009**.

SUMMARY

Matrix-assisted laser desorption/ionization (MALDI) has been celebrated as a soft ionization method for analyzing very diverse biological species including large proteins, peptides, carbohydrates, lipids and metabolites. The fact that MALDI is tolerant to salts and buffers and that it mostly produces singly charged ions from intact biomolecules is considered highly advantageous over electrospray ionization (ESI). Almost two decades after the introduction of vacuum MALDI, the technique was successfully implemented under atmospheric pressure (AP) conditions by Laiko and co-workers. Some of the most salient advantages of AP-MALDI over vacuum MALDI are its ability to generate intact ions from labile species with minimal fragmentation due to collisional cooling under AP, the ability of performing MS^n experiments, and its exchangeability with other ion sources. However, AP-MALDI suffers from limited sensitivity due to low ion transmission efficiency under AP conditions. Because sensitivity is a function of the sample pretreatment method of choice, both preconcentration and selective sample fractionation can be used during the initial stages of the analytical pipeline to improve detectability.

To that end, the first part of the work presented in this thesis is aimed at investigating various approaches to improve the sensitivity of AP-MALDI for mass spectrometric analysis of biomolecules. Chapter 1 reviews the history of laser desorption ionization (LDI), presenting salient features of vacuum MALDI and AP-MALDI, and concludes with a brief overview of leading ambient ionization techniques, such as Direct Analysis in Real Time (DART) ionization. Chapter 2 presents an investigation of an

on-chip sample preconcentration approach coupled to AP-MALDI for high-sensitivity analysis of neuropeptides extracted from *Aedes aegypti* mosquito heads. The theme of exploring efficient and reproducible purification methods for complex biosamples is continued in Chapter 3, where an evaluation of new on-tip solid-phase extraction (SPE) micro columns with various functional groups is presented. A second approach for enhancing AP-MALDI sensitivity by constructing a new pneumatically-assisted (PA)-AP-MALDI ion source is presented in Chapter 4, where various factors affecting the performance of this device are investigated. Chapter 5 describes work involving the evaluation of DART ionization as a high-throughput method for the detection and identification of small terpene molecules central to the *Aedes aegypti* mosquito lifecycle.

CHAPTER 1. ATMOSPHERIC PRESSURE LASER DESORPTION IONIZATION AND AMBIENT IONIZATION TECHNIQUES: AN OVERVIEW

1.1. Abstract

Laser desorption/ionization (LDI) traces its roots to the work of Muma and Vastola in late 1960s[1] and since then this technique evolved as a mainstream method of ionizing macromolecules[2]. The recently-invented atmospheric pressure (AP) version of LDI has further extended the advantages of the established vacuum LDI and therefore needs special attention. This chapter presents an overview of the evolution of LDI techniques and later describes some of the key advantages and limitations of the traditional vacuum LDI and its AP counterpart followed by a brief overview on the technological advancements in other ionization techniques under ambient conditions.

1.2. Laser Desorption/Ionization: History and Milestones

Producing gaseous phase ions of large, nonvolatile and thermally unstable biomolecules has been a challenge to mass spectrometrists of all generations. The thermal lability of these macromolecules demands 'soft' ionization methods[3] to generate predominantly-intact molecular ions with minimal fragmentation. The introduction of field desorption (FD) ionization by Beckey[4, 5] provided such a soft ionization method in which sample is chemisorbed as a thin film on a metal emitter anode to which a high electric field is applied[5, 6]. Direct ionization of the samples by the external electrostatic field in FD was reported to ionize nonvolatile molecules with $m/z < 10{,}000$[5, 7, 8]. However, FD ionization was limited by poor reproducibility of both, absolute and relative

signal abundances, which were a function of the type of emitter and analyte[5, 9]. Concurrently, a new technique known as laser desorption ionization (LDI) was gathering attention amongst the scientific community as a way of quasi-instantaneously vaporizing nonvolatile polyatomic molecules[10]. The larger the size of a molecule, the more difficult it is to transfer it into gaseous state, therefore requiring larger energy amounts for evaporation. It was found that the high energy deposition required for the vaporization of a macromolecule often caused increase in its internal energy, consequently fragmenting it[11]. Because unimolecular decompositions rates are smaller than desorption rates achievable in LDI, rapid heating was expected to have the advantage of promoting vaporization over decomposition or fragmentation[11]. Various ultraviolet (UV) and infrared (IR) lasers with pulse width ranging between nanoseconds[12] to microseconds[7] and power densities from 10^{3} to 10^{-11} W cm^{-2} were sought after by researches as a source of instantaneous heating of thermally labile molecules[13]. Typically, LDI experiments were carried out by first depositing the sample solution on a glass or a metallic rod as a thin film by direct evaporation or electrospraying the sample solution, followed by positioning of this rod into the vacuum region of the ionization source[7, 12, 14-18]. In the next step, a focused laser beam was pulsed onto a 10^{-2} cm^{2} – 10^{-6} cm^{2} sample area and the desorbed ionized analyte species were directed into the mass spectrometer.

The observed LDI mass spectra of various types of analytes showed cationized species as common features of the mass spectrum[1, 7, 19, 20] along with low intensity protonated analyte ions depending upon analyte basicity. Various groups suggested different mechanisms for desorption and ion formation in LDI which would explain the observed ionic species. In that, Van der Pely and coworkers proposed a thermal model of

desorption followed by gas phase ion-molecular reactions and cationized ion formation[21]. Their experimental data showed that a continuous wave or a pulsed CO_2 laser irradiation of a solid sample generated neutrals at low temperatures (400-500 K) and cationized ions at much higher temperatures (> 800 K)[21]. Based on the experimental evidence, Van Der Pely et al. proposed that laser irradiation produced a steep temperature gradient on the sample surface where alkali ions were emitted from the hot locus (> 700 K) while neutrals were desorbed from much colder areas (400-500 K) on the sample surface. The gas phase alkali ions and neutrals then combined to form quasimolecular ions just over the sample surface. Hardin et al. proposed that metastable decomposition of desorbed cluster ions was responsible for generating cationized or protonated ions after observing the wide kinetic distributions of the molecular ions in LDI-MS experiments[15]. Stoll et al. suggested the involvement of multiphoton absorption along with thermal heating in explaining the LDI process[19]. In a yet another separate study, Hillenkamp suggested that a non-thermal mechanism is predominant in the desorption of ions from thin films, while thermal pathways dominate the ion evaporation from bulk solids[14]. Antonov and coworkers also supported a non-thermal desorption pathway by proposing electronic excitation of surface analyte ions or neutral molecules upon photon absorption leading to an increase in vibrational energy, consequently releasing the analyte ions/neutrals from the surface[10]. The same group suggested an alternative desorption pathway, by Columbic repulsion of ions near the surface due to the fact that the excited state electrons formed by photoionization possess energy of several eV and penetrate into the crystal surface as much as 50 A° [10].

Although no unified theory of ion formation in LDI was established, researchers continued to explore the technique for various applications[12, 13, 15, 16, 19, 22]. Most of the early work with LDI mass spectrometry (MS) was centered around inorganic molecules. A milestone was reached with the first report of the application of LDI-MS by Posthumus et al. for analyzing biomolecules such as nucleotides, polypeptides and oligosaccharides with *m/z* as high as 1251[7]. The intensity of the cationized digitonin ion (*m/z* 1251) was relatively low as the acceleration voltage of the magnetic sector instrument used in this study had to be reduced in order to reach the high mass range. A few years later, Linder et al. used a time-of-flight (TOF) instrument to detect dodecasaccharide isolated from *Shigella flexneri*[17]. Furthermore, the use of delay extraction mass analysis in TOF instruments[8] and the availability of high mass resolution instruments such as Fourier transform (FT) mass spectrometers [18] significantly improved the upper mass limit to about *m/z* 3600 and 7000 for analyzing phosphazines and polymers, respectively. However, the goal to desorb intact higher molecular weight protein and large peptide molecules using pulsed lasers remained elusive for almost two decades after the report by Posthumus and coworkers. The history of LDI-MS changed in 1987 when a large protein with *m/z* 35,000 Da, namely carboxipeptidase A, was successfully desorbed and ionized by Tanaka and coworkers[23, 24]. The large protein molecules were first embedded into a matrix of metal nanoparticles, and the dried co-crystallized sample was then irradiated using a pulsed N_2 laser. This was the beginning of the era of Matrix-Assisted Laser Desorption Ionization (MALDI).

1.3. Matrix-Assisted Laser Desorption/Ionization

1.3.1. Nobel Prize and Controversy

The term matrix-assisted laser desorption/ionization was coined by Hillenkamp and Karas[25] in 1985. However, Koichi Tanaka was first to introduce MALDI in the field of biochemistry and received a Nobel Prize in 2002 for this significant contribution[24]. The fact that Hillenkamp, Karas and Tanaka are equally credited for the introduction of MALDI in mass spectrometry triggered the 2002 Nobel Prize controversy. Additionally, some researchers argued that since the crystalline organic MALDI matrix used by Hillenkamp and Karas group is more widely used than the inorganic matrix used by Tanaka, the former group deserves the prestigious Nobel Prize more than the later. Despite of the debate, the introduction of MALDI is considered one of the greatest feats in the history of mass spectrometry.

1.3.2. Development of New MALDI Matrices

In MALDI, the sample solution is air dried on a stainless steel substrate also known as target plate together with an excess amount of MALDI matrix forming a co-crystallized sample-matrix spot. The dried spot is irradiated under vacuum using a UV or IR laser and the sample-analyte molecules are ablated or desorbed from the target plate. The MALDI matrix absorbs and transfers laser energy to analyte molecules embedded in it and subsequently facilitates ionization of the analyte (Figure 1.1.).

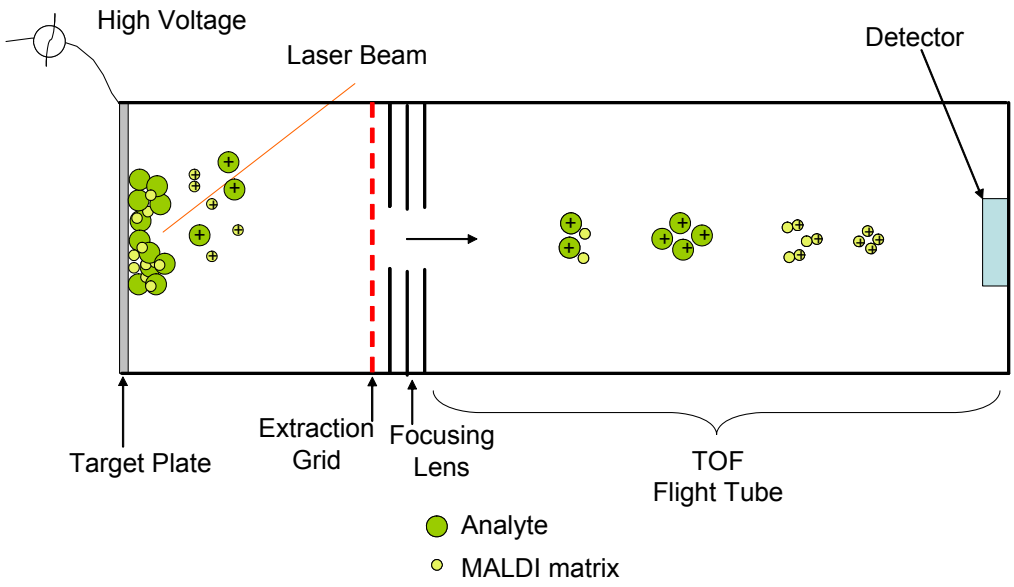

Figure 1.1. Schematics of MALDI-MS apparatus.

The gaseous analyte ions along with matrix ions and clusters are extracted into a mass analyzer under the influence of a high electrostatic field. UV lasers with 337 nm wavelength are most commonly used, however, IR lasers have shown a tremendous potential in analyzing water-containing biological samples such as tissues and cells, and in matrix-free softer laser ionization by IR-MALDI[26]. The most commonly used MALDI matrices are small polar organic or inorganic compounds or in some cases mixtures of two or more components. It is well known that one matrix that is optimal for one class of compounds may not be the best for another. Therefore, efforts to formulate new MALDI matrices continue. Table 1.1 summarizes the chronological discoveries of some of the most widely used MALDI matrices.

Hillenkamp and Karas showed that the ion yield and types of ions generated in MALDI are the result of linear energy absorption of an analyte at its near-irradiance threshold[25]. By mixing such an absorbing analyte in molar excess with a non-absorbing

analyte sample, it is possible to control the total energy deposited to promote soft desorption of the non-absorbing molecules. Hillenkamp tested two solid organic matrices namely, nicotinic acid (NicAc) and trytophan (Trp) and two liquid organic matrices, namely, 3-Nitrobenzyl alcohol (NOBA) and 2-nitrophenyl octyl ether (NPOE) in methanol for their suitability as UV MALDI matrices[22]. Out of the two solid matrices, NicAc was preferred over Trp as the later fragmented easily and its fragments caused background noise in the low mass region of the spectrum. The liquid matrix NOBA performed better due to more solubility of the tested proteins in this matrix solution as compared to NOPE.

In a separate study, Tanaka used a fine cobalt metal powder; know as Ultra Fine Metal Powder (UFMP) mixed with glycerol as a MALDI matrix[23, 24]. As compared to the bulk metal, UFMP with nanometer-range particle diameters was suggested to absorb light more efficiently without heat loses by thermal dissipation as depicted in Figure 1.2. Due to the proximity of the nanoparticles, any scattered light would be absorbed within the matrix, resulting in rapid heating of the sample spot. UFMP also offered low heat capacity and larger surface area per unit volume as compared to the bulk metal.

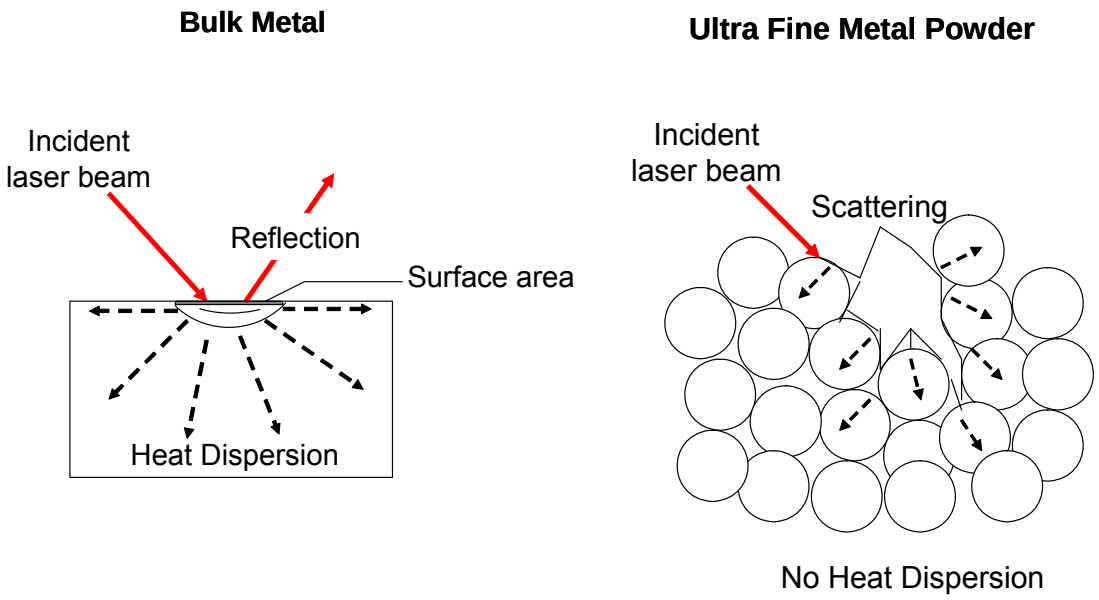

Figure 1.2. Comparison of bulk metal and UFMP matrix.

(Adopted from Tanaka, Nobel lecture, 2002)

In Tanaka's work, protein samples were embedded into the UFMP-glycerol liquid matrix and the mixture was then irradiated using a N_2 laser with wavelength of 337 nm, with a pulse width of 15 nsec and pulse energy of 4 mJ. The TOF mass spectrometer used in this work was modified by incorporating a gradient-electric field ion reflector to improve mass resolution by better energy focusing and the conventional micro-channel plate (MCP) detector was modified by adding a blind type ion-electron converter to achieve better sensitivity[24]. The resulting TOF mass spectra showed unfragmented singly charged $[n\times M+Cation]^+$ (n = 1to 7), and many of the doubly charged $[n\times M+2\times Cation]^{2+}$ cluster ions of lysozyme (M.W. 14306 Da), carboxypeptidase-A (M.W. 34472 Da), and Poly(-propylene glycol) (PPG 20K, M.W. 20 KDa). In the following years, several other UV and IR compatible MALDI matrices were discovered, including: cinnamic acid derivative matrices[27], most specifically caffeic and sinapinic acid,[27, 28]

α-cyano-4-hydroxycinnamic acid (CHCA)[29], a picolinic acid derivative named 3-hydroxypicolinic acid (HPA)[30], a carboxylic acid derivative named 2,5-dihydroxybenzoic acid (DHB)[31], 3-nitrobenzyl alcohol (NBA)-rhodamine 6G mixture[32], urea[33-35], ice[36], and glycerol[33, 34]. Recently, room-temperature ionic liquids (RTILs) with very low vapor pressures and good thermal stability were also successfully used as liquid matrices[37], however their ability to generate gas-phase ions varied substantially depending upon the availability of cationic and anionic moieties in their compositions. McLean and coworkers used size-selected gold nanoparticles ranging from 2 to 10 nm as MALDI matrices for desorption and ionization of small proteins and peptides[38] where the smaller molar ratio of matrix/ analyte required during the analysis suggested enhanced ionization efficiency as compared to conventional organic matrices.

Existing MALDI matrices can be solid or liquid, with each type having some advantages and limitations. Solid matrices have lower vapor pressures compared to liquid matrices, which allows for longer analysis time without changing the dynamics of the co-crystallized sample-matrix spot by evaporation under vacuum. The use of solid matrix also facilitates sample desalting and concentration and thus generates better signal as compared to liquid matrices. However, inhomogeneous sample-matrix co-crystallization creates ‘sweet spots’ within the dried sample area and causes significant variations in the signal intensity obtained from the same spot or amongst spots with the same analyte concentrations. Conversely, a liquid matrix offers self-renewing capability after each laser shot, resulting in a more stable ion signal. However, liquid matrices suffer from low overall sensitivity attributed mostly to sample dilution. Although finding a universal

MALDI matrix is not yet possible, the basic requirements of a solid/liquid MALDI matrix are as follows:

1. It must co-crystallize (solid matrix) or completely dissolve (liquid matrix) the sample.
2. It should not react with the sample molecules embedded or dissolved in it and ensure stability of the analyte
3. It should strongly absorb the laser light and promote analyte desorption and ionization, and lastly,
4. It should be stable under vacuum conditions

Apart from mediating laser energy transfer to the embedded analyte molecules, the MALDI matrix has been proposed to play a significant role in ionizing the desorbed analyte by photoionization (electronic excitation) or proton transfer in a series of secondary reactions occurring in the MALDI ionization process.

Table 1.1. List of commonly used MALDI matrices, in chronological order

MALDI matrix	Year of discovery	Inventor	Matrix type	Laser wavelength (nm)	Suits for analyte
Ultra Fine Metal Powder (UFMP) in glycerol	1987-88	Tanaka et al.	Liquid	337	large proteins, peptides and polymers
Nicotinic Acid (NicAc)	1987	Hillenkamp et al.	Solid	266-290, 2.94 μm, 10.6 μm	proteins, peptides and organic molecules
3-Nitrobenzyl Alcohol (NOBA)	1987	Hillenkamp et al.	Liquid	266	small peptides and organic molecules
3-Pyridinecarboxylic Acid	1989	Beavis et al.	Solid	266	large proteins
2-Pyrazinecarboxylic Acid	1989	Beavis et al.	Solid	266	large proteins
Thymine	1989	Beavis et al.	Solid	266	large proteins
3-Methoxy,4-hydroxybenzoic Acid	1989	Beavis et al.	Solid	266	large proteins
Thiourea	1989	Beavis et al.	Solid	266	large proteins
Sinnapic Acid (SA)	1989	Beavis et al.	Solid	266, 355, 337, 2.94 μm, 2.79 μm, 10.6 μm	large proteins, polymers

Table 1.1. continued

MALDI matrix	Year of discovery	Inventor	Matrix type	Laser wavelength (nm)	Suits for analyte
Caffeic Acid	1989	Beavis et al.	Solid	266, 355, 337,2.94 μm, 2.79 μm, 10.6 μm	large proteins
Ferulic Acid	1989	Beavis et al.	Solid	266, 355, 337, 2.94 μm, 2.79 μm, 10.6 μm	large proteins
Urea	1990	Overberg et al.	Solid	2.94 μm, 2.79 μm, 10.6 μm	large proteins
Glycerol	1990	Overberg et al.	Liquid	2.94 μm, 2.79 μm, 10.6 μm	large proteins
Succinic Acid	1990	Overberg et al.	Solid	2.94 μm, 10.6 μm	large proteins
Fumaric Acid	1990	Overberg et al.	Solid	2.94 μm	large proteins
Nitrobenzyl Alcohol (NBA), MeOH, Water (3:2:1)	1991	Zhou et al.	Liquid	265	large proteins
2,5- Dihydroxybenzoic Acid (DHB)	1991	Strupat et al.	Solid	266, 355, 337, 2.94 μm, 2.79 μm, 10.6 μm	large proteins, polymers
α-Cyano,4-hydroxycinnamic Acid (CHCA)	1992	Beavis et al.	Solid	266, 355, 337	peptides, glycopeptides and proteins

Table 1.1. continued

MALDI matrix	Year of discovery	Inventor	Matrix type	Laser wavelength (nm)	Suits for analyte
3-Nitrobenzyl Alcohol (NBA), Rhodamine 6G mixture	1992	Cornett et al.	Liquid	532, 337	large proteins
3-Hydroxypicolinic acid (HPA)	1993	Wu et al.	Solid	266,337,355	Oligonucleotides
2-Amino,4-methyl,5-nitropyridine	1993	Fitzgerald et al.	Solid	266,355	small peptides
2-Amino,5-nitropyridine	1993	Fitzgerald et al.	Solid	266,355	Oligonucleotides
Dithranol	1996	Belu et al.	Solid	337	polystyrene
4-Hydroxyazobenzene	1996	Liu et al.	Solid	337	polar polymers
2,2'-Dihydroxyazobenzene	1996	Liu et al.	Solid	337	polar polymers
4-(Phenylazo)-resorcinol	1996	Liu et al.	Solid	337	polar and non-polar polymers
Chromoionophor IV	1996	Liu et al.	Solid	337	polar and non-polar polymers
Graphite added glycerol	1996	Dale et al.	Liquid	337	peptides, proteins
Salicylamide	1996	Krause et al.	Solid	337	small peptides

Table 1.1 continued

MALDI matrix	Year of discovery	Inventor	Matrix type	Laser wavelength (nm)	Suits for analyte
2,4-, 2,5-, and 2,6-Dihydroxyacetophenone	1996	Krause et al.	Solid	337	proteins, oligoglycines
Ice	1996	Berkenkamp et al.	Solid	2.94 μm	frozen protein crystal
CHCA: 3-aminoquinoline:glycerol (1:4:6)	1998	Sze et al.	Liquid	337	peptides and proteins
2-(4-Hydroxyphenylazo) benzoic Acid :3-aminoquinoline:glycerol	1998	Sze et al.	Liquid	337	peptides and proteins
nano Sn in glycerol	1998	Schurenberg et al.	Liquid	337,500-760, and 1064	proteins
Ionic liquids	2001	Armstrong et al.	Liquid	337	proteins, oligomers, polymers
Size-selected gold nanoparticles	2005	Mclean et al.	Solid	337	small peptides
Solid ionic matrices	2006	Lemaire et al.	Solid	337	MALDI imaging of peptides

1.3.3. MALDI Mechanisms

Although MALDI has matured over the last three decades in terms of technological advancements and better sample preparation strategies, the underlying MALDI mechanisms are still poorly understood[2, 22, 25]. The basic MALDI ionization mechanism can be divided into three steps, starting with a desorption (or ablation) process, followed by formation of a gas plume of matrix and analyte species, and lastly the ionization of gaseous analytes by the MALDI matrix.

The desorption process in MALDI mainly involves breaking intermolecular bonds between neighboring molecules, molecules-substrate, and individual molecules following absorption of the laser energy. If this energy is sufficiently low to match the intermolecular oscillations, intact molecules are desorbed from the surface by sudden phase transition leading to the formation of gas jet or MALDI plume[39, 40]. The amount of energy deposited during desorption determines the types of molecules formed within the plume. Vertes et al.[41] suggested that the laser radiation creates hot spots in the co-crystallized sample-matrix spot where the radiation electronically excites mostly the matrix molecules, and with a lower cross section, also the sample molecules. Within several picoseconds, the electronic excitation leads to internal vibrational excitation, which is then transferred to the matrix lattice, as well as to the sample molecules embedded in it. Thus, out of the high laser energy deposited on the sample-matrix spot, only a part of the energy is transferred to the analyte molecules leading to softer desorption.

MALDI ion generation should not be described as a single process due to the presence of variety of ionic species observed in the corresponding mass spectra. Based on

the time scale of the desorption (few nanoseconds) to adiabatic gas jet plume expansion (many microseconds)[42], the ionization processes in MALDI can be divided into primary and secondary processes. Primary ions are generated immediately after the laser pulse when the MALDI matrix molecules are still in excited states, lasting for only a few nanoseconds[43, 44]. As the plume expansion occurs over the longer time scale ranging from few hundred nanoseconds to many microseconds, a combination of complex chemical reactions generate the various types of ionic species that dominate typical UV MALDI MS spectra.

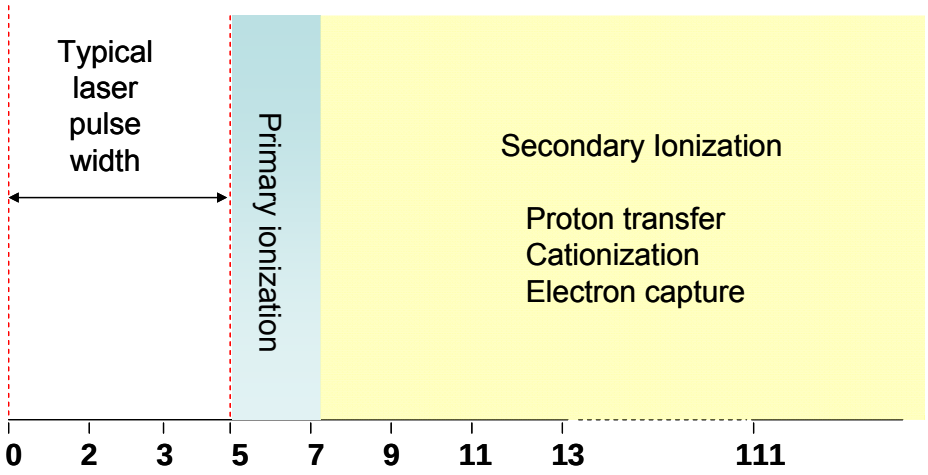

Figure 1.3. Time scale of MALDI ionization processes in nanoseconds (ns).

These chemical reactions are referred to as secondary ionization processes. The reactions discussed here are those for UV-MALDI since a UV laser was used to perform all experiments described in the following chapters (Chapter 2, 3 and 4). The excellent review by Knochenmuss and Zenobi discusses various types of in-plume secondary reactions in MALDI ionization in detail[45]:

A. Proton Transfer: Protonated molecular ions are the most commonly observed species in the MALDI mass spectra of several analyte classes, especially of proteins and peptides. Proton affinities (PA) of these proteins are usually higher (approximately 900 KJ/mol)[46-48] or greater than the PA of the commonly used basic MALDI matrices (850-900 KJ/mol)[49-51], which results in proton transfer from protonated MALDI matrix ($M+H^+$) to the neutral analyte (A). Stevenson et al.[52] showed that a strong correlation between matrix anion gas-phase basicities and analyte ion internal energies suggesting an exothermic gas-phase matrix to analyte proton transfer reaction.

B. Cationization: Although cationized ions are commonly seen in MALDI mass spectra, these may not be the dominant ions. This is explained by the fact that in general the cation affinities of most matrices are much lower than their PA values[45]. Therefore, analytes with lower PA values but higher cation affinities[53, 54] than the matrix tend to generate abundant cationized ions.

C. Electron capture: This type of reaction can explain the dominance of singly charged ions in the MALDI mass spectrum. Low energy electrons are emitted from the metal target plate during laser irradiation[55, 56]. These photoelectrons are then captured by multiply charged analyte species, which are neutralized to +1 charge states.

In a separate cluster model postulated by Karas et al.[57], it is proposed that the charge state of the analytes is conserved from solution to the dried sample spot in the condensed phase. As MALDI matrix clusters carrying embedded multiply charged analyte ions are desorbed by the laser radiation, analyte ions are progressively liberated from the matrix clusters by evaporation. The presence of these large clusters has been shown experimentally[58] and by simulations[59], reinforcing the idea that they are the ion precursors in MALDI[60]. While the cluster model can prove the appearance of most of the observed ions, the kinetic and thermodynamic studies of the species and reactions involved are yet to be performed.

The lack of a universally accepted theory to explain the underlying mechanisms in MALDI did not stop practitioners from applying this technique in fields spanning from proteomics[61-63], metabolomics and biomarker discovery[64] to tissue imaging mass spectrometry[65]. The rapid gain in the popularity of MALDI is due to some of its key advantages over other ionization techniques. The salient features of MALDI are discussed in the next section.

1.3.4. Advantages and Limitations of MALDI

The intrinsic feature of MALDI to produce predominantly singly charged ions reduces the complexity of MALDI mass spectra in analyzing complex mixtures of biomolecules and polymers[24, 66, 67]. MALDI also offers relatively higher tolerance to salt and buffer contaminants as compared to electrospray ionization (ESI). The technological advancements in mass spectrometers such as delayed extraction and reflectron TOF geometries, and the coupling of MALDI with ultrahigh resolution Fourier transform-ion

cyclotron resonance (FT-ICR) and Orbitrap instruments has dramatically improved the quality of mass spectral data. However, like all other ionization techniques, MALDI also suffers from a few limitations.

The first and foremost limitation is the dependence of the technique on the sample preparation method chosen. Although MALDI is tolerant to salt contamination, it is not completely immune to interferences from inorganic salts, buffers, detergents and chaotropic agents present in a typical biological sample. Secondly, MALDI matrix ions cause interfering background or chemical noise in the lower mass range region making it difficult to analyze small molecules. In the high mass range, neutral matrix cluster form adducts of the protein and the presence of these satellite adduct peaks is difficult to resolve from a protonated peak of a higher mass protein. The third limitation of MALDI lies in its dependence on the uniformity of the co-crystallized sample-matrix spot. MALDI also suffers from intra- and inter-reproducibility in the relative and absolute signal intensity due to the presence of 'sweet spots' within the dried spot. Therefore, researchers are on a constant pursuit for new and effective sample preparation procedures for MALDI applications. Offline sample desalting and preconcentration strategies such as purification using magnetic beads[68], solid-phase extraction micro columns[69-71] and offline and online nano-LC separation methods[62 72] are becoming routine prior to MALDI MS analysis of complex biological samples along with new electrophoretic fractionation and concentration methods[73]. Recently Aerni and coworkers developed an acoustic reagent multispotter to improve reproducibility of depositing matrix onto a sample surface for MALDI imaging applications and reported improved spot-to-spot variability compared to the conventional matrix deposition techniques used in MALDI imaging[65]. Additional

attempts to increase MALDI sensitivity include, new MALDI substrates such as porous silica, porous gold substrates[74], polymeric substrates[75]; surface-enhanced laser desorption/ionization (SELDI)[76], desorption/ionization on porous silicon (DIOS)[77], and gold nanoparticles-assisted surface-assisted laser desorption/ionization (SALDI)[78].

Despite their differences and advantages over other LD methods, MALDI, DIOS, SELDI and SALDI inherit one common limitation: the requirement of vacuum conditions, which is not conducive for coupling MALDI to online sample fractionation and for using liquid or high vapor pressure MALDI matrices. To that end, the invention of the atmospheric pressure variant of MALDI by Laiko et al.[79, 80] marked a paradigm shift towards the development of more versatile AP ionization sources.

1.4. Atmospheric-Pressure MALDI: Breaking the Vacuum Constraints

The schematic view of a typical AP-MALDI ion source coupled to a mass spectrometer is shown in Figure 1.4. AP-MALDI shares many common features with vacuum MALDI such as the use of a MALDI matrix, sample preparation procedures, types of lasers used for desorption and the applied high extraction voltages (HV), except that in the case of AP-MALDI the applied HV are much lower than those used in vacuum MALDI. AP-MALDI set-up differs from MALDI in terms of the use of an AP interface (API) in order to transfer the ions generated under AP conditions to the high vacuum region of the mass spectrometer (Figure 1.4).

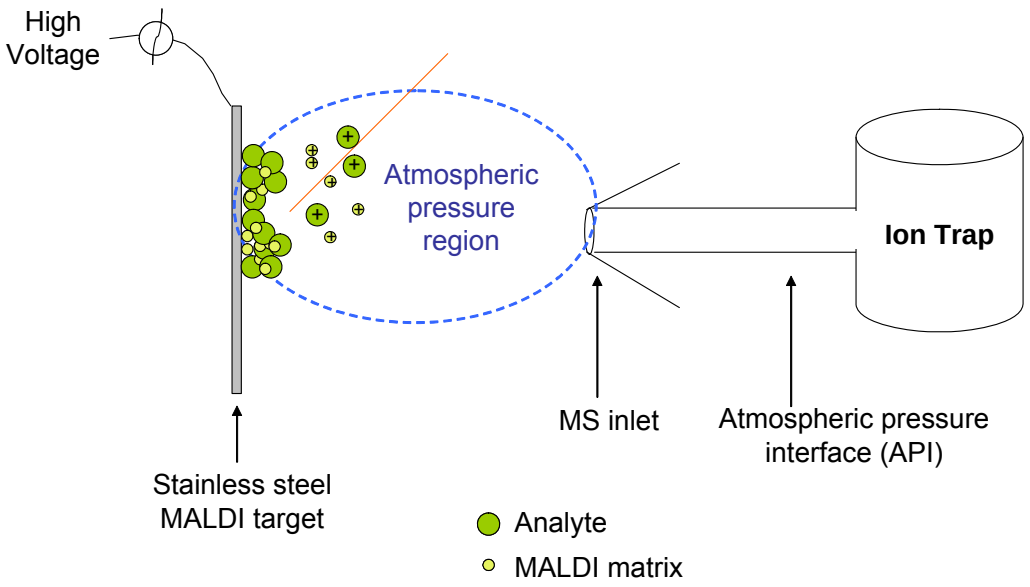

Figure 1.4. Schematics of AP-MALDI technique.

In an AP-MALDI ion source, the distance between the target plate and the API inlet (~2mm) is crucial for efficient ion collection. Such a small distance restricts the workable HV to about 2-3 KV in order to avoid electric discharges. A cylindrical stainless steel capillary with few hundred micrometers diameter serves as an API. In the commercial version of the AP-MALDI ion source, the target plate is mounted on a X-Y stage which allows for computer controlled sample positioning. The laser beam is focused on a sample spot by means of a set of mirror and lens and a UV or an IR laser can be used alternatively with the same ion source. Lastly, the compact ion source design offers compatibility with various types of mass spectrometers.

1.4.5. Advantages of AP-MALDI

AP-MALDI combines the benefits of the conventional vacuum MALDI technique with the key advantages of other AP ionization sources such as APCI and ESI. Firstly,

the AP-MALDI ion source is interchangeable with ESI or other AP ionization sources, which enables complementary analyses on a single mass spectrometer, offering more options to laboratories with limited resources. Also, when mounted on an ion trap, AP-MALDI offers MS^n capabilities[80]. Secondly, the AP nature of the source allows simple sample introduction, which enables a straightforward way for coupling on-line separation techniques such as LC and capillary zone electrophoresis (CZE). Additionally, AP-MALDI offers versatility in the type of MALDI matrices, not restricting to low vapor pressure, vacuum-stable matrices. Lastly, AP-MALDI is more amenable for analyzing fragile and thermally labile biomolecules as compared to its vacuum counterpart due to the softer ionization pathway resulting from rapid thermalization of AP-MALDI ions under AP conditions. These key advantages have made AP-MALDI a fast growing technique with several important applications, including the identification of peptides, differentiating structural isomers of oligosaccharides[81], study of phosphopeptides[82] and for the rapid screening of complex biological fluids for drugs[83] and pathogens[84].

1.4.6. Ion Transmission in AP-MALDI

Along with the above-mentioned advantages of being an AP ionization method, AP-MALDI shares a common disadvantage with the other API techniques, which is the relatively poor ion transmission into the vacuum region of the mass spectrometer. Researchers have utilized various approaches to overcome this challenge. Earlier work by Miller et al.[85] and Laiko et al.[80] used N_2 gas flowing countercurrent in or at an angle with respect to the direction of ion transit to assist ion transfer, both approaches claiming to improve sensitivity. However, important factors such as the investigation of optimal gas

flow-rates, orientation of the pneumatic flow, relative position of the sample holder and the gas outlet were not provided. In a separate study, Tan et al.[86] developed a pulsed dynamic focusing (PDF) technique in which the ions are focused into the API inlet by periodically pulsing the extraction electric field between the target plate and the API inlet, few microseconds after each laser pulse. This approach significantly improved AP-MALDI ion transmission and increased the sensitivity by almost 3-4 times. Even with this new development, AP-MALDI sensitivity is still not comparable with that of conventional MALDI.

Part I of my thesis explores the possibility of improving the sensitivity of AP-MALDI. In that, Chapter 2 describes a novel approach where on-chip sample preconcentration and focusing is coupled with AP-MALDI in an effort to increase the total amount of analyte available for AP-MALDI MS analysis. The research work explained in Chapter 3 is geared towards improving MALDI sample preparation procedures using novel on-tip SPE micro columns with various functionalities. The micro columns were evaluated for their fractionating specificities and reproducibility using model protein digest and serum control sample. As a next step in improving the AP-MALDI sensitivity, the existing AP-MALDI source was modified to accommodate a co-axial gas flow. Chapter 4 describes the evaluation of this new AP-MALDI design using various carrier gases.

1.5. Towards Open Air Ionization

The progressive transition in the ionization sources going from vacuum to AP conditions further progressed when desorption by electrospray ionization (DESI)[87] was

first performed under ambient conditions by Takats and coworkers. The success of DESI invigorated efforts to develop newer and better ambient ionization methods such as direct analysis in real time (DART)[88], extractive electrospray ionization (EESI)[89] and others[90, 91]. Open air ionization methods can be grouped under spray-based, laser-based, or heat-based techniques. One example of each type of technique is described briefly in the following sections. The power of these approaches lies in their ability to perform high throughput analysis without sample preparation.

1.5.7. Spray-based Ambient Ionization: DESI

The first technique reported in this group is DESI, invented by Cooks and coworkers, in which sample solution is dried on a freely moving substrate and is desorbed by means of an electrospray jet. The desorbed analyte is then solvated by the electrospray solution and ionized by the 'droplet pick-up mechanism'. DESI has been applied for rapid screening of drug molecules[89], steroids, and chemical warfare agents[87], among other analytes.

1.5.8. Laser-based Ambient Ionization: MALDESI

In MALDESI[92], a premixed sample-MALDI matrix spot is ablated using a laser and the desorbed neutrals are ionized by directing an electrospray over the sample spot. Muddiman et al. coupled MALDESI to a high resolution FT-ICR for obtaining good quality mass spectral data for peptides and protein samples in the open air.

1.5.9. Ambient Ionization via Gaseous Metastables

In DART[88], a stream of heated metastable gases such as N_2 or Helium (He) is directed on to a sample, which is placed in the gap between the exit of the DART source and the API inlet of a mass spectrometer. The heated metastables desorb and ionize the sample. Several DART ionization mechanisms including Penning ionization have been suggested by Cody et al., which are described in detail in Chapter 5. DART is best suited for analyzing small and volatile molecules and several hundreds of samples can be screened in a single day emphasizing the high throughput nature of the technique. Recently, experimental evidence along with computer simulations showed that DART sensitivity is greatly affected by the metastable gas flow rate, temperature, and the position of the sample.

Part II of my work describes a novel application of the DART technique for analyzing small volatile terpenes and terpenoids, which play a key role in the growth of a disease vector, *A. aegypti*. In Chapter 5, the work related to the optimization of DART parameters for analyzing various terpene alcohols and their oxidation products is described.

1.6. Conclusions

After experiencing a plateau in the development of ionization techniques for almost three decades, a growth surge was experienced in the last decade as new atmospheric and ambient pressure ionization methods were successfully developed and applied for analyzing a wide class of samples by MS. However, less-than-optimal sensitivity of ionization methods such as AP-MALDI has not yet been completely

alleviated. The introduction of better sample preparation strategies and the development of a new ion source design described in this thesis attempts to circumvent some of these challenges.

PART I: ADVANCES IN ATMOSPHERIC PRESSURE MATRIX-ASSISTED LASER DESORPTION/IONIZATION

CHAPTER 2. IMPROVED SENSITIVITY FOR AP-MALDI-MS ANALYSIS USING ON-CHIP SOLID-PHASE EXTRACTION PRE-CONCENTRATION/FOCUSING SUBSTRATES

2.1. Abstract

This chapter presents the implementation of a chip-based sample pretreatment approach for improving AP-MALDI sensitivity. The characteristics of the new focusing targets are discussed, followed by a brief description of the steps involved in the on-chip sample preconcentration/focusing process. The performances of the focusing targets in terms of AP-MALDI MS sensitivity, reproducibility, and detection limits are evaluated and compared with conventional AP-MALDI targets using a model peptide and a derivatized protein digest. Finally, the coupling of focusing targets with AP-MALDI is extended for successful tandem mass spectrometric (MS/MS) sequencing of dilute solutions of a derivatized tryptic digest of a protein standard and for the detection and profiling of low abundance neuropeptides from crude mosquito head extracts.

2.2. Introduction

The advantages of AP-MALDI over its vacuum counterpart have been discussed in the previous chapter. Besides of being a facile, easy to swap ion-source, and being compatible to solid as well as liquid matrices, the main power of AP-MALDI lies in generating cooler ions of thermally labile biomolecules such as conotoxins[93] and phosphopeptides[82] with minimal fragmentation. The rapid thermalization of AP-MALDI ions due to the collisional-cooling under AP conditions modulates the internal energy

deposited in the ions, preserving intact precursor ions. Although advantageous, softer ionization in AP-MALDI leads to the formation of analyte-salt and analyte-matrix adducts showing satellite peaks at slightly higher *m/z* than the analyte. The satellite peaks can merge with the analyte signal peaks of higher mass component in a complex biological sample, resulting in low quality mass spectra where the background noise contributes to loss of AP-MALDI sensitivity[94]. The problem of adduct formation has been partially resolved by using a heated API stainless steel capillary[95], and by using a capillary inlet incorporating a concentric flow of heated N_2 gas directed at the sample to de-cluster adducts[85]. However, these approaches were directed towards instrument development whereas the simpler approach of sample pretreatment remained open for investigation.

Historically, as the use of MS for analyzing biological samples became customary, newer and better sample pretreatment strategies were developed, including magnetic beads[68] and centrifuge mass cut-off filters[96, 97], and solid-phase extraction (SPE) based on-tip[70] and on-chip[69, 98-100] sample pretreatment methods, with the main focus being vacuum MALDI applications. Although proven efficient, some of these SPE-based techniques suffer from day-to-day reproducibility[70, 101]. Other techniques such as surface-enhanced laser desorption/ionization (SELDI) requires vacuum chambers for sample preparation. Recently, Turney et. al. developed functionalized silica nanoparticles for selective extraction of hydrophobic peptides, which served the dual purpose of also being part of the AP-MALDI MS matrix[102]. However, their performance was not evaluated for real-world complex samples, where competitive binding between the analyte of interest and other concomitant species can affect binding efficiency.

Therefore, the work described in this chapter was motivated by the need for improved AP-MALDI sensitivity and by the need for better sample pretreatment platforms for complex biological samples prior to AP-MALDI MS analysis. An evaluation of the analytical performance (i.e. sensitivity gain, reproducibility) afforded by two types of on-chip SPE preconcentration/focusing targets, namely hydrophobic and weak cation exchange (WCX) is presented. Later, the two targets were tested for two biologically significant applications requiring high sensitivity: (a) in the detection and profiling of low abundance neuropeptides obtained from the extracts of *Aedes aegypti* mosquito heads, and (b) in sequencing of dilute sulfonated tryptic peptides of a model protein by tandem MS (MS^2) analysis. The results were compared with those obtained using conventional AP-MALDI targets for determining dynamic range and reproducibility. The results presented here extend the application of AP-MALDI MS for neuropeptide profiling and present the first report of coupling on-chip surface preconcentration/focusing to AP-MALDI.

2.3. Experimental

2.3.1. Chemicals

Angiotensin I, equine heart myoglobin, proteomic grade trypsin and ammonium dihydrogen phosphate were purchased from Sigma-Aldrich (St. Louis, MO, USA). Ammonium hydroxide was purchased from Fisher Scientific (Pittsburgh, PA, USA), and ammonium bicarbonate, 1,4-dithoi-DL-threitol, and 2-sulfobenzoic acid cyclic anhydride were purchased from Fluka (St. Louis, MO, USA). O-Methylisourea hemisulfate was purchased from Acros Organics (Morris Plains, NJ, USA). Ethanol (EtOH), HPLC grade

acetonitrile (ACN), ammonium citrate diabasic and α–cyano-4-hydroxycinnamic acid (CHCA) were purchased from Qiagen Inc. (Valencia, CA, USA). Neuropeptides allatostatin-C (AS-C) and allatotropin (AT) were synthesized by Alpha Diagnostic International Inc. (San Antonio, TX, USA), and Center for Biotechnology Research, Kansas State University (Manhattan, KS, USA). These standards were purified chromatographically and assessed to be ≥100 % (AS-C), and ≥ 97% (AT) pure by reversed-phase (RP) liquid chromatography (LC) with MS detection (LC-MS) and amino acid analysis. All aqueous solutions were prepared with pure water from a Nanopure Diamond laboratory water system (Barnstead International, Dubuque, IA, USA). C18 particle-embedded pipette micro tips (NuTips, 1-10 μL) were purchased from Glygen Corp. (Columbia, MD, USA).

2.3.2. Aedes. aegypti Mosquito Sample Collection

Mosquito head sample collection was performed by in the groups of Prof. Fernando G. Noriega from Florida International University (FIU, Miami, FL, USA) and Salvador Hernández-Martínez from Instituto Nacional de Salud Pública (Cuernavaca, Morelos, México).

Mosquito head samples were collected by decapitation, followed by homogenization in Bennett's solution[103] (1% NaCl, 5% formic acid, and 1% trifluroacetic acid (TFA) in 1 M HCl). The homogenized sample was centrifuged for 10 minutes at 14,000 *g* and the supernatant was lyophilized and stored at -80°C until the next step of on-chip desalting/ focusing as described in the next section.

2.3.3. Focusing Target Geometry and Surface Functionalities

The desalting/focusing hydrophobic targets (64 wells, MassSpecFocus Desalting Type 4), weak cation exchange (WCX) targets (25 wells, prototype chip), and gold-coated stainless steel 'tuning targets' without surface functionality, but otherwise identical to the hydrophobic/WCX focusing targets, were obtained from Qiagen Inc.

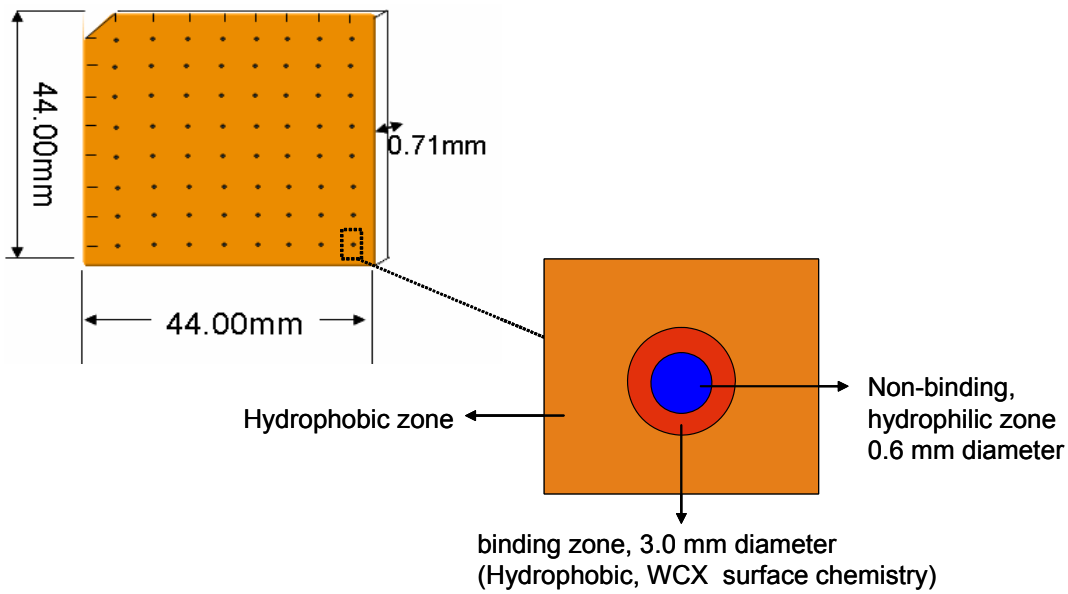

Figure 2.1. On-chip preconcentration/focusing target surface morphology.

The focusing targets used in this work consist of gold-coated stainless steel plates with their surfaces modified by arrays of concentric rings of alkanethiol self-assembled monolayers (SAMs) as shown in the Figure 2.1. Depending upon the nature of the terminal groups of these alkanethiols, three distinct wettability zones, namely the outermost hydrophobic, a central, moderately hydrophobic, and the innermost hydrophilic zone exist on the plate surface. The central zone can be alternatively modified with either hydrophobic or weak cation exchange surface functionalities, which

serve as binding sites to retain hydrophobic or positively charged chemical species. The diameters of the central and inner most zones are approximately 3.0 mm and 0.6 mm, respectively. Together, the central and the innermost zone form one sample-loading site, with a total number of 64 and 25 sites on hydrophobic and WCX focusing targets, arranged in 8× 8 and 5 × 5 matrices, respectively. The locations of the sample loading sites are marked by gridlines since the zones are not visible to the naked eye. The focusing targets were stored in a desiccator before and after the use.

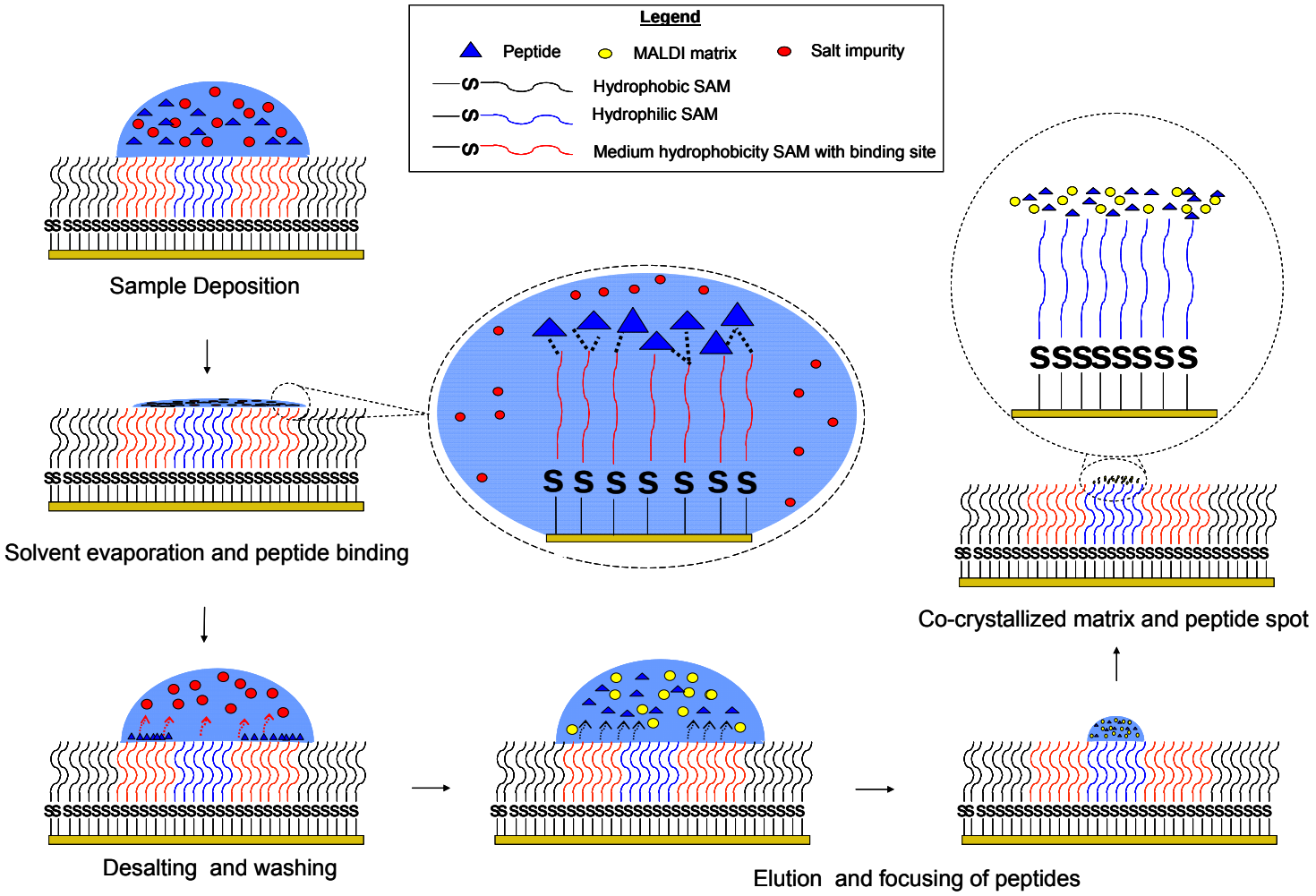

Figure 2.2. Schematic diagram illustrating the steps involved in the on-chip sample preconcentration/focusing process.

2.3.4. Optimized On-chip Sample Preconcentration/Focusing Procedure

Variable volumes ranging from 5-20 μL of sample solution prepared in 50:50 ACN/ 0.1 % TFA in deionized water were deposited on hydrophobic loading sites and the solution was allowed to dry completely in a humidity chamber. Controlled evaporation of 10 μL solution required approximately 45 minutes with humidity maintained between 45-65%. In the next step, on-chip desalting was achieved by twice depositing and subsequently removing after 2 minutes 10 μL of 0.1% TFA solution. In the last step, elution and focusing were performed simultaneously by spotting 2 μl of 0.063 mg/mL CHCA solution prepared in 84:13:3 v/v/v ACN/ EtOH/5 mM ammonium citrate solution. The optimum concentration of the working CHCA matrix solution was determined in exploratory experiments, which are described in detail under the results and discussion section.

For WCX targets, variable volumes of samples prepared in 20 mM ammonium phosphate buffer with pH 6.6 were deposited on the loading sites for 30 minutes and rinsed prior to complete dryness. Elution and focusing steps were carried out separately, by first eluting the bound peptide in 5 μL of 50:50 ACN/ 0.1%TFA. The solution was allowed to dry completely before focusing the eluted peptides by depositing 2 μL of CHCA matrix solution.

2.3.5. Procedures for Reproducibility and Signal-to-Noise(S/N) Gain Study

Serial dilutions of peptide standards angiotensin I and AS-C containing 0.1-5 pmol/ 0.5 μL were prepared in 50:50 ACN/ 0.1% TFA solution. Triplicates of each solution were premixed with equal volumes of 10 mg/mL of CHCA solution prepared in

the same solvent and the mixture was spotted on a gold-coated conventional AP-MALDI target and allowed to air dry to form co-crystallized peptide-matrix spots. A second set of the diluted peptide solutions with concentrations ranging from 0.075-1 pmol / 5 μL of angiotensin I were spotted on the hydrophobic and WCX focusing targets followed by on-chip desalting and focusing the peptide in triplicate and duplicate, respectively, using the optimized on-chip preconcentration/focusing procedure as described in the previous section.

For S/N gain studies at fixed peptide concentration, 0.5 μL the of 2×10^{-7}M angiotensin I solution, premixed with equal volume of 10 mg/mL CHCA matrix was spotted on the conventional AP-MALDI target. Varied volumes from 5-20 μL of the same solution were deposited on the hydrophobic and WCX focusing targets and subjected to on-chip desalting/focusing procedures. In S/N gain studies at fixed peptide amounts, 1 μL of premixed solution of 1×10^{-6} M angiotensin I and 10 mg/mL CHCA solution was spotted on the conventional focusing target. Five μL of the peptide solution with 2×10^{-7} M concentration were desalted and focused on the hydrophobic and WCX targets, resulting in equal amounts of angiotensin I (1 pmol/spot) on each investigated targets.

2.3.6. Preparation of Model protein Digest and Tryptic peptide Derivatization

A 1×10^{-4} M myoglobin solution was prepared in 50 mM ammonium bicarbonate/ 40% ACN, and 100 μL of this solution were incubated sequentially with (a) 5 μL of 200 mM 1,4-dithio-DL-threitol in 100 mM NH_4HCO_3 for 1 h, followed by with (b) 4 μL of 1 M iodoacetamide in 100 mM NH_4HCO_3 for 20 min at room temperature in

order to perform reduction and alkylation of the protein. Trypsin working solution (20 μg/mL, prepared as per the manufacturer's protocol) was added to the mixture and incubated for 18 h at 37°C. Later, the protein digest solution was dried in a Speed-Vac (Savant Instruments Inc., Holbrook, NY, USA) and reconstituted in 60 μL of deionized water. Guanidination of 20 μL of the reconstituted digest was carried out using 7 M NH_4OH and 8 M O-methylisourea hemisulfate solution for 10 min at 65°C[104]. A 26 μL aliquot of this solution was dried, reconstituted in 10 μL of 50:50 ACN/ 0.1% TFA and purified using C18 NuTip, by following the procedure developed earlier in our lab[64]. The eluate was subsequently dried, reconstituted in 40 μL of 0.1 M ammonium bicarbonate. The N-terminal sufonation was carried out following the procedure described by Keough et al.[105], with the exception that ammonium bicarbonate instead of trimethylamine was used to maintain a pH value of 8. The derivatized tryptic digest was serially diluted and each dilution was spotted on the conventional, tuning and hydrophobic focusing targets in duplicate. The dried spots on all the targets were subjected to tandem MS analysis performed in a data dependent analysis mode using the quadrupole ion trap instrument.

2.3.7. Aedes aegypti Mosquito Head Extract Samples

Frozen lyophilized mosquito head extracts obtained from 10 mosquito heads were reconstituted and dissolved in 30 μL of 50:50 ACN/ 0.1% TFA solvent. The reconstituted solution was subject to on-tip SPE prior to the on-chip preconcentration/focusing on the hydrophobic focusing target. The on-tip SPE procedure was as follows: A C18 NuTip was first washed 5 × 10 μL 50% ACN, and equilibrated with 3 × 10 μL 0.1% TFA. The equilibrated NuTip with a set pipette volume of 10 μL was immersed in 30 μL of

reconstituted head extract solution and the solution of aspirated in and expelled through the NuTip micro-column 10 times, followed by a washing step with 2 × 10 µL of 0.1% TFA. During the sample loading and washing steps, precautions were taken to avoid introduction of air into the micro-column. Finally, the bound components were eluted with 5 µL of 50:50 ACN/0.1% TFA. The eluate containing an extract equivalent to 4 mosquito heads was deposited on a hydrophobic focusing target for on-chip preconcentration/focusing. A second frozen lyophilized extract obtained from 10 mosquito heads was reconstituted and dissolved in 30 µL of 20 mM ammonium hydrogen phosphate (pH 6.4), and a 10 µL aliquot was directly spotted on a WCX focusing target for on-chip preconcentration and focusing.

2.3.8. AP-MALDI MS Set-up

The schematic of the AP-MALDI ion source equipped with a nitrogen laser (337 nm wavelength, pulse width of 4 ns, repetition rate of 10 HZ) and a pulse dynamic focusing (PDF) module is shown in Figure 2.3a. The AP-MALDI ion source (model 611, MassTech Inc., Columbia, MD, USA) housing consists of two cap-like aluminum flanges, namely, the optical flange and the target flange. The optical flange supports a mount which holds an optic fiber and a lens. An adjustable mirror is held inside the optical housing by a setscrew. The height of the optic fiber and the direction of the lens and the mirror can be adjusted to direct and focus the laser beam delivered by the optic fiber. The other end of the optic fiber is connected to the laser unit.

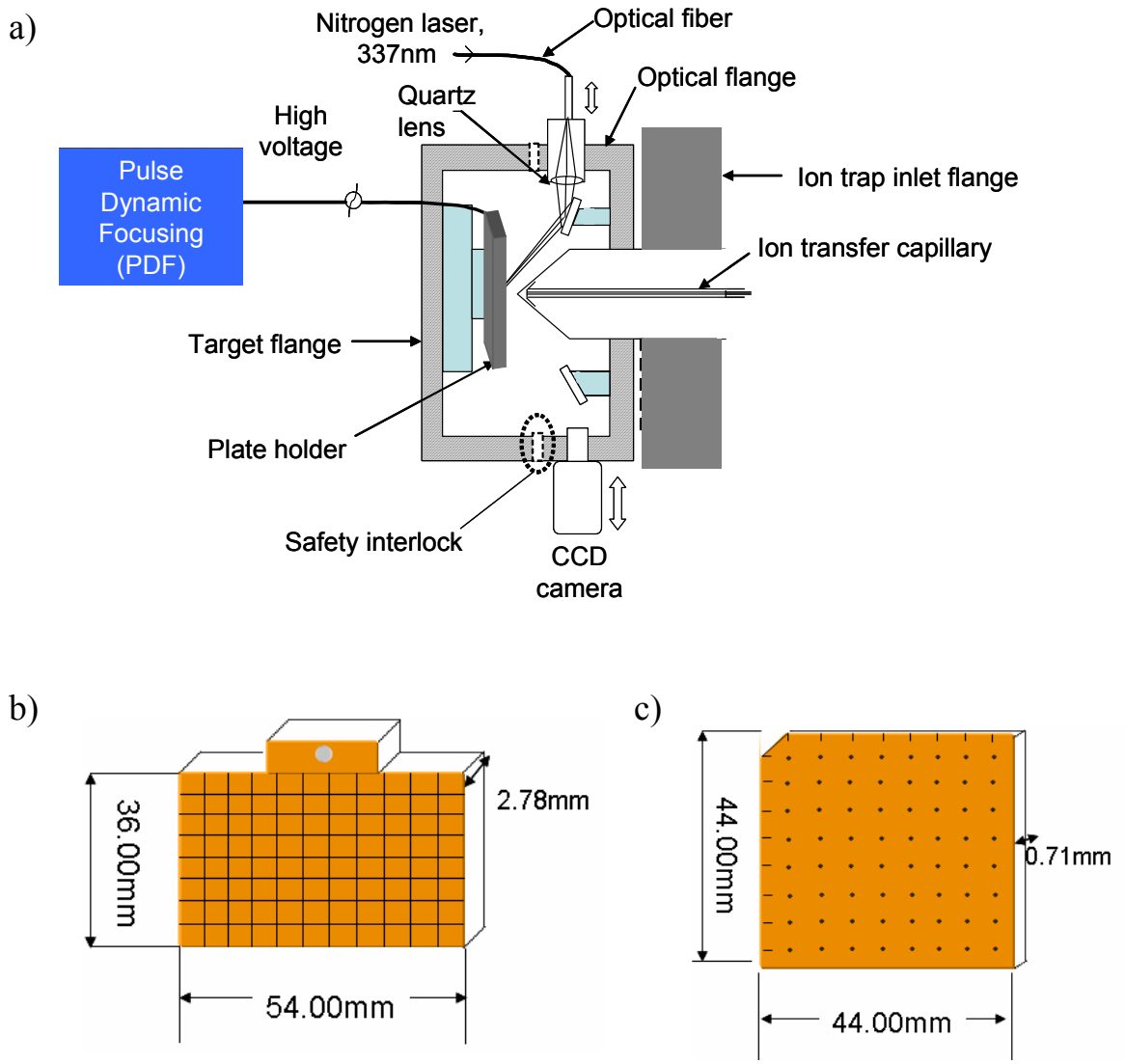

Figure 2.3. Schematic diagram of (a) AP-MALDI MS set-up, (a) a conventional AP-MALDI target (64 wells, 8 × 8 array), where each square marked by gridlines shows sample spotting position, and (c) a focusing target, with location of the innermost zone shown by dots.

A CCD camera to view sample spot location is mounted on the ion source flange. The ion source also houses an X,Y-linear translational stage which holds a magnetic target adaptor (2.3b). In order to mount the focusing targets (2.3c), the conventional magnetic sample adaptor was replaced by an Opti-TOF plate holder (Applied Biosystems, Foster city, CA, USA). The AP-MALDI ion source was mounted on an LCQ DECA XP+

quadrupole ion trap (IT) mass spectrometer (Thermo Finnigan, San Jose, CA, USA). The target flange is placed on the LCQ slider so that the two flanges of the ion source can be connected to each other during the experiments and can be moved away in between experiments for inserting and removing the targets. A safety interlock activated when the source is closed is turned off as soon as the target flange is moved away from the optical flange, and as a result, the high voltage (HV) supplied to the target is switched off automatically as a safety measure.

The HV extraction potential to the target is provided by the mass spectrometer. When the pulse dynamic focusing (PDF) module (Figure 2.3a) is operational, this HV is periodically pulsed to focus the AP-MALDI ions towards the instrument's inlet. The principle of PDF technology, first described by Tan et al.[86], is illustrated in Figure 2.4. When the PDF mode is functional, each laser pulse is used to trigger a delay/pulse generator that activates a fast HV transistor switch at a user-defined set 'time-extraction interval' after the laser pulse. The time-extraction interval marks the delay between the firing of the laser pulse and when the HV is switched off. Once the switch is activated, after this interval, the HV supplied to the target is immediately pulsed off for a given 'hold time'. Typically, the hold time is set to be less than the time between the laser pulses (100 ms with 10 Hz laser frequency) so that the HV can be delivered to the target plate before next laser pulse.

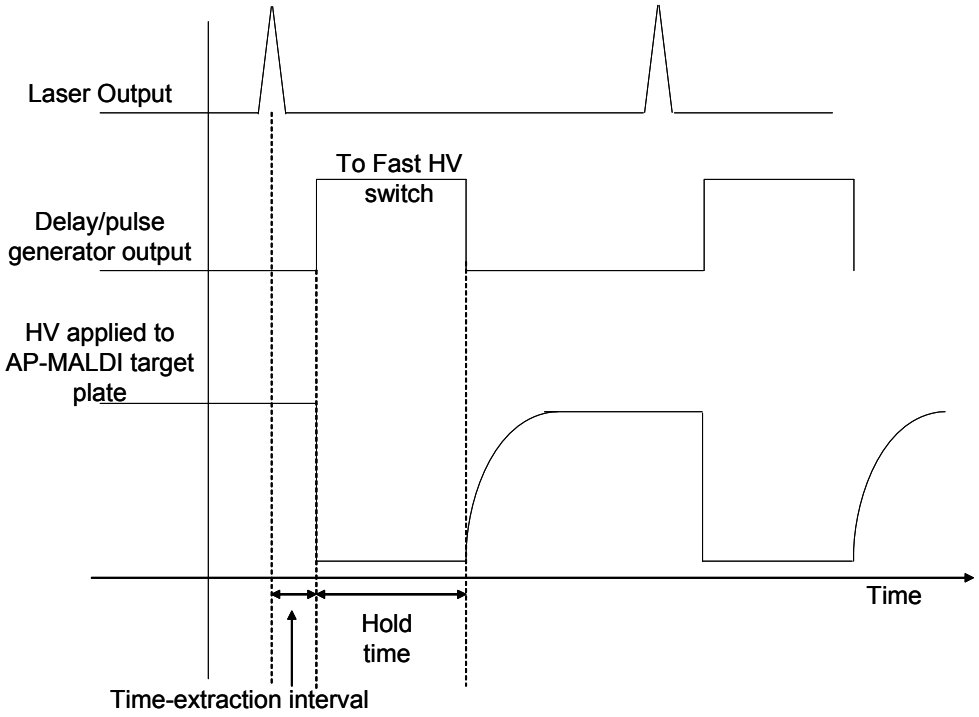

Figure 2.4. Sequence of events in the pulsed dynamic focusing (PDF) mode of operation.
(Adopted from Tan et al., *Anal. Chem.*, 2004 (76), 2462-2469)

The AP-MALDI target layout stored in the ion source control software (Mass Tech Inc.) was custom modified in order to accommodate for the plate geometry of the new focusing targets as follows: For the 64-well hydrophobic target and the 25-well WCX target, the X,Y target position offsets were (10 mm, 1 mm), and (4.7 mm, -3.50 mm), respectively. Sample spacing parameters were set to 4.5 mm (X) and 9.0 mm (Y) for both types of targets. The spiral motion velocity of 2 mm/min with a between-turn spacing of 0.08 mm were used throughout all the experiments.

The target plate high voltage was kept to an optimal value of 3.0 KV. The tuning of the laser was performed by spotting 5 pmol of angiotenin I on 'tuning targets', which are identical to the focusing targets but lack the surface functionalities. The IT mass

spectrometer settings were as follows: Ion transfer capillary voltage and temperature, 43 V and 300°C, tube lens offset voltage: 15 V, multipole 1 offset: 0.25 V, multipole 2 offset: -7.00 V, intermultipole lens voltage: - 16 V, and entrance lens: -66 V. The skimmer-multipole 1 voltage difference was set to 60 V to promote declustering of analyte-matrix adducts by increasing low-energy collisions. The optimum PDF module pulse delay was set to 23 μs for conventional targets and 17.5 μs for focusing targets. Automatic gain control (AGC) was turned off, and the ion injection time was fixed to 220 ms. Data was acquired for one minute and averaged over the entire acquisition time with approximately 30 scans. Averaged spectra were smoothed using a 9-point Boxcar filter and exported to Origin Lab 7.5 (OriginLab Corp., MA, USA) for baseline correction.

For protein identification experiments in data dependent scan mode, the data were acquired for 2 minutes in two sequential events. The first event was a full MS scan for 1 minute over the mass range *m/z* 1300- 1805. In the second event, successive MS/MS scans on five different precursor ions were performed, with each MS/MS scan acquired for 0.2 min, and the precursor mass was automatically added to the exclusion list. The MS/MS parameters were as follows: isolation width: 5.0, normalized collision energy: 100%, activation Q: 0.25, activation time: 80 ms, minimum signal required for Full MS and MS^2 scans were 2×10^4 and 2×10^3, respectively, exclusion mass width: 2.0, ion injection time: 500 ms, and number of microscans: 20. The raw data was directly imported to PEAKS studio (PEAKS studio, 4.2, Bioinformatics Solutions Inc., Waterloo, ON, Canada) for auto *de novo* sequencing and subsequent protein database search against SwissProt. The PEAKS data refinement feature used were noise filtering, peak centroiding, and merging scans of the same precursor ion. The database searching mass

error tolerance used for the precursor and fragment ions were 2.0 and 0.8 Da, respectively. Three post-translational modifications, namely, C-terminal guanidination, N-terminal sulfonation (both, user-defined modifications), and cysteine carbamidomethylation (built-in modification) were considered as fixed peptide modifications for the auto *de novo* and database searches.

2.4. Results and Discussion

The typical appearance of an on-chip preconcentrated and focused sample-matrix co-crystallized spot is shown in Figure 2.5. The average diameter of the focused spots measured with an optical microscope (2.5x magnification, Olympus, USA) was 569 ± 48 µm.

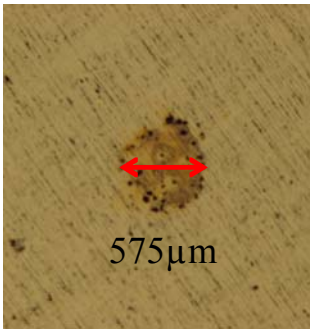

Figure 2.5. Typical sample-matrix focused spot on a focusing target.

The dependence of the focused spot diameter on the evaporation speed of the matrix solution was apparent during method development. The optimal speed of evaporation was achieved by maintaining % humidity between 45%-65% and by using

80% ACN in the matrix solution composition. Additionally, the concentration of CHCA matrix solution influenced the evaporation rate and needed further optimization.

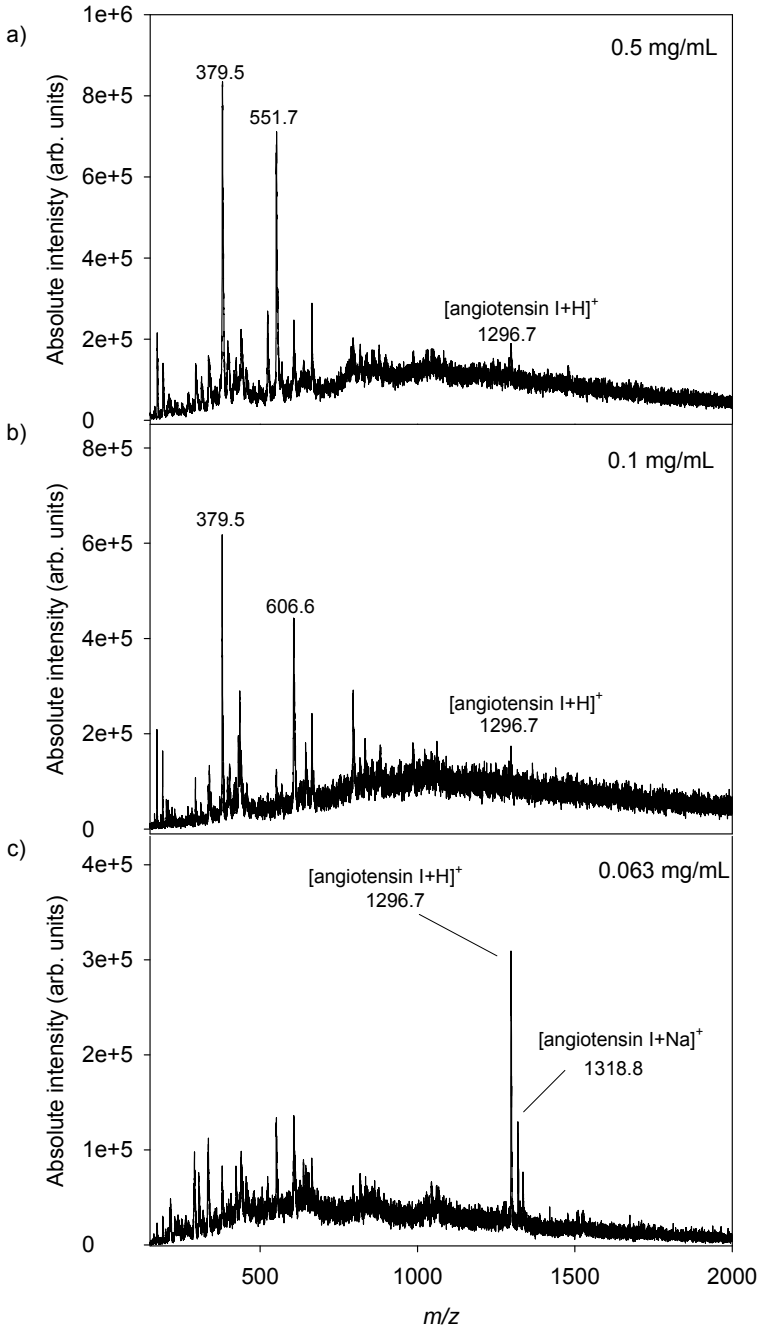

Figure 2.6. AP-MALDI-MS mass spectra obtained from 0.1 pmol/spot of angiotensin I focused using (a) 0.5 mg/mL, (b) 0.1 mg/mL, and (c) 0.063 mg/mL of CHCA matrix solution on a hydrophobic focusing target.

2.4.1. Optimization of Amount of CHCA Matrix for On-chip Focusing

The optimal concentration of CHCA matrix solution was determined experimentally as 0.063 mg/mL. Matrix concentrations above the optimized values reduced the mass spectral quality with poor S/N ratio due to the appearance of high intensity matrix adducts, such as at *m/z* 379, corresponding to $[2CHCA + H]^+$, along with other unknown background peaks and a low intensity peak corresponding to the protonated angiotensin I ion at *m/z* 1296.7 (Figure 2.6a). The low intensity of the protonated peptide ion peak was attributed to the ionization suppression of peptide ions in the presence of a more dense matrix plume. It is worthwhile mentioning that concentrated CHCA matrix solutions evaporated much faster than diluted matrix solutions, resulting into incomplete elution of the bound peptide from the central zone into the innermost zone. Therefore, a 0.063 mg/mL CHCA concentration was used for all experiments.

2.4.2. Signal-to-Noise Ratio (S/N) Gains

Initial characterization studies were directed at investigating the extent to which focusing targets enhanced AP-MALDI sensitivity. Two phenomena factor into the observed S/N gains. First, focusing targets enable the deposition of a larger sample volume than in the conventional AP-MALDI experiment, effectively resulting in a preconcentration effect where more peptide is probed by the AP-MALDI laser. The second effect is related to the focusing of the co-crystallized matrix and analyte into a spot of a smaller diameter than what is obtained in a conventional AP-MALDI plate provided by the manufacturer. Two sets of experiments were designed to investigate these phenomena independently from each other. We first deposited variable volumes of

a fixed concentration (2 x 10^{-7} M) angiotensin I solution to investigate the preconcentration effect (Figure 2.7a-c). These experiments were followed by a second set of runs where a fixed amount (1 pmol/spot) of peptide was deposited to investigate the focusing effect, independently of any pre-concentration factors (Figures 2.8a-c). Both conventional and focusing AP-MALDI targets were used in these experiments, and S/N gains were calculated from the resulting baseline-corrected mass spectra.

For experiments performed with a fixed peptide concentration per spot (Figures 2.7 a-c), the observed S/N were 0.5, 117 and 56, for conventional, hydrophobic and WCX focusing substrates, respectively. This is equivalent to S/N gains of 234 and 112 for the hydrophobic and WCX focusing targets. The observed higher absolute signal of the protonated peptide on the focusing targets (Figure 2.7b-c) compared to that on the conventional target (Figure 2.7a) was attributed to the fact that the improved spot homogeneity reduced the appearance of 'sweet-spots', with in the co-crystallized peptide-matrix spot, yielding on average more ions per laser shot, along with the preconcentration effect.

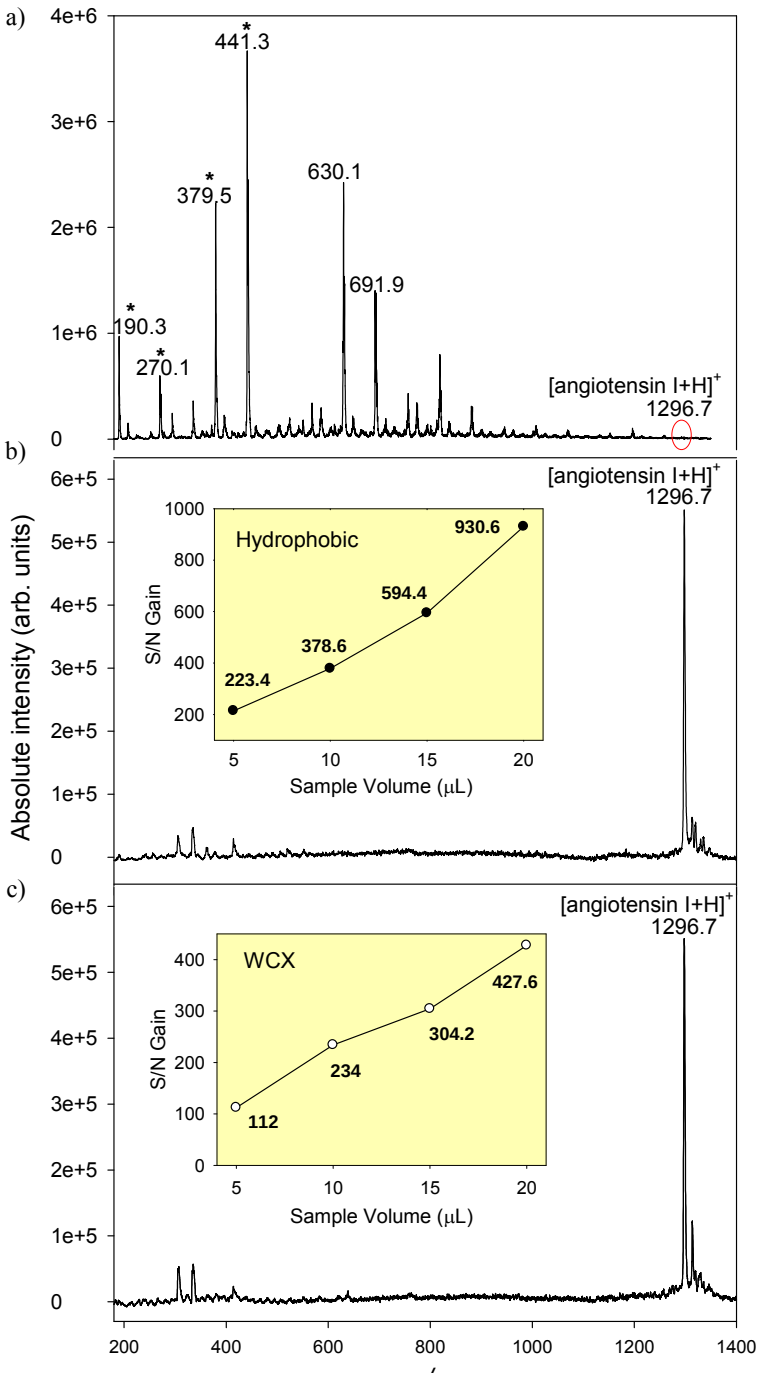

Figure 2.7. AP-MALDI MS spectra of 2 x 10^{-7} M/spot angiotensin I spotted on (a) conventional AP-MALDI target, 5 µL on (b) hydrophobic, and (c) WCX focusing targets. The inserts show the S/N gain as a function of sample volume deposited. Peaks corresponding to CHCA matrix peaks are denoted by asterisks.

The focusing targets produced mass spectra with clean baselines, devoid of matrix species such as the protonated CHCA matrix ion at *m/z* 190, matrix clusters and salt adducts at *m/z* 270.8 ($[M+Na+K+H_2O+H]^+$), 379 ($[2M+H]^+$), 442 ($[2M+Na+K+H]^+$), and 630 ($[3M+Na+K+H]^+$), commonly observed with conventional targets. This observation was partially attributed to the fact that the surface matrix density was almost 10 times higher for the conventional (5.76×10^{-3} mg/mm^2) than for the focusing targets (4.95×10^{-4} mg/mm^2). Additionally, on-chip desalting minimizes the abundance of Na^+ and K^+ ions necessary for forming the above-mentioned clusters. The addition of diabasic ammonium citrate to the CHCA matrix solution further suppresses the most common matrix adducts, resulting in reduction of baseline chemical noise[106-108].

The inserts in Figures 2.7b and 2.7c show the S/N gains observed for independent experiments were 5-20 μL of sample solution were deposited on the two types of focusing targets investigated. These ranged from 223 to 931 for hydrophobic targets and from 112 to 428 for WCX targets. As compared to the hydrophobic target, lower S/N gains were observed for the WCX focusing target. This could be due to the fact that the recommended pH of the binding solution used for on-chip sample preconcentration on WCX targets was 6.6, which is close to the pI of this peptide (6.69)[109] , leading to a lower proportion of positively-charged angiotensin in the investigated solution. Secondly angiotensin I is hydrophobic (hydrophilicity value of -0.5) and hence it has high binding affinity for hydrophobic sites. This hydrophilicity value was calculated using an online tool{, #258}, based on the Hopps-Woods scale[111]. Regardless of the substrate type considered, the large increase in observed S/N demonstrates the main advantage of these substrates for AP-MALDI analysis.

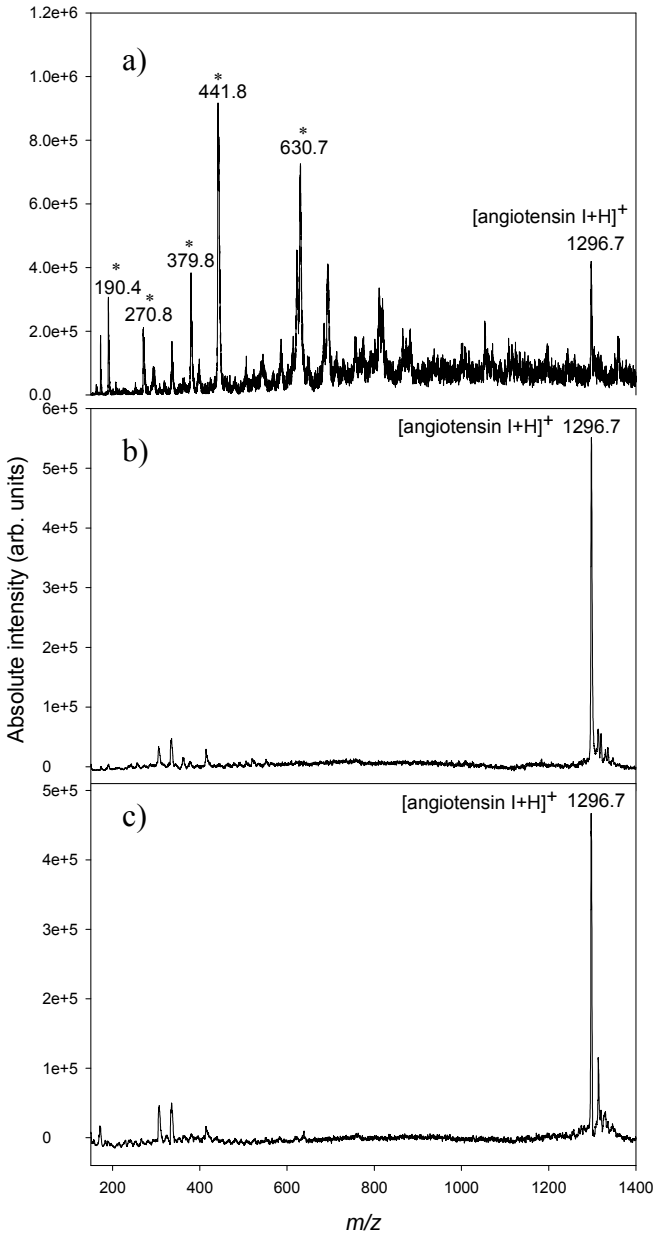

Figure 2.8. AP-MALDI mass spectra of 1 pmol/spot of angiotensin I on (a) conventional AP-MALDI target, and on (b) hydrophobic, (c) WCX focusing targets. Peaks corresponding to CHCA matrix adducts are denoted by asterisk.

Results for experiments with a fixed amount (1pmol/spot) of peptide are shown in Figures 2.8a-c. S/N values of 7.8, 126 and 74 for conventional, hydrophobic, and WCX focusing targets were observed, respectively. This corresponds to S/N gains of 16 and 9.5 due solely to the focusing effect. The angiotensin I detection limits (LOD) calculated for

these experiments were 384 fmol/μL for conventional targets, and 5 and 8 fmol/μL for hydrophobic and WCX focusing targets, as a direct consequence of the tighter sample spots. Results for experiments with a fixed amount (1 pmol/spot) of peptide are shown in Figures 2.8a-c. S/N values of 7.8, 126 and 74 for conventional, hydrophobic, and WCX focusing targets were observed, respectively. This corresponds to S/N gains of 16 and 9.5 due solely to the focusing effect.

When the CHCA concentration used for the focusing targets (0.063 mg/mL) was spotted on the conventional target, there was no signal observed for 1 pmol of angiotensin I due to insufficient matrix (data not shown). However with the 10 mg/mL CHCA concentration, peptide signal was observed with S/N ratio of 7.2 (Figure 2.9a). The addition of ammonium citrate did not improve the spectral quality and detection limits (Figure 2.9b). This suggested that for the conventional target, a higher matrix concentration should be used without the addition of diabasic ammonium citrate salt. Therefore, the matrix concentrations and solvent compositions used for the two types of targets were independently optimized for the subsequent sensitivity and reproducibility experiments.

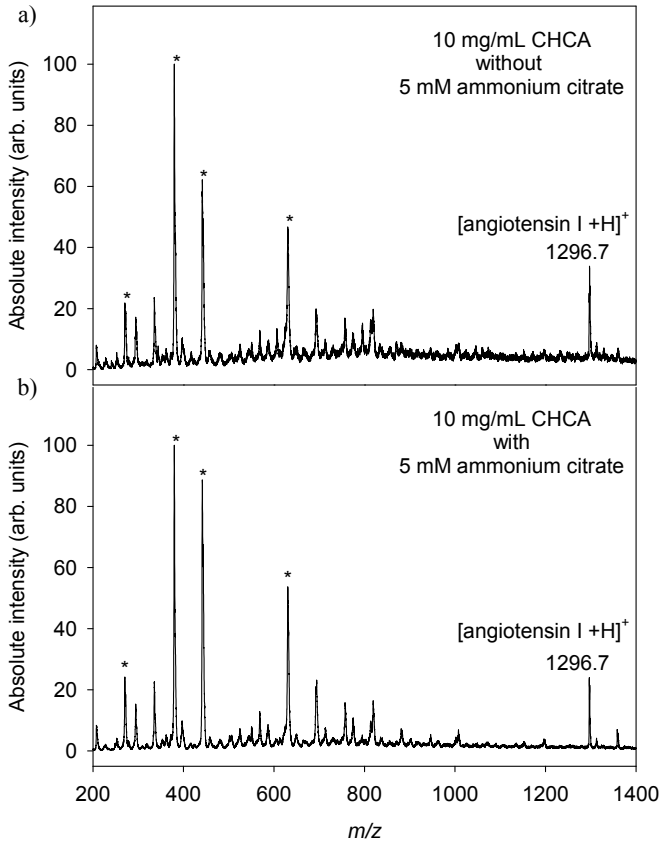

Figure 2.9. AP-MALDI mass spectra of 1 pmol/spot of angiotensin I spotted on a conventional AP-MALDI target. Angiotensin I was co-crystallized with 10 mg/mL CHCA matrix (a) with and (b) without 5 mM ammonium citrate added into the matrix solution.

2.4.3. Comparison of Focusing and Conventional AP-MALDI Targets in Terms of Dynamic Range and Reproducibility

Both types of focusing targets were compared with conventional AP-MALDI targets to determine the dynamic range, spot-to-spot variability and inter-day reproducibility. The observed dynamic range for conventional targets (0.1-5 pmol, Figure 2.10 a) was approximately 5 times larger than for hydrophobic and WCX focusing targets (0.075-0.5 pmol, Figure 2.10b). The signal for hydrophobic and WCX focusing targets was observed to increase at a lower rate after ~0.7 pmol angiotensin I were deposited (Figure 2.10b), suggesting partial saturation of the binding surface. Further loading of

higher volumes of peptide solution (10-20 μL) did not increase the peptide signal in a linear fashion (data not shown).

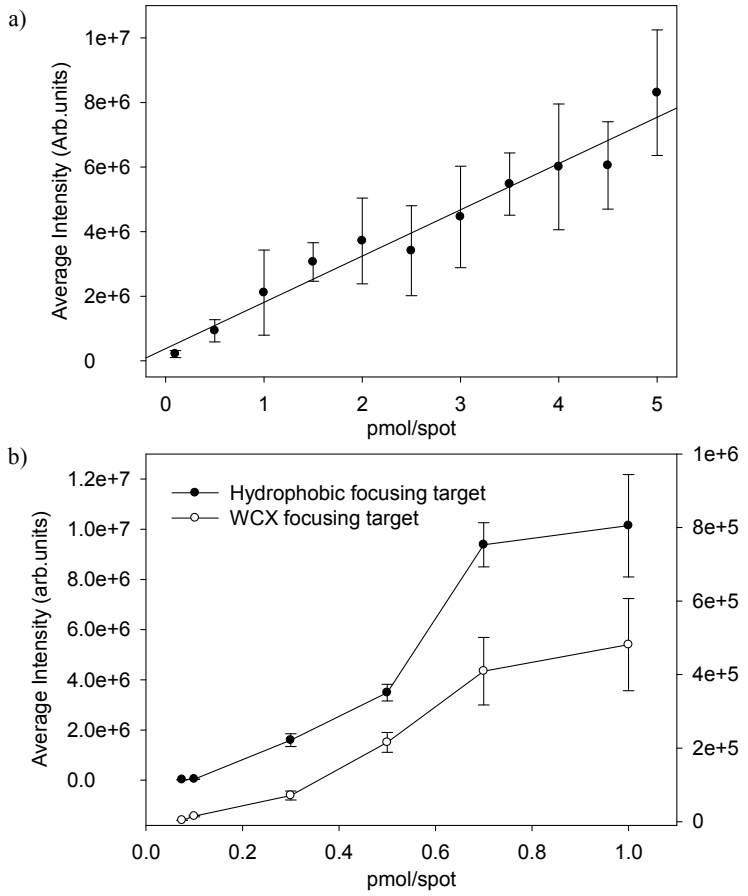

Figure 2.10. Average signal intensity of the protonated angiotensin I ion as a function of the amount of peptide spotted on a (a) conventional AP-MALDI target, and on (b) hydrophobic focusing (y-axis, left) and WCX focusing targets (y-axis, right).

As a result of the more uniform analyte-matrix co-crystallization, the absolute signal variability measured in terms of % CV was comparatively lower for hydrophobic (2%-10%) and WCX (4%-17%) focusing targets than for conventional targets (11%-37%), as shown by the magnitude of the error bars in Figures 2.10 a-b.

a)

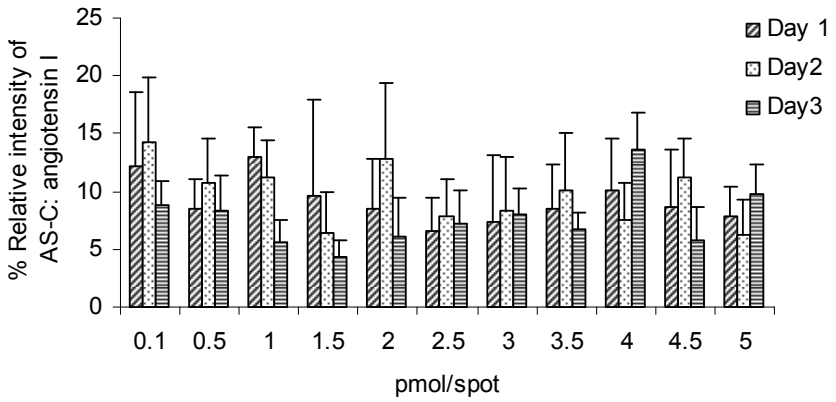

b)

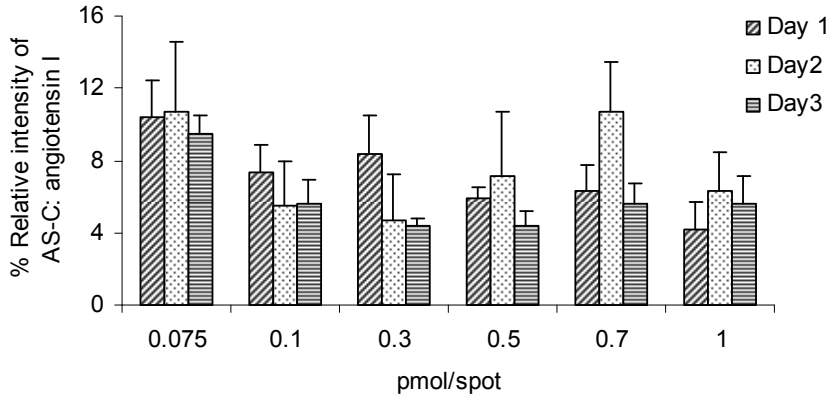

Figure 2.11. Variance in the % relative intensity of allatostatin C (AS-C) with respect to angiotensin I as a function of the total amount of equimolar peptide mixture deposited per spot on (a) conventional AP-MALDI and (b) hydrophobic focusing targets. The inter-day experiments were performed on three separate days.

Reproducibility studies performed for a binary mixture spotted onto conventional (0.1-5 pmol/spot, Figure 2.11a) and hydrophobic (0.075-1 pmol/spot, Figure 2.11b) focusing targets showed % CVs of 25% and 24% for the relative intensity of AS-C respect to angiotensin I, when averaged over 3 days of measurements and the entire concentration range. Overall, the reproducibility for both absolute and relative signal intensities was found to be acceptable for the focusing targets, indicating that the manual operations involved did not significantly add to the variability of the method.

2.4.4. Application of Focusing Targets to the AP-MALDI-IT MS Analysis of Neuropeptides from Aedes aegypti Mosquito Heads

Allatostatins (AS) and allatotropins (AT) are structurally diverse peptides first described as modulators of juvenile hormone biosynthesis in the *corpora allata* of a number of insect species[112-116]. A *corpora allatum* is one of a pair of ganglionic bodies present in the heads of insects. It has been recognized that AS and AT have multiple physiological effects, controlling processes such as heart rate and gut motility, control of nutrient absorption, migratory preparedness, and modulation of circadian cycle[117-121]. Profiling AS-C and AT levels in mosquitoes is therefore critical to further understand the physiological roles of these peptides. However, only a few neuroendocrine cells present in mosquito heads[122] are responsible for all of the AS-C and AT production, which is estimated to be in the 30-50 fmol range per insect[121, 123], thus presenting a challenge in terms of analytical sensitivity.

Initial attempts to analyze mosquito head extracts by AP-MALDI MS using conventional targets were unsuccessful. Therefore, we evaluated the usefulness of on-chip pre-concentration via focusing targets for analyzing mosquito head extracts by AP-MALDI MS. When crude extracts were directly spotted on focusing plates a film was found to form irreversibly on the target surface where the sample was spotted, probably due to irreversible binding of sample components, such as lipids and proteins. This film caused surface fouling resulting in highly increased wettability which translated in evaporation of the solution droplet at rates too high to enable focusing during the elution step. Previous studies by Kanari et. al., have shown that the layer of surface bound water on the hydrophobic SAM stimulates strong protein adsorption[124]. To further prevent surface fouling, a single

pre-purification step via on-tip SPE was used for treating the raw mosquito head extracts prior to on-chip preconcentration and focusing. With this approach, pre-purified mosquito head extracts were observed to focus effectively, yielding AP-MALDI mass spectra with detectable signals (Figure 4). Mass spectra acquired in both wide (4a) and narrow (4b) mass ranges using a hydrophobic focusing target showed peaks at *m/z* 1614.5, 1920.8 and 1936.1, corresponding to protonated AT, and two forms of AS-C, namely, with and without N-terminal glutamine cyclization. These spectra correspond to material extracted from approximately 4 mosquito heads.

When WCX focusing targets were tested, the sample focused without the additional pre-purification step. Figure 4c shows the AP-MALDI mass spectrum corresponding to 3 mosquito heads. Two forms of protonated AS-C ions were observed in this experiment, along with peaks corresponding to unknown species not seen in the mass spectra obtained from hydrophobic focusing targets. This is most likely due to the different binding specificities of the two targets, which can thus be used to obtain complementary information. The peak at *m/z* 1636.8 was assigned to the AT sodium adduct while the peak at *m/z* 1654.8 was attributed to a water cluster with the former ionic species. Being both a hydrophobic and basic peptide (pI > 7), AS-C was also detected on the WCX target (Figure 4c).

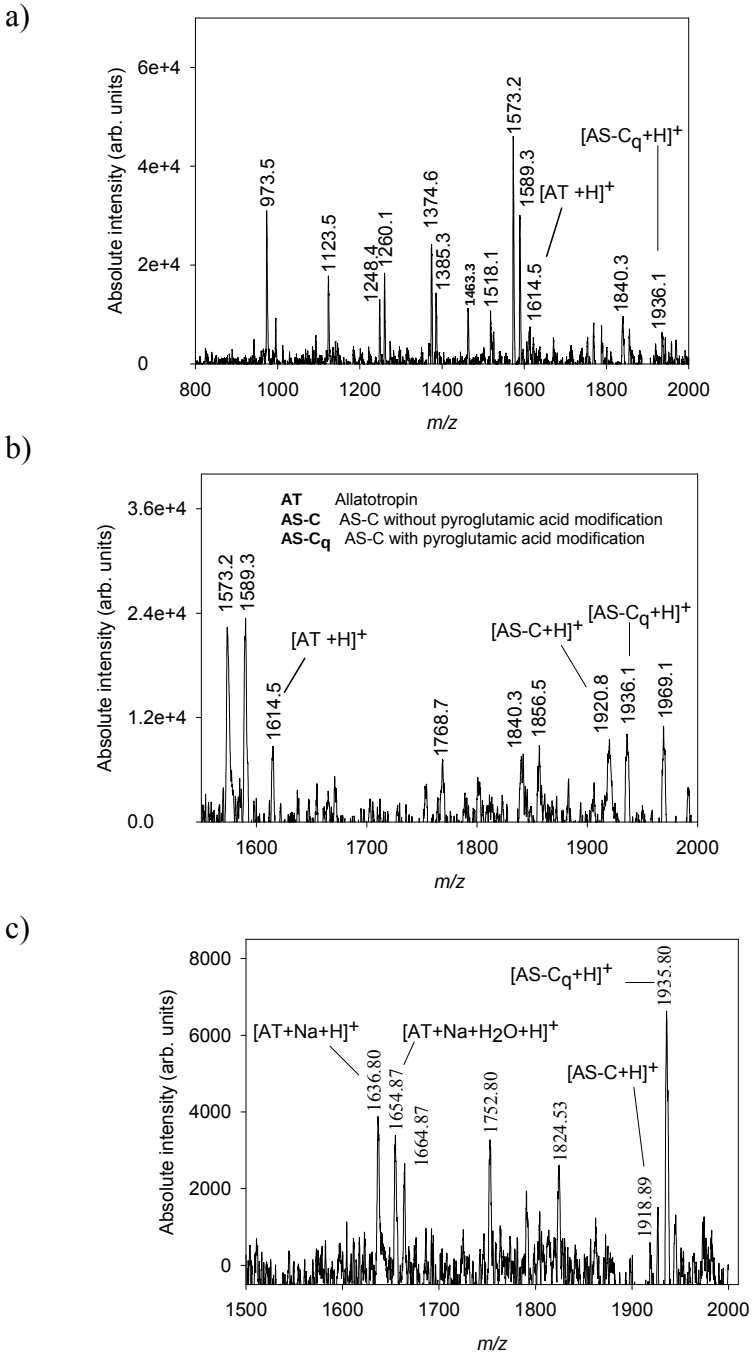

Figure 2.12. AP-MALDI IT mass spectra of desalted and focused mosquito head extracts, using hydrophobic and WCX focusing targets. The amount of extract deposited corresponded to 4 and 3 heads/spot respectively. The mass spectra were acquired in the *m/z* ranges (a) 800-2000 and (b) 1550-2000 for hydrophobic focusing and in *m/z* (c) 1500-2000 for the WCX focusing targets.

Despite the improvements in sensitivity enabled by the use of focusing targets, the observed gains were not sufficient for performing tandem MS experiments. However, it is expected that by coupling of focusing chips and AP-MALDI to a higher trapping capacity mass analyzer such as a linear ion trap, or by performing AP-MALDI analysis with higher repetition rate lasers now available, sensitivity could be further improved to a point where neuropeptide MS/MS would be possible for these challenging samples.

2.4.5. Use of the Focusing Targets for Enhancing Protein Identification by AP-MALDI IT MS

AP-MALDI, when coupled to trapping instruments such as linear or quadrupolar ion traps (IT), is in principle appealing for proteomic and peptidomic experiments, as it could enable multi-stage mass spectrometric (MS^n) analysis in a compact and rather inexpensive platform[125]. However, the difficulty in obtaining good sequence coverage from singly-charged peptide ions by low-energy collision-induced dissociation (CID) as predicted by the mobile proton model[126] limits the applicability of this approach for *de novo* peptide sequencing and protein identification via database searches[127]. In an effort to increase fragment ion yields of singly-protonated MALDI peptides, Keough et al. introduced a derivatization technique based on C-terminal sulfonation followed by lysine guanidination[105, 128]. Addition of a negatively charged group at the C-terminus of tryptic peptides counterbalances the charge of the protonated N-terminal basic amino acid, facilitating charge-directed cleavage of backbone amide bonds by a second, more mobile proton[126]. In AP-MALDI ion trap experiments, peptide derivatives prepared by C-terminal sulfonation have been shown to fragment more extensively than the

corresponding native peptides, generating contiguous y-ion series[129]. However, C-terminal sulfonation further decreases AP-MALDI sensitivity, as two protons are to be transferred from the UV-absorbing matrix to the analytes in order to produce positively-charged ions[128].

As a second demonstration of the sensitivity enhancement that focusing chips afford for AP-MALDI MS, we tested their performance for protein identification using dilute sulfonated tryptic digests of a model protein. Automated data dependent acquisition (DDA) was performed on 2 x 10^{-6} M, 2 x 10^{-7} M, and 2 x 10^{-8} M solutions of a derivatized myoglobin digest. Five μL of each digest dilution were deposited on the hydrophobic focusing target and 0.5 μL on conventional and tuning targets. Figure 2.13a shows a typical full scan AP-MALDI mass spectrum obtained for a 2 x 10^{-8} M derivatized myoglobin digest spotted on a hydrophobic focusing target. The five selected guanidinated-sulfonated peptide precursor ions are denoted by asterisks. Subsequent MS/MS spectra for three of the five pre-selected precursors with protonated precursor ions at *m/z* 1604.8, *m/z* 1497.7, and *m/z* 1790.8 are shown in Figures 2.13b-d. Fragmentation of precursor ions produced guanidinated (gu*) peptide ions $[M\text{-gu*}+H]^+$ by loss of $O_3S\text{-}C_6H_5\text{-}CO$ (184 Da) and a series of high intensity y-ions. It was noted that y-ions smaller than y_5 were not observed for any of the three types of targets.

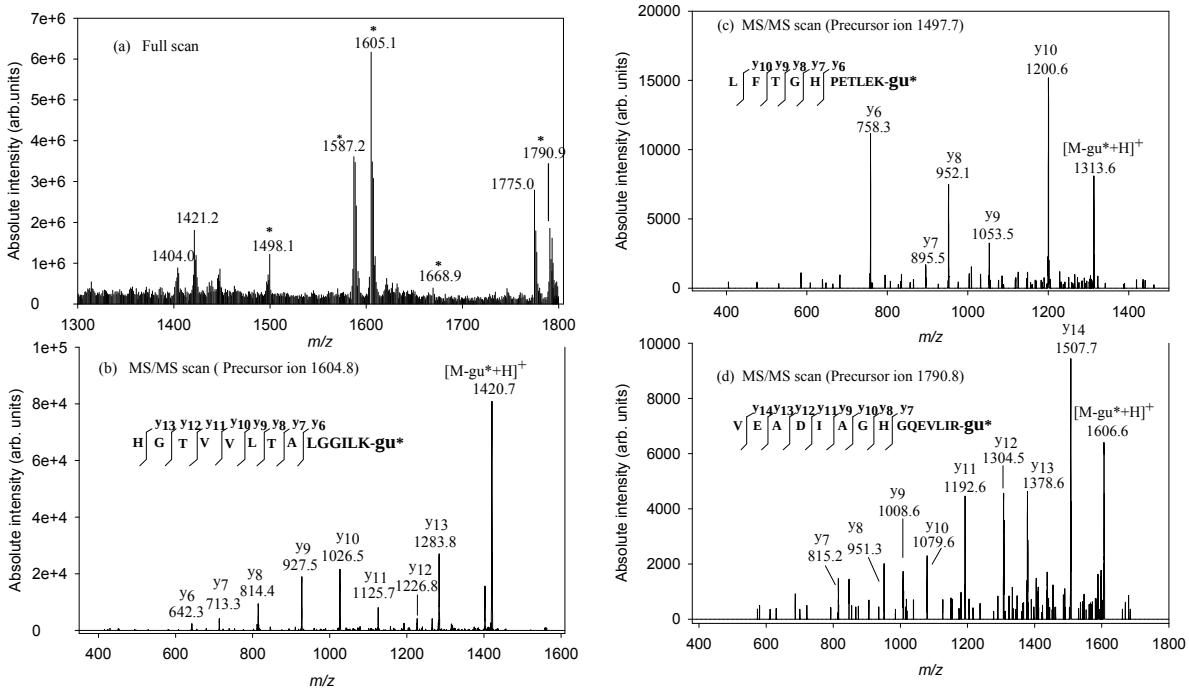

Figure 2.13. Data dependant analysis of the derivatized myoglobin tryptic digest using AP-MALDI IT MS. (a) Full scan AP-MALDI mass spectra obtanined from 100 fmol of the derivatized digest spotted (5 µL) on a hydrophobic focusing target with precursor ions selected for tandem MS marked with asterisks, followed by MS/MS scans of guanidinated and sulfonated precursor ions at *m/z* (b) 1604.8, (c) 1497.7, and (c) 1790.8.

We believe that the second, more mobile proton in these derivatized peptide ions tends to populate carbonyl groups further away from the positively charged guanidinated C-terminus due to charge repulsion[126].This effect, together with the limited energy imparted during ion trap collisional activation, limits the extent of fragmentation. In the case of FTGHPEILEK, fragmentation N-terminal to proline is also favored[128, 130]. No b-ions were observed, as when the charge is retained in the N-terminus, the negatively-charged SO_3 group neutralizes the fragment ion's charge.

Table 2.1. Comparison of PEAKS identification scores for derivatized myoglobin tryptic digests spotted on focusing (hydrophobic), conventional, and tuning targets

Concentration of derivatized digest	Hydrophobic focusing target		Conventional AP-MALDI target		Tuning target	
	Spot 1	*Spot 2*	*Spot 1*	*Spot 2*	*Spot 1*	*Spot 2*
2.10^{-6}M	61	79	56	59	54	33
2.10^{-7}M	55	51	0	0	0	0
2.10^{-8}M	45	30	0	0	0	0

Table 2.1 shows the PEAKS protein identification scores obtained when the AP-MALDI mass spectral data obtained from different substrates and various dilutions was subject to database searching. All three concentrations deposited on the hydrophobic focusing target, with the lowest (2×10^{-8} M) containing 100 fmol digest, yielded the correct protein identification. For conventional and tuning targets, only the highest concentration (2×10^{-6} M) was positively matched. The quality of the MS/MS spectra obtained from lower concentrations was extremely poor (SNR < 3) for conventional and tuning targets. The amounts of digest spotted on these two targets were 100 fmol (0.5 μL, 2×10^{-7} M) and 10 fmol (0.5 μL, 2×10^{-8} M) per spot. As a result, most of the fragment peaks were removed during auto noise filtration by the database search software. Again, these results show that focusing targets improved AP-MALDI sensitivity, increasing the quality of MS/MS spectra and protein identification scores. Additionally, focusing targets enabled shorter acquisition times (2 minutes), which compares favorably to previous reports that used acquisition times of 5-7 minutes[131, 132].

2.5. Conclusions

The results presented here are the first successful demonstration of the implementation of focusing targets with unique surface properties for AP-MALDI experiments. Improvements in sensitivity with S/N gains of approximately 200-900 and 100-430 were obtained for peptide standards using hydrophobic and WCX focusing targets, respectively. The improved sensitivity was a direct consequence of the on-chip preconcentration effect, which enabled to deposit larger sample volumes on the MALDI plate, and the subsequent elution onto tightly focused spots. Coupling the on-chip preconcentration and focusing strategy to AP-MALDI enabled positive identification of sulfonated peptides from nanomolar solutions with higher sensitivity. The new on-chip sample preconcentration and focusing approach not only minimized the number of sample purification steps, but also enhanced AP-MALDI sensitivity for high-throughput MS analysis of various biomolecules, including mosquito neuropeptides. Combination of on-tip SPE pretreatment with the focusing targets allowed successful detection of allatostatin-C and allatotropin neuropeptides in extracts from as low as three mosquito heads. A detail study on the characterization of the on-tip SPE micro-columns is described in the next chapter.

CHAPTER 3. HIGH-THROUGHPUT SAMPLE PURIFICATION BY SOLID-PHASE MICROEXTRACTION WITH PARTICLE-EMBEDDED MICROTIPS FOR MALDI APPLICATIONS

3.1. Abstract

Presented in this chapter is a detailed characterization of an on-tip sample preconcentration approach for application in high-throughput serum profiling by MALDI-MS. The study presents an evaluation of the new class of solid-phase extraction (SPE) pipette tips embedded with different chromatographic media for fractionation of model protein digests and serum samples. The materials embedded include strong anion exchange (SAX), weak cation exchange (WCX), hydrophobic (C4, C8, C18), and immobilized metal affinity chromatography (IMAC), and zirconium dioxide particles. Simple and rapid serum proteome profiling protocols based on these SPE micro tips are described and tested using a variety of MALDI matrices. The effect of different sample pretreatments, such serum dilution and ultrafiltration using molecular weight cut-off membranes, and the reproducibility observed for replicate experiments, are evaluated. The chapter concludes with a discussion of the results obtained from the different types of particle-embedded SPE micro tips and their utility in providing complementary information in terms of spectral features detected for β-casein digests and control human serum samples.

3.2. Introduction

Specific serum biomarker panels are urgently needed in many areas of medicine, particularly in cancer diagnostics. Great effort is thus being directed towards the identification of molecular disease markers with high selectivity and sensitivity, with mass spectrometry (MS) being one of the detection tools of choice. MS-based serum biomarker discovery workflows are based on two main approaches: uni- or bi-dimensional chromatography followed by single stage or tandem MS, which provides high peak capacity; and MALDI-MS or MS/MS without prior fractionation, which provides lower coverage in terms of the maximum number of spectral features that can be detected without spectral overlap, but orders of magnitude higher sample throughput[133].

Serum profiling by MALDI-MS is widely used by medical researchers due to the frequent need for rapid analysis of large quantities of clinical samples[99, 101, 134-141]. In this high-throughput approach, careful bioinformatic comparison of the abundance of proteins and peptides inferred from MALDI mass spectra obtained under standardized conditions enables the multivariate comparison of sample groups, with the aim of identifying proteomic patterns or "fingerprints" that can be used for diagnostic purposes. Despite its unquestionable throughput, MALDI-MS serum proteomic profiling can be negatively affected by the high complexity of serum samples, the presence of interfering salts, and the large dynamic range of protein concentrations, all of which can result in ionization suppression[142] and/or space-charge effects in trapping instruments[143], with the concomitant inability to detect or identify low abundance biomarkers.

In this trend, one of the major challenges in serum proteome profiling is to develop optimal front end sample preparation procedures for removing salts, separating

high abundance protein fractions, and selectively enriching for subsets of serum proteins and peptides (i.e. "subproteomes"), which can be probed in deeper detail than the original sample. A number of techniques have been developed to fractionate serum samples prior to mass spectrometric analysis, including depletion columns for removal of high abundance proteins[144-147], ultrafiltration with different molecular weight cut-off membranes[96, 97], solid-phase extraction (SPE) columns[70], coated magnetic beads[148] and precipitation by organic solvents[149]. The biggest challenge for users of these techniques is to obtain high-enough day-to-day and batch-to-batch reproducibility to correctly evaluate biologically significant differences within the bewildering number of mass spectral features detected[70, 101, 145].

One of the most popular tools for high-throughput serum profiling in the biomedical community is surface-enhanced laser desorption/ionization (SELDI)-MS, a MALDI-based technique which integrates on-target sample preparation with time-of-flight (TOF) MS peptide/protein ion detection[150]. Unique to this method are functionalized MALDI targets with specific SPE or affinity-capture properties[76]. Interest in this technique was sparked by early work by Liotta and coworkers which exploited the potential of SELDI-TOF MS combined with sophisticated bioinformatics algorithms for ovarian cancer diagnostics[151, 152]. Other research groups also applied this SELDI approach, further demonstrating the utility of applying specific surface chemistries for serum proteome partitioning, one of the most promising being strong cation exchange functionalized targets[153]. However, SELDI TOF mass spectrometers offer limited resolving power, mass accuracy and tandem MS capabilities, making biomarker identification difficult. In addition, there have been questions regarding the long term

stability of SELDI experiments. Difficulties in baseline correction, irreproducibility in sample preparation protocols, and unstable TOF mass calibration have been reported[154]. More recently, in-source collision-induced dissociation has been suggested to be the origin of much of the structure uncovered by SELDI[155].

As an alternative to SELDI, many groups have been investigating functionalized MALDI targets that can be used across many MALDI-TOF MS platforms for on-chip sample fractionation[156, 157]. Another popular option is the combination of off-line serum fractionation protocols with MALDI MS, which have the advantage of decoupling sample preparation from mass analysis, thus allowing the optimization of those two steps separately[70, 158]. Both the on-chip and off-line methodologies share the advantage of not relying on proprietary MALDI instrumentation, and can thus be implemented in combination with a variety of high-end MALDI MS or MS^n spectrometers. Such a combinatorial approach as described in Chapter 2 has allowed for successful detection and profiling of mosquito neuropeptides by AP-MALDI, by combining on-chip sample preconcentration using focusing targets with offline fractionation using a new class of reverse-phase SPE micro tips.

In this work, we further evaluate the performance of these particle-embedded SPE pipette micro tips, in which the inner plastic walls are covered with chromatographic particles with different functionalities, such as strong anion exchange (SAX), weak cation exchange (WCX), hydrophobic (C18, C8, C4), ZrO_2, and immobilized metal affinity chromatography (IMAC). We first present a detailed characterization of these SPE micro tips using tryptic digests of a standard protein, and then extend these studies to human serum for fractionation of low mass proteins and peptides.

3.3. Experimental

3.3.1. Chemicals

Trifluoroacetic acid (TFA), ammonium hydroxide and formic acid were obtained from Fisher Scientific (Fair Lawn, NJ, USA), acetonitrile (ACN) was from EMD Chemicals (Gibbstown, NJ, USA), nickel (II) chloride and gallium (III) nitrate hydrate were from Alfa Aesar (Ward Hill, MA, USA). Healthy human serum (stock No. S7023-50ML), ammonium citrate, β-casein, trypsin (proteomics grade), ammonium bicarbonate, α-cyano-4-hydroxycinnamic acid (CHCA), 2,5-dihydroxybenzoic acid (DHB), sinapinic acid and indoleacrylic acid (IAA) were from Sigma-Aldrich (St. Louise, MO, USA). Microcon ultrafiltration 3 kDa and 50 kDa cut-off membranes were purchased from Millipore (Bedford, MA, USA). NuTip particle-embedded pipette micro tips (1-10 µl) were obtained from Glygen Corp. (Columbia, MD, USA). All aqueous solutions were prepared with nanopure water from a Nanopure Diamond laboratory water system (Barnstead International, Dubuque, Iowa, USA).

3.3.2. In-solution Tryptic Digestion of β-casein

A (2.4 µg/µL) solution of β-casein was prepared in 6 M urea containing 50 mM ammonium bicarbonate and separated into 20 µL aliquots, which were first heated for 1 h at 65°C. After cooling, 180 µL of 50 mM ammonium bicarbonate were added to each aliquot followed by addition of 48 µL of trypsin working solution (20 µg/mL) and the mixtures were incubated in a water bath for 20 h at 38°C. One aliquot was then basified by adding approximately 6 µL of 20 mM NH_4Cl/NH_3 aqueous buffer (pH 8.5) and the remaining aliquot was acidified using 2% TFA solution to a final pH of approximately

2.0. Purification and concentration of the acidified and basified digest aliquots was achieved by using SPE micro tips containing different chromatographic media as described below.

In-silico tryptic digestion was performed with ProteinProspector{, #262}. Variable modifications namely, methionine oxidation (Met-Ox), phosphorylation at serine, threonine, tyrosine residues (denoted as s,t, and y, respectively), and carbamylation of lysine and arginine were selected. The total number of theoretically generated peptides was 225 as a result of combinations of the variable post-translational modifications. Each peptide thus generated was then characterized for its hydropathy using an online tool{, #261} based on the Hopps-Woods scale[111]. In this process, a line plot is generated for each peptide by averaging hydrophobicity values assigned to sequential amino acids in windows of 5 residues. If the obtained hydrophobicity line was predominantly above zero, the corresponding peptide was considered hydrophilic and vice versa. Terms such as 'predominantly' or 'partially' hydrophilic/hydrophobic are used if a significant part of the line lies above or below zero respectively.

3.3.3. Serum Sample Pretreatment Prior to SPE

The serum sample pretreatment and subsequent fractionations using various SPE micro-tips were performed by Dr. Manshui Zhou, a former post-doctoral fellow in the Fernández group. Immediately upon arrival from the vendor, the frozen serum sample was thawed, aliquoted into 1.5 mL Safe-Lock Eppendorf micro test tubes and frozen at -80°C until further use. All measurements were performed on identical 500-µL aliquots of twice-thawed serum. Prior to SPE, the serum was denatured by adding 25 µL of 80%

ACN to 200 µL of sample to disrupt intermolecular interactions. The mixture was then vortexed, and incubated for 30 minutes at ambient temperature (22-25°C). Microcon membranes (50 kDa cut-off) were rinsed three times with 0.2 ml deionized water, and used to filter 240 µL of the denatured serum mixture at 13,000g for 25 minutes. A 120-µL aliquot of the filtrate was acidified by addition of 30 µL of 2% TFA solution to a final pH of ~2.0. Similarly, a second 120-µL serum filtrate was basified to pH ~8.5 by addition of dilute NH_4Cl/NH_3 aqueous buffer. The acidified and basified serum filtrate aliquots were treated with SPE micro tips as described below.

I. Procedure for SPE via Hydrophobic (C18, C8, C4) NuTips

C18, C8 and C4 NuTips were washed with 5×4 µL (5 times, 4 µL each time) of 50% ACN, and equilibrated with 3×4 µL of 0.1% TFA solution. Then, 30×4 µL of β-casein protein digest or acidified serum filtrate were aspirated and expelled through the tip. The tip was then washed with 2×4 µL of 0.1% TFA solution. Retained components were eluted with 2 µL of 50% ACN / 0.1% TFA. The elunt was pipetted up and down 10 times in a clean vial to ensure complete elution.

II. Procedure for SPE via Ion-Exchange NuTips

Silica Strong Anion-Exchange (SAX): SAX NuTips were conditioned with 5×4 µL of 50% ACN, and equilibrated with 3×4 µL of 20 mM NH_4Cl/NH_3 aqueous buffer (pH 8.5). Then, 30×4 µL of β-casein protein digest or basified serum filtrate were aspirated and expelled through the tip. The tip was then washed with 2×4 µL of deionized water. Retained components were eluted with 2 µL of 0.5% TFA / 20% ACN, as described above for C18 tips.

Poly(aspartic acid)-silica(polyCAT A) Weak Cation-Exchange (WCX): WCX NuTips were first washed with 5×4 µL of 50% ACN, and equilibrated with 3×4 µL of 0.1% TFA solution. 30×4 µL of acidified of β-casein protein digest or serum filtrate were sequentially aspirated and expelled through the tip. The tip was then washed with 2×4 µL of deionized water, and elution of the retained peptides was performed with 2 µL of 2% aqueous ammonia solution containing 20% ACN.

III. Procedure for SPE via IMAC NuTips

IMAC-Ga (III) and IMAC-Ni (II) NuTips were metal loaded with 10×4 µL of 200 mM $Ga(NO_3)_3$ and $NiCl_2$ aqueous solutions respectively, followed by washing with 3×4 µL of dH_2O. Tip equilibration was performed with 3×4 µL of 1% acetic acid / 10% ACN and with 5×4 µL of 0.1% acetic acid / 10% ACN respectively. Then 30×4 µL of the acidified protein digest or serum filtrate were aspirated and expelled through the micro tips. Washing was done with 2×4 µL of deionized water, followed by elution with 2 µL of 2% aqueous ammonia solution containing 20% ACN by aspirating up and down (10 times) into a clean vial.

IV. Procedure for SPE via ZrO_2 NuTips

ZrO_2 NuTips were first washed with 10×4 µL of 0.33% formic acid. Then, 30×4 µL of acidified serum filtrate or digest aliquot were aspirated / expelled, the tips were washed with 2×4 µL of deionized water, and the retained species were eluted with 2 µL of 2% aqueous ammonia solution containing 20% ACN.

The eluate obtained from different NuTips was mixed in a 1:1 v/v ratio with 10 mg/mL CHCA solution in 50% ACN / 0.1% TFA. One µL of this mixture was spotted on a stainless steel MALDI plate. The CHCA matrix solution (10 mg/mL) used to

co-crystallize with IMAC and ZrO_2 eluates was prepared in 50% ACN / 0.4% acetic acid / 10 mM ammonium citrate.

3.3.4. MALDI-MS

MALDI-TOF MS analyses were performed using a Voyager DE-STR (Applied Biosystems, Framingham, MA) MALDI-TOF mass spectrometer equipped with a nitrogen laser (337 nm, 3 ns pulse width). All experiments were carried out in positive ion mode. All mass spectra were acquired in linear mode with 25 kV acceleration voltage, 92.8% grid voltage and 300 ns extraction delay. In all cases, 240 laser shots were averaged for each mass spectrum. The instrument was externally calibrated prior to running any samples using angiotensin II $[M+H]^+$=1046.54, ACTH (18-39) $[M+H]^+$= 2464.12, insulin chain β $[M+H]^+$=3494.65, bovine insulin $[M+H]^+$=5730.61, and cytochrome C $[M+H]^+$=12361.96. All spectra were baseline corrected, and smoothed prior to exporting them as ASCII files.

3.4. Results and Discussion

3.4.1. MALDI Matrix Selection

The choice of a suitable MALDI matrix, sample-matrix preparation procedure, and the composition of the MALDI matrix solution greatly influence the quality of MALDI mass spectra of biopolymers[161, 162]. Various properties of matrix molecules such as their ability to induce analyte fragmentation, ionization potential, and proton affinity are some of the determinants of MALDI matrix suitability. Additionally, it is demonstrated that proteins co-crystallize with the matrix based on their amphiphilic

nature, i.e. the hydrophobic portions of the protein become associated with the relatively hydrophobic crystal faces of the matrix crystals.[163] A suitable matrix for one type of compound may not be optimal for others, and hence matrix selection for a particular application is typically determined by comparing the experimentally observed performances of the different matrixes under similar experimental conditions[164]. We performed preliminary experiments to determine a suitable MALDI matrix using four compounds, namely, α-cyano-4-hydroxycinnamic acid (CHCA), 2,5-dihydroxybenzoic acid (DHB), sinapinic acid and indoleacrylic acid (IAA). The results showed that CHCA, DHB and IAA showed high intensity signals for peptides below *m/z* 4000 as compared to sinnapinic acid, which showed better performance for analyzing larger peptides or proteins (Figures 3.1a-d). However, CHCA outperformed DHB and IAA in terms of observed signal-to-noise (S/N) ratio and therefore CHCA was chosen as the MALDI matrix for all subsequent experiments.

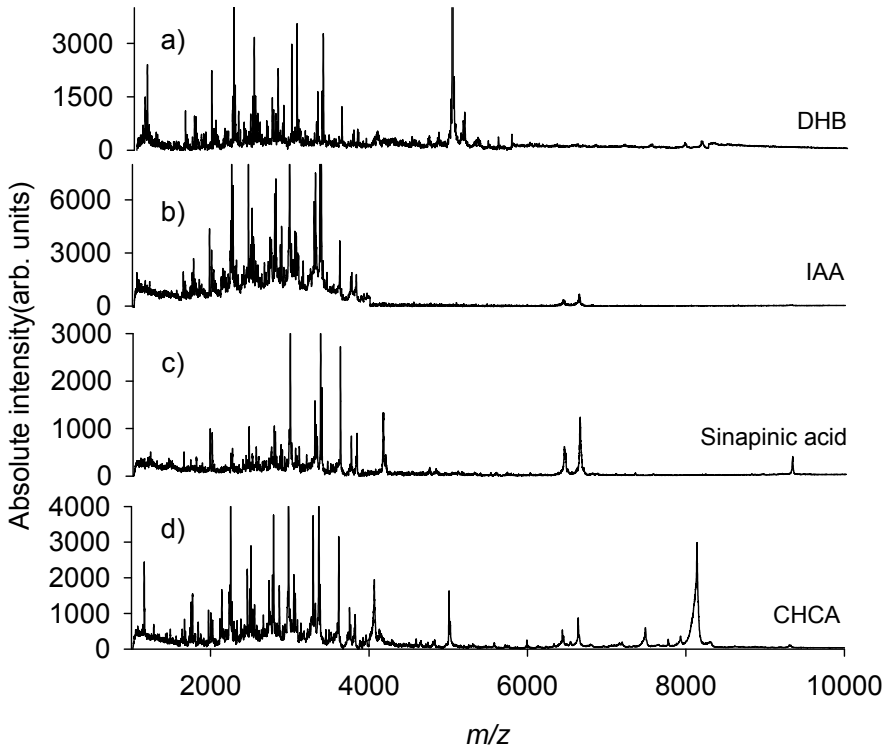

Figure 3.1. MALDI-MS mass spectra of a control serum sample fractionated using C18 micro tips and co-crystallized with various MALDI matrices including (a) DHB, (b) IAA, (c) sinnapinic acid, and (d) CHCA.

3.4.2. Selectivity Study of Different SPE Micro Tips Using a Model Protein Digest

A comparison of β-casein tryptic digest fractionation using particle-embedded micro tips coated with eight different materials (Figures 3.2a-e) revealed the extent to which each support selectively enriched various peptide fractions. The left panel shows the 700 to 2000 *m/z* range and the right panel, the 2000-3400 *m/z* range. Figures 3.2a, 3.2b and 3.2c show the MALDI spectra of digests treated with C4, C8 and C18 hydrophobic SPE micro tips respectively. Peaks corresponding to predominantly hydrophobic or hydrophilic peptides are denoted by filled or empty squares. A detailed list of the peptides identified, along with their respective degrees of hydropathy is given in Table 3.1.

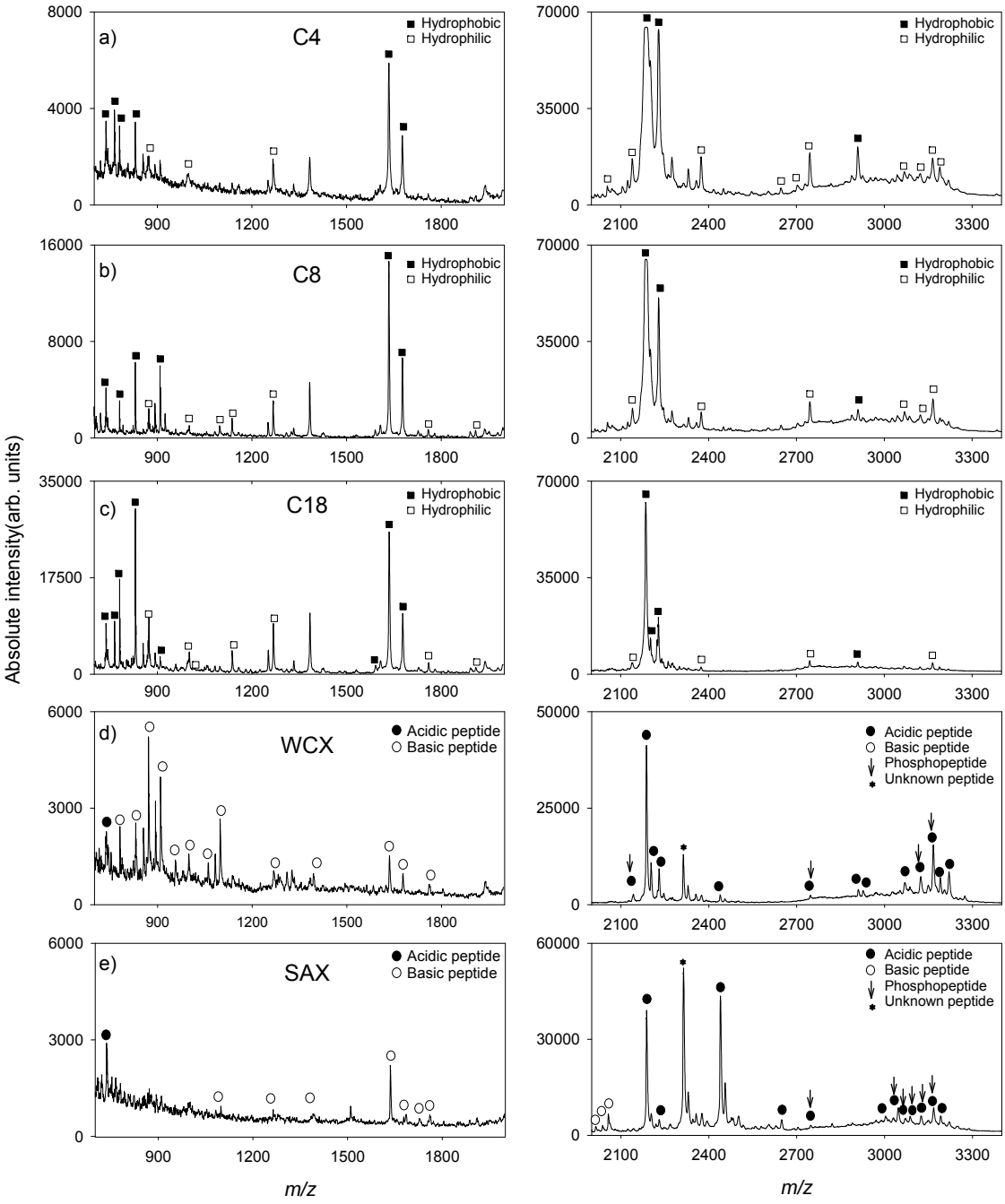

Figure 3.2. MALDI-TOF mass spectra of β-casein tryptic digest fractionated with (a) C4, (b) C8, (c) C18, (d) WCX, and (e) SAX SPE micro tips, in the mass ranges of *m/z* 700-2000 (left panel) and *m/z* 2000-4000 (right panel). Hydrophobic and hydrophilic peptides are denoted by filled and empty squares respectively in (a), (b) and (c). Acidic peptides (pI < 7) and basic peptides (pI > 7) are denoted by filled and empty circles respectively, in (d) and (e). Phosphopeptides in (d) and (e) right panels are marked by vertical arrows.

Table 3.1. List of hydrophobic and hydrophilic peptides retained by C4, C8 and C18 SPE micro tips and corresponding signal-to-noise (S/N) ratios. Peptides detected as their water and salt adducts are marked by asterisks. All other peptides were detected as protonated ions. The following modifications were considered: oxidation of methionine(Met-Ox), carbamylation of lysine and arginine (Carm), and phosphorylation of serine (s), threonine (t) and tyrosine (y).

m/z	Peptide	Modifications	Hydropathy	C4	C8	C18
742	GPFPIIV		Hydrophobic	1.7	2.8	4.1
762	EMPFPK	1-Met-Ox	Hydrophobic	2.8	0.9	7.2
780	VLPVPQK		Hydrophobic	2.6	6.4	14.0
830	AVPYPQR		Predominantly Hydrophobic	4.1	12.7	22.6
873	VKEAMAPK		Hydrophilic	1.75	5.0	8.0
910	AVPyPQR		Hydrophilic	1.0	8.0	11.2
1001	INKKIEK	3 Carm	Hydrophilic	2.0	2.6	7.5
1099	HKEAMPFPK	2 Carm	Hydrophilic	-	3.6	4.0
1138	VKEAMAPKHK		Hydrophilic	1.6	9.3	15.6
1267	VKEAMAPKHK	3 Carm	Hydrophilic	3.3	13.1	28.5
1592	VLPVPQKAVPYPQR		Predominantly Hydrophobic	-	-	7.4
1634	VLPVPQKAVPYPQR	1 Carm	Predominantly Hydrophobic	16.7	29.7	46.7
1678	VLPVPQKAVPYPQR	2 Carm	Predominantly Hydrophobic	8.7	14.9	9.3
1760*	EAMPKHKEMPFPK	1 Met-Ox,2 Carm	Hydrophobic	-	-	14.8
1910	VKEAMAPKHKEMPFPK	1 Carm	Hydrophilic	-	8.8	6.7
2141	FQsEEQQQtEDELQDK		Hydrophilic	6.4	5.6	4.1
2186	DMPIQAFLLYQEPVLGPVR		Hydrophobic	24.9	18.7	28.0
2202	DMPIQAFLLYQEPVLGPVR	1 Met-Ox	Hydrophobic	20.0	7.3	7.5
2229	DMPIQAFLLYQEPVLGPVR	1 Carm	Hydrophobic	28.9	11.3	4.6
2375*	IEKFQSEEQQQTEDELQDK		Hydrophilic	5.5	2.7	2.4
2646	ELEELNVPGEIVESLSSSEESITR		Hydrophilic	3.0	-	-
2703*	ELEELNVPGEIVESLSSSEESITR		Hydrophilic	2.1	-	-
2746*	KIEKFQsEEQQQtEDELQDK	1 Carm	Hydrophilic	3.6	2.5	2.5
2909	DMPIQAFLLYQEPVLGPVRGPFPIIV		Hydrophobic	5.0	1.8	1.7
3044	ELEELNVPGEIVESLSSSEESITR	1 Carm	Hydrophilic	3.8	-	-
3068*	ELEELNVPGEIVEsLsssEESItR		Hydrophilic	2.0	1.7	1.0
3168	INKKIEKFQsEEQQQtEDELQDK	4 Carm	Hydrophilic	2.3	3.0	2.6
3190*	ELEELNVPGEIVESLSSSEESITRINKK	1 Carm	Hydrophilic	2.4	-	-

Table 3.2. List of β-casein tryptic peptides retained by WCX, SAX, IMAC-Ga, IMAC-Ni and ZrO_2 micro tips and corresponding S/N. Peptides detected as their water and salt adducts are marked by an asterisks.

m/z	Peptides	Modifications	pI	WCX	SAX	IMAC-Ga	IMAC-Ni	ZrO_2
742	GPFPIIV		6.0	1.6	3.3	2.8	2.2	12.3
780	VLPVPQK		10.1	2.3	-	-	-	3.3
872	INKKIEK		9.8	3.2	-	3.0	2.8	9.4
910	AVPyPQR		9.9	7.0	-	2.5	-	3.4
1001	INKKIEK	3 Carm	10.3	2.2	-	-	-	4.7
1056	HKEAMPFPK	1 Carm	9.9	3.2	-	-	-	4.3
1099	HKEAMPFPK	2 Carm	9.9	5.2	2.0	-	-	-
1267	VKEAMAPKHK	3 Carm	10.3	3.0	2.5	8.2	5.2	6.1
1634	VLPVPQKAVPYPQR	1 Carm	10.4	8.6	10.6	10.3	12.2	28.7
1678	VLPVPQKAVPYPQR	2 Carm	10.4	3.0	-	5.2	6.2	15.3
1683	EAMPKHKEMPFPK	1 Carm	9.8	-	3.2	-	-	-
1726	EAMPKHKEMPFPK	2 Carm	9.8	-	4.1	-	-	-
1728*	VLPVPQKAVPyPQR		10.4	-	-	-	-	3.5
1760*	EAMPKHKEMPFPK	1 Met-Ox, 2 Carm	9.8	4.7	5.7	-	-	9.2
2013	VKEAMPKHKEMPFPK	1 Met-Ox, 3 Carm	10.2	-	3.6	-	-	-
2040	VKEAMPKHKEMPFPK	4 Carm	10.2	-	3.0	-	-	-
2056	VKEAMPKHKEMPFPK	1 Met-Ox, 4 Carm	10.2	-	7.2	-	-	-
2061	FQSEEQQQTEDELQDK		3.4	-	-	8.7	-	4.3
2141	FQsEEQQQtEDELQDK		3.4	4.0	-	8.5	5.0	12.8
2186	DMPIQAFLLYQEPVLGPVR		4.1	22.8	21.3	17.8	16.4	10.3
2202	DMPIQAFLLYQEPVLGPVR	1 Met-Ox	4.1	7.3	3.7	12.1	14.2	8.2
2229	DMPIQAFLLYQEPVLGPVR	1 Carm	4.1	6.2	2.1	5.0	5.6	15.2
2266	DMPIQAFLLyQEPVLGPVR		4.1	-	-	-	-	3.2
2438	IEKFQSEEQQQTEDELQDK	2 Carm	3.7	-	18.5	-	-	-
2747*	KIEKFQsEEQQQtEDELQDK	1 Carm	4.0	1.7	2.0	4.2	3.0	6.5
2909	DMPIQAFLLYQEPVLGPVRGPFPIIV		4.4	2.3	-	1.5	1.6	2.3
2926	DMPIQAFLLYQEPVLGPVRGPFPIIV	1 Met-Ox	4.4	2.2	-	1.3	1.0	-
2966	ELEELNVPGEIVEsLsssEESITR		3.5	-	-	-	1.8	2.0
3001	ELEELNVPGEIVESLSSSEESITRINK		3.9	-	3.1	-	-	-
3004	DMPIQAFLLyQEPVLGPVR		4.4	-	-	1.5	-	-
3046	ELEELNVPGEIVESLsssEEsItR		3.5	-	2.0	2.5	2.8	2.3
3068*	ELEELNVPGEIVEsLsssEESItR		3.5	-	2.0	1.7	2.5	1.5
3087	INKKIEKFQsEEQQQTEDELQDK	4 Carm	4.3	2.5	1.8	1.5	1.9	1.3
3124	ELEELNVPGEIVEsLSSSEESITRINK	1 Carm	4.3	1.7	3.2	-	3.5	1.4
3168	INKKIEKFQsEEQQQtEDELQDK	4 Carm	4.3	5.2	4.0	-	6.5	2.5
3190*	ELEELNVPGEIVESLSSSEESITRINKK	1 Carm	4.1	-	3.5	-	-	-
3204	ELEELNVPGEIVEsLsSSEESITRINK	1 Carm	3.9	-	-	1.5	2.2	1.3

The most intense peaks in Figures 3.2a-c corresponded to hydrophobic peptides at *m/z* 780, 873, 2186, 2202, 2229, and 2909 and to predominantly hydrophobic peptides at *m/z* 830, 1634, and 1678. A set of less intense peaks corresponding to hydrophilic peptides was detected at *m/z* 1267, 907 ($[M+H_2O+H]^+$ of VKEAMAPK, 1 Met-Ox), and at *m/z* 2375 ($[M+Na]^+$ of IEKFQSEEQQQTEDELQDK) with lower S/N ratio. Out of the 225 theoretical peptides generated in this tryptic digest, only 22% are hydrophobic, mostly found in the *m/z* < 1000 range and the remainder, which are more hydrophilic, are predominantly present in the higher *m/z* range. The binding of hydrophilic peptides to hydrophobic SPE micro tips is thus explained by their higher relative abundance in the initial tryptic mixture. S/N ratios of the detected hydrophilic peptides were lower than for the hydrophobic peptides in both the higher and lower mass ranges as a result of the hydrophobic nature of SPE micro columns. Overall, inspection of the mass spectra of hydrophobic SPE eluates showed that the performance of C18 micro tips was superior in the lower *m/z* range, both in terms of sensitivity, reflected in the higher S/N ratios and number of peaks observed. In the higher *m/z* range, the MALDI mass spectrum of the C4 eluate showed more spectral features and higher intensity peaks when compared to the MALDI spectra of C8 and C18 eluates. The observed mass spectral patterns reflect the effects of the different chain lengths in each of the three materials. The shorter chain length in C4 makes it less hydrophobic and larger peptides are thus more likely to expose sufficiently-large hydrophobic regions to efficiently interact with this material. The MALDI spectra shown in Figures 3.2d and 3.2e correspond to WCX and SAX eluates. Peaks corresponding to acidic or basic peptide are denoted by filled and empty circles, respectively. Theoretically, WCX materials should first retain mostly basic peptides with

a net positive charge at the lower pH used for binding, and SAX material should bind acidic peptides with a net negative charge at the basic pH used. Clear differences are observed between these materials in both *m/z* ranges providing complementary information from the same protein digest. A detailed list of acidic and basic peptides identified in the WCX and SAX eluate mass spectra is presented in Table 3.2. In the low *m/z* range, the WCX eluate showed many peaks corresponding to eight peptides and their various modifications. One acidic peptide at *m/z* 742.4 (pI 6) and several basic peptides with their pI values in the 9-10.5 range were observed. The spectrum from the SAX eluate in this *m/z* range showed a signal corresponding to one acidic peptide, at *m/z* 742, and weak signals corresponding to carbamylated peptides at *m/z* 1099, 1267, 1634, 1678, 1683, 1726, and 1760. It has been suggested that carbamylation lowers peptide isoelectric points, providing a possible explanation for the partial retention of these peptides by the SAX micro tip[165]. The acidic peptide at *m/z* 742 (pI 6) was seen in the mass spectra of both WCX and SAX eluates, as the net charge on this peptide shifts upon changes in the pH of the binding buffers used in either extraction and hence it will bear a net positive change in the acidic binding buffer (pH 2) used for WCX and a net negative charge in the basic binding buffer (pH 8.5) used for SAX SPE. The peak intensity and S/N ratio corresponding to this peptide were higher in the SAX eluate mass spectrum in accordance to its predominantly acidic character, whereas the carbamylated peptides at *m/z* 1099, 1267, 1678, 1683 and 1670, retained by the SAX and WCX micro tips, showed higher intensity peaks in the latter due to their more basic nature (pI>7).

In the higher *m/z* range, the WCX eluate produced signals corresponding to peptides with an average pI value of 3.9 (*m/z* 2141, 2186, 2202 and 2229), higher than the

pH to which the binding solution was adjusted (pH 2.0), making these peptides positively charged. The SAX spectrum (Fig 3.2e, right panel) showed intense peaks corresponding to mostly carbamylated peptides such as at *m/z* 2056 (1 Met-Ox, 4 Carm), *m/z* 2013 (3 Carm), 2438 (2 Carm, pI 3.7), and 3168 (4 Carm). A comparison of WCX and SAX eluates in the higher mass range (Figures 3.2d-e) showed that peaks corresponding to acidic peptides (pI < 7) were more intense with higher S/N ratios in the mass spectrum of the SAX eluate. A few peaks corresponding to phophorylated peptides at *m/z* 2747 ($[M+H_2O+K]^+$, 3 Carm), *m/z* 3046, 3068, 3087 (4 Carm), 3124 (1 Carm), and at *m/z* 3168 (4 Carm) were also detected. Retention of phosphopeptides by the SAX column is expected due to electrostatic interactions with the negatively charged phosphate groups. Only four phosphopeptides at *m/z* 2141, 2747, 3124 and 3168 were also retained by WCX micro tip with comparable peak intensities, as these peptides are positively charged at the acidic binding pH.

A comparative analysis of the MALDI spectra of eluates purified by hydrophobic and ion exchange SPE micro tips further illustrates the binding specificity of these materials. Hydrophilic peptides of basic nature, such as INKKIEK (*m/z* 872) and its carbamylated form at *m/z* 958, HKEMPFPK (*m/z* 1099, 2 Carm and *m/z* 1082 with loss of ammonia), VKEAMAPKHKEMPFPK (*m/z* 2056, 1 Met-Ox, 4 Carm) were observed in the WCX eluate mass spectra, but not in eluates from hydrophobic micro tips. Hydrophobic peptides retained by the C18, C8 and C4 SPE micro columns showed intense peaks at *m/z* 780, 830, 1634, 2186, and 2229 but their peak intensities were significantly lower in the WCX eluate mass spectrum with lower S/N ratios. Hydrophilic, acidic peptides (pI < 7) were seen in the mass spectrum of SAX eluate at *m/z* 2062 (pI

3.4), 2438 (pI 3.7), 2395 (pI 3.7), 2518 (pI 3.7), and were absent in the mass spectra of eluates from hydrophobic materials

In addition to SPE and ion exchange, affinity enrichment of phosphopeptides is becoming an increasingly important tool in proteomic science and biomarker discovery, as protein phosphorylation plays a crucial role in a number of biological processes[166, 167]. Metals such as Ga (III), Ni (II), and Zr (IV) form complexes by coordination of the phosphate group with the zirconium electrophilic metal center. Porous ZrO_2 surfaces also contain hydroxyl groups, and Lewis acid and base sites located on the Zr cation, and coordinatively unsaturated oxygen, respectively[168, 169]. Zirconia has recently drawn significant attention as a promising separation material due to its higher thermal stability, wider operational pH range[170], and improved selectivity towards phosphopeptides when compared to IMAC materials such as TiO_2[171]. Figures 3.3a-.3c show MALDI-MS spectra obtained for eluates from the IMAC-Ni, IMAC-Ga and ZrO_2 SPE micro tips, respectively. A detailed list of phosphopeptides retained by IMAC and ZrO_2 materials is shown in Table 3.2. For completion, phosphopeptides retained by SAX and WCX microtips are also included in this table.

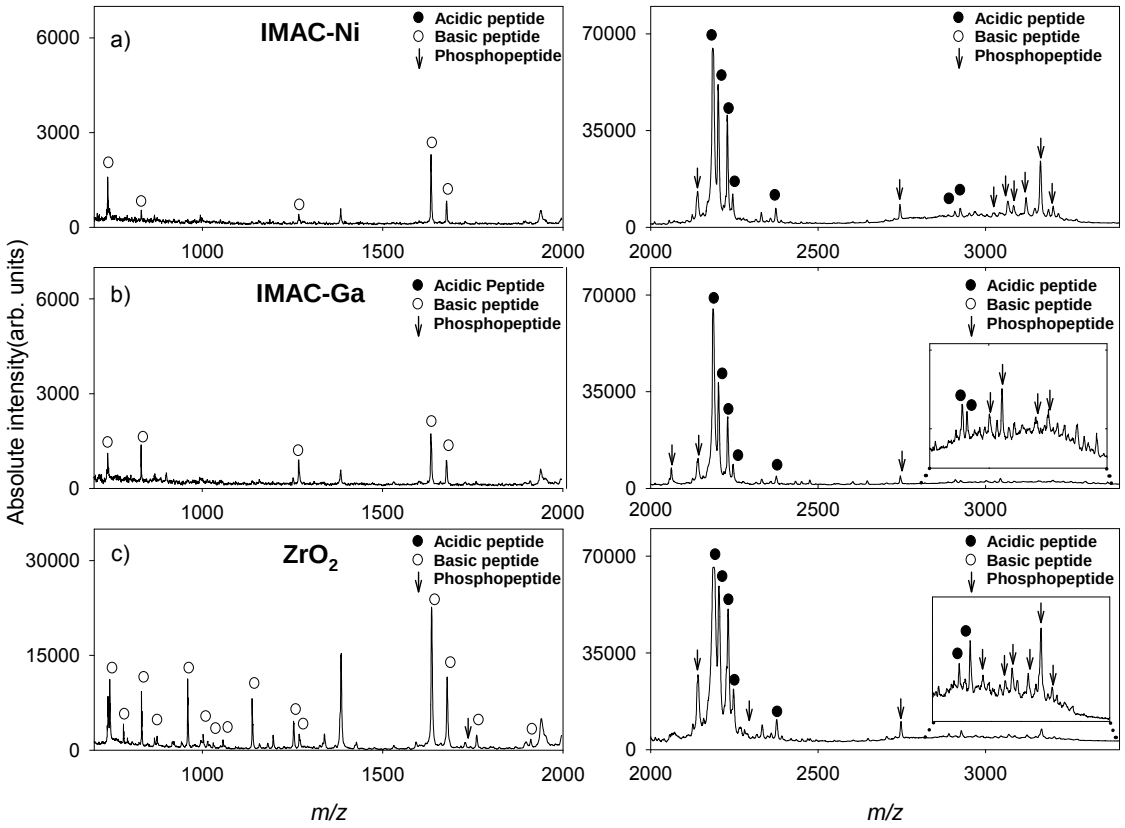

Figure 3.3. MALDI mass spectra of b-casein tryptic digest treated with (a) IMAC-Ni, (b) IMAC-Ga, and (c) ZrO2 micro tips in the mass ranges between *m/z* 700-2000 (left panel) and *m/z* 2000-4000 (right panel). Phosphopeptides are denoted by vertical arrows. Non-phosphopeptides with acidic and basic characters are marked by filled and empty circles, respectively.

Out of the three possible phosphopeptides in the lower *m/z* range, AVPyPQR (*m/z* 910) and VLPVPQKAVPyPQR (*m/z* 1671 and *m/z* 1714 with 1 Carm), only one peak corresponding to $[M+H_2O+K]^+$ of VLPVPQKAVPyPQR was observed at *m/z* 1728 in the ZrO_2 eluate, but was absent in the IMAC eluate spectra. For the higher *m/z* range, a phosphopeptide at *m/z* 2061 was found in the eluates of IMAC-Ga and ZrO_2 but was absent in the mass spectrum of IMAC-Ni eluate whereas a phosphopeptide at *m/z* 2266 was found only in the ZrO_2 eluate mass spectrum. Phosphopeptides retained by IMAC materials and ZrO_2, at *m/z* 2141 and *m/z* 2747 were more intense in the ZrO_2 eluate.

Phosphopeptides at *m/z* 3046, 3068, and 3087 (4 Carm) corresponding to $[M+H]^+$, $[M+Na]^+$ and $[M+H_2O+H]^+$of ELEELNVPGEIVEsLsssEESITR, at *m/z* 3124 (1 Carm), 3167 (4 Carm) and *m/z* 3204 (1 Carm), were of highest S/N ratios in the IMAC-Ni eluate spectrum as compared to their respective S/N ratios in the IMAC-Ga and ZrO_2 eluates. Both, IMAC and ZrO_2 materials showed retention of a few basic and acidic non-phosphopeptides but their number and peak intensities were significantly higher in the ZrO_2 eluate spectrum. These peptides are captured non-specifically due to the amphoteric character of the ZrO_2 surface functional groups, which results in additional ion exchange properties. At high pH values, the predominant surface species is $Zr\text{-}O^-$ which binds positively charged species, while at low pH values, $Zr\text{-}OH_2^+$ species predominate, which are able to exchange anions. Recent studies have also demonstrated that the protein/peptide fraction retained on ZrO_2 particles is a function of the pH to which the sample is preconditioned prior to SPE[168, 171].

As mentioned earlier, SAX micro tips showed non-specific retention of phosphopeptides. Therefore, the mass spectral features of SAX, IMAC materials and ZrO_2 eluates were compared to investigate their phosphopeptide-binding characteristics. In the low mass range spectrum of the SAX eluate, no peaks corresponding to phosphopeptides were observed. In the higher mass range, SAX showed retention of a few phosphopeptides at *m/z* 2747, 3068, 3087, 3124, and 3167 that were also retained by the ZrO_2 and IMAC materials, but their peak intensities were significantly lower in the of SAX eluate mass spectrum(Table 3.2). WCX micro tips were observed to retain four different phosphopeptides, although their peak intensities were much smaller if compared to their corresponding peaks in the SAX, ZrO_2 and IMAC-Ni eluates. Acidic,

carbamylated, non-phosphorylated peptides at *m/z* 1098, 1683, 2439 (pI 3.5-4.0) were found in the SAX eluate mass spectrum but were absent in the spectra of IMAC and ZrO_2 eluates. When extracted using IMAC and ZrO_2 micro tips, these peptides exhibit net positive charges (pH of binding buffer < pI of peptide) and hence show no significant affinity for the electrophilic metal centers.

In summary, binding specificities and efficiencies of these new particle-embedded micro tips were highly dependent on their surface functionalities, isoelectric points, and hydropathy of sample peptides and pH of binding buffer solution. Following the characterization of these SPE micro tips with a model protein digest system, these were further evaluated for their applicability to human serum profiling.

3.4.3. Pre-conditioning of Serum Sample by Denaturing Ultrafiltration

Due to the biological complexity of human serum, ultrafiltration using molecular weight cut-off membranes facilitates the generation of mass spectrometric proteome profiles by removing high abundance proteins[96, 97]. Figure 3.4 shows the MALDI mass spectra of human serum purified by C18 NuTips after different pre-treatments. Solid-phase extraction of the filtrate from a 50 kDa cut-off membrane by C18 micro tips yielded mass spectra with abundant features in the *m/z* 1000 to 4000 (Figure 3.4a) and *m/z* 4000 to 10000 (Figure 3.4c) ranges.

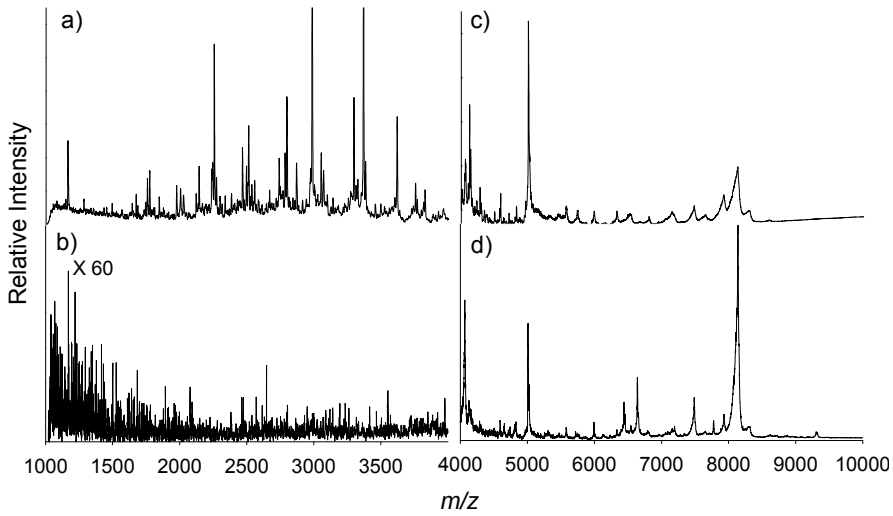

Figure 3.4. MALDI mass spectrometric profiles obtained by SPE with C18 micro tips of control human serum pre-processed by ultrafiltration using a 50 KDa membrane (a,c), without ultrafiltration (b), and with subsequent removal of low molecular weight peptides from the 50 KDa filtrate by a 3 KDa membrane (d).

No useful mass spectral data was obtained when the serum sample was directly analyzed by MALDI-MS without ultrafiltration (Figure 3.4b, high *m/z* range not shown). To further explore if mass spectral information shown in Figure 3.4c could be further improved, the 50 kDa filtrate was subsequently treated using a 3 kDa cut-off membrane (13,000g for 25 minutes) and the *retentate* was reconstituted by addition of 100 µl of 0.1% TFA solution. The analysis of the resulting sample showed improved sensitivity for molecular weight species in the 4000-10000 *m/z* range (Figure 3.4d), but no new mass spectral features were observed (data not shown). As expected, no signals below 4 kDa were detected. Based on these results, we concluded that a single, 50 kDa membrane ultrafiltration step was sufficient for processing samples prior to SPE, giving the best coverage in terms of number of features detected, and with the highest sample throughput.

3.4.4. Effects of Serum Dilution

In order to improve the filtration speed of serum samples through molecular weight cut-off filters, several dilutions were tested to optimize the experimental conditions. As shown in Figure 3.5a, a high serum concentration enhanced protein and peptide binding to the surface of C18 micro tips, resulting in optimum mass spectrometric profiles. As the serum was progressively diluted, the peak at *m/z* 1162.9 was observed to increase in intensity both in relative and absolute terms, while the other mass spectral features observed in Figure 3.5a decreased, and eventually disappeared when the serum to 0.5% TFA ratio reached 1:5 (Figure 3.5c). One possible explanation for these observations is that, as dilution increases, there is less competition for binding sites among the species present in serum, and only species with higher initial abundance are observed in the mass spectrum. The binding and ionization of these species is progressively enhanced with increasing dilution, due to the increased availability of surface binding sites, and the decrease in the number of eluted species, which reduces ionization suppression. At a certain point (Figure 3.5d and 3.5e) the dilution effect overcomes the enhanced binding and ionization, with a concomitant decline in signal intensity. From these experiments, a ratio of 1:0.5 (v/v) of serum to 0.5% TFA aqueous solution was selected as the optimum ratio for further SPE of serum samples. This dilution was kept constant for all types of micro tips in order to compare the differences in mass spectral profiles on an equal basis.

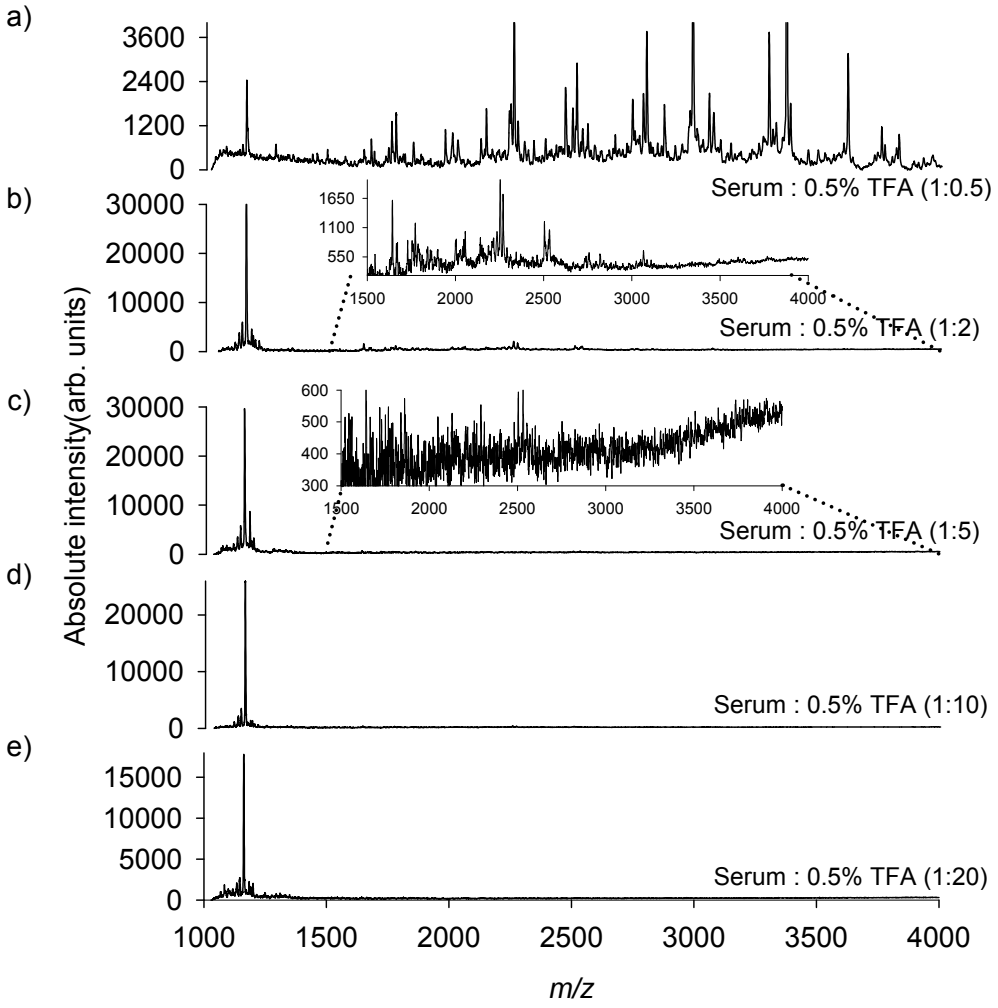

Figure 3.5. MALDI mass spectrometric profiles obtained by SPE of control human serum with C18 micro tips at different dilution ratios. Healthy individuals sera samples were diluted with a 0.5% TFA solution at different serum: TFA volume ratios (v/v), (a) 1:0.5, (b) 1:2, (c) 1:5, (d) 1:10, and (e) 1:20.

3.4.5. Application of SPE NuTips for Serum Proteome Fractionation

The MALDI MS profiles of serum samples treated with SAX, WCX, C18, C8, C4, and IMAC-Ni, IMAC-Ga, and ZrO_2 micro tips are displayed in Figures 3.6 and 3.7, respectively. Mass spectra obtained from serum extracted by C8 and C18 tips were very similar, as shown in Figures 3.6b-c but the one extracted with C4 generated a very different spectrum (Figure 3.6a), with peaks in a wider mass range, up to *m/z* 66,000.

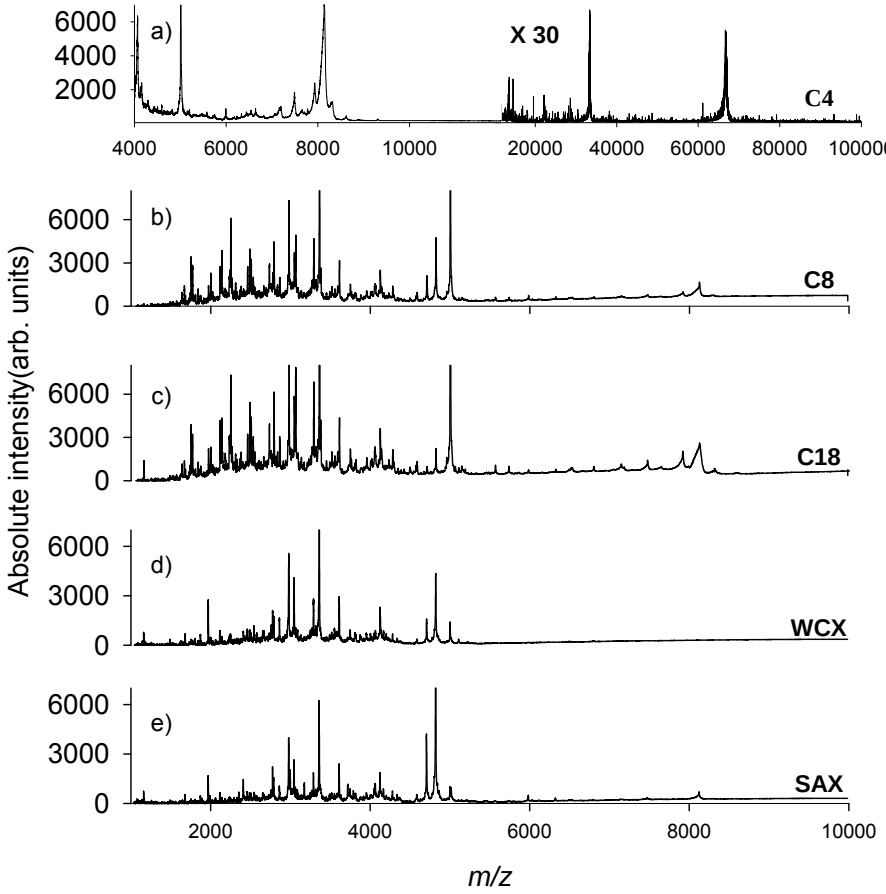

Figure 3.6. MALDI mass spectrometric profiles obtained by SPE of control human serum with (a) C4, (b) C8, (c) C18, (d) WCX, and (e) SAX micro tips.

These results are in accordance with the results obtained for the pure protein digest, which showed a correlation between the length of the alkyl chain of the

hydrophobic media used and the *m/z* range of proteins and peptides bound to it. WCX and SAX materials have oppositely charged surfaces, thus human serum SPE using these tips should lead to the generation of different MALDI mass spectra. Visual inspection of the corresponding spectra, shown in Figures 3.6d and 3.6e, revealed some apparent similarities, but closer examination and comparison of the *m/z* values of these profiles showed that both spectra had only very few peaks in common.

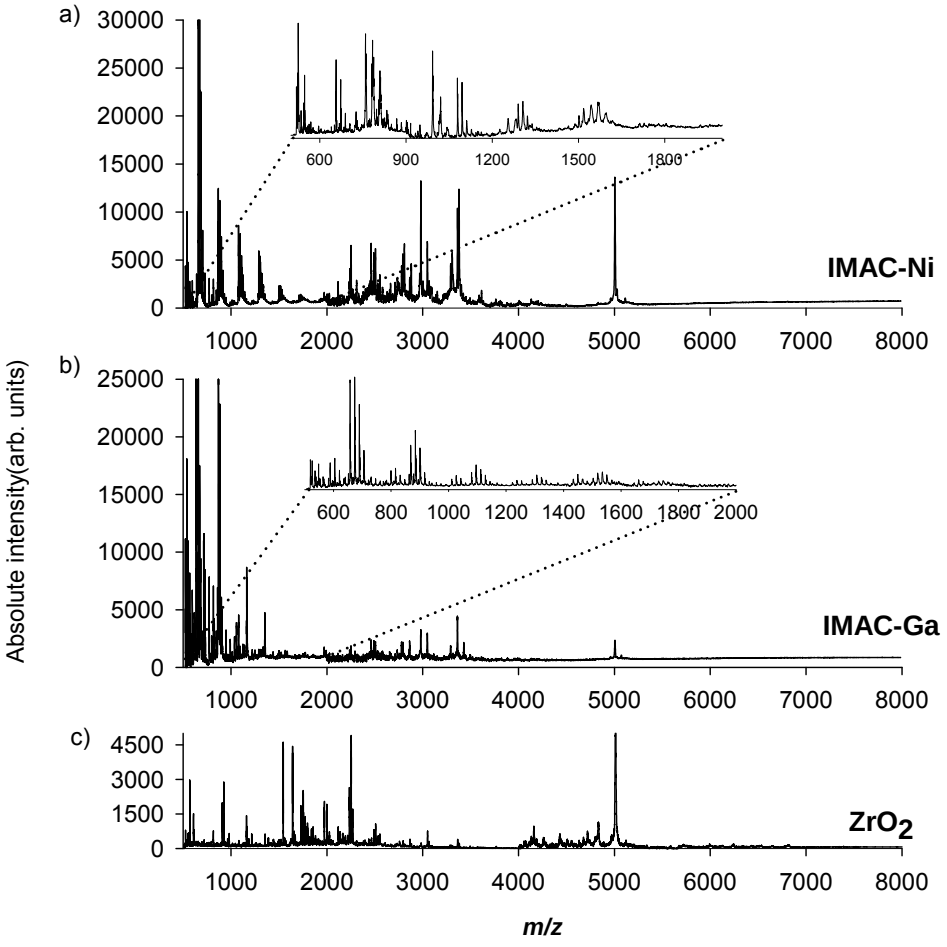

Figure 3.7. MALDI mass spectrometric profiles obtained by SPE of control serum fractionated using (a) IMAC-Ni, (b) IMAC-Ga and ZrO_2 micro tips.

Figures 3.7a-3.3c show the MALDI mass spectra of human serum extracted by IMAC-Ni, IMAC-Ga and ZrO_2 micro tips, with the inset spectra showing a detail of the peaks observed in 500-2000 *m/z* range. The extraction efficiency of IMAC-Ga micro tips in the 2000-6000 *m/z* range was low compared to that of IMAC-Ni. The mass spectrum obtained for a serum sample processed using porous ZrO_2 micro tips clearly differed from the ones obtained with IMAC-Ni and IMAC-Ga micro tips, suggesting that the unique surface characteristics of porous ZrO_2 result in a different fraction being extracted from the same serum sample.

Peak by peak comparison of all the mass spectral profiles showed varying degrees of overlap in the species extracted and detected from the same serum sample and a simplified representation of these common and unique species was compiled in a Venn diagram (Figure 3.8). Serum fractionation using C18 micro tip produced 106 peaks, while 113 peaks were detected using C8 micro tip (Figure 3.8a). A total of 86 of these peaks overlapped between C18 and C8, but only 14 peaks overlapped when C18 and C4 were compared (Figure 3.8b). Extraction with SAX and WCX micro tips produced a profile with 128 and 112 peaks respectively for the same serum sample (Figure 3.8c), with only 18 peaks in common within the *m/z* accuracy afforded by the linear MALDI instrument used in this study. This observation further verified that the two oppositely charged materials offer highly complementary chemistries for serum profiling. Extractions with IMAC-Ga, IMAC-Ni and ZrO_2 produced 86, 89 and 150 peaks respectively. There were 32 overlapping peaks between the spectra obtained for C18 SPE and SAX (Figure 3.8d), and 26 overlapping peaks between the spectra obtained for SAX and ZrO_2 materials (Figure 3.8e), while 32 peaks overlapped between IMAC-Ga and IMAC-Ni (Figure 3.8f).

Comparison of the spectral features extracted by ZrO_2 and IMAC materials showed that there were only 18 peaks in common (Figure 3.8g), and 25 overlapping peaks between ZrO_2 and IMAC-Ni (Figure 3.8h).

These results indicate that different embedded particles with unique surface characteristics produce different MALDI mass spectra for an identical serum sample; hence, these micro tips could be used to obtain complementary proteomic information with high sample throughput. It is important to note that the overlaps of spectral features of serum fractions extracted from different SPE microtips is the consequence of intrinsic properties like hydropathy, isoelectric point of the respective unknown proteins or peptides of the serum sample.

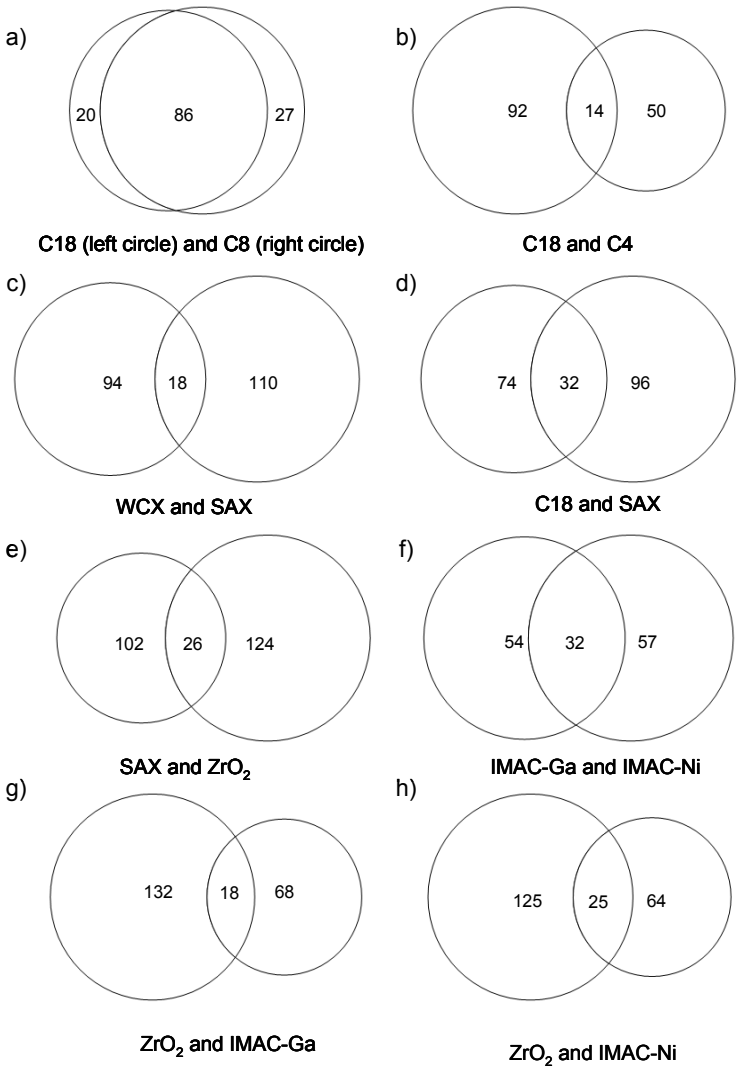

Figure 3.8. Venn diagrams comparing the overlap in the number of unique species extracted from control human serum samples by micro tips embedded with different materials (a) C18 (left circle) vs. C8 (right circle), (b) C18 vs. C4, (c) WCX vs. SAX, (d) C18 vs. SAX, (e) SAX vs. ZrO_2, (f) IMAC-Ga vs. IMAC-Ni, (g) ZrO_2 vs. IMAC- Ga, and (h) ZrO_2 vs. IMAC-Ni.

3.4.6. Inter-run Reproducibility of SPE Micro Tips

A study of the spectral reproducibility obtainable by these sample preparation protocols is of utmost importance in profiling studies where identifying potential biomarkers from a complex sample system is the main objective. By performing significance tests between the intensity profiles of the control and test samples, it is

possible to identify potential biomarkers. The significance of these tests is strongly affected by the variability arising from sample handling. An intra-run reproducibility study was thus performed using C18 and WCX micro tips in order to assess the maximum degree of variability that would be observed amongst serum profiles obtained from a single serum sample within a given experiment. This variability sets the floor of minimum biological differences that can be detected between sample groups. Eight replicate MALDI mass spectra were obtained from the same serum sample, fractionated using eight different C18 and WCX micro tips in a single laboratory session (Figure 3.9). Two 2-µL eluates were obtained from each SPE micro tip and were spotted as two different spots with equal volumes of CHCA matrix. Thus there were a total of sixteen spots each for the eight C18 (Figure 3.9, left panel) and eight WCX (Figure 3.9, right panel) micro tips. For all C18 and WCX fractions, mass spectra acquired in the higher (*m/z* 5000-8000) mass ranges were appended to those acquired in the lower mass range (*m/z* 1000-5000) and were normalized with respect to the highest intensity peaks in the individual spectrum. The asterisks denote the peaks used for coefficient of variance (CV) calculations of *m/z* and peak intensity. The peaks were selected randomly over a wide mass range, disregarding peak intensities and S/N ratios. Mean relative peak intensity of each selected *m/z* was calculated by averaging peak amplitudes at that *m/z* in the individual spectra. Spot to spot variations for all the selected peaks were measured in terms of their absolute intensity and the CV for each peak was calculated.

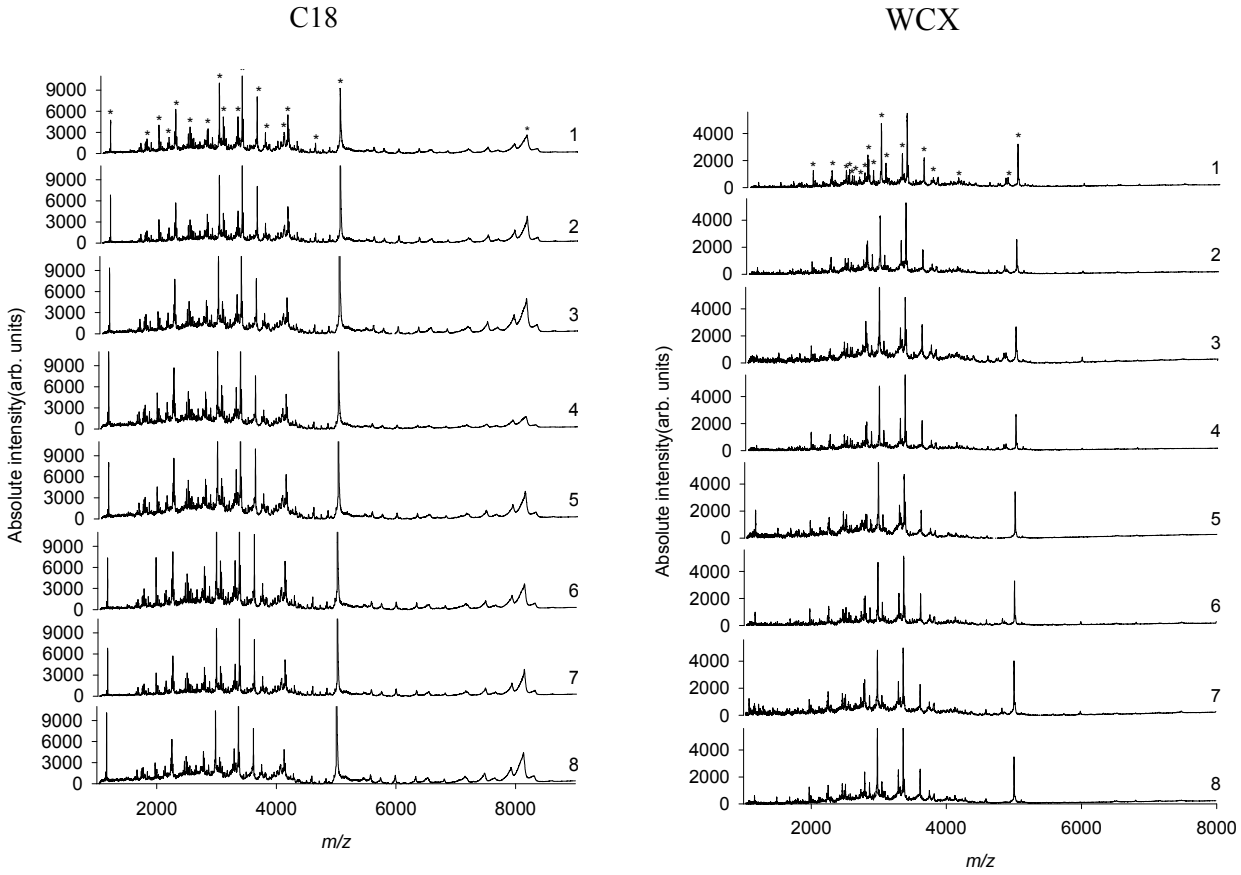

Figure 3.9. MALDI mass spectra of a control human serum sample treated with 8 individual C18 (left panel) and WCX (right panel) microtips, respectively. The marked peptide signals were used in the statistical calculations shown in the Tables 3.3 and 3.4.

An average CV of approximately 0.04% for each *m/z* value was obtained in both experiments (Table 3.3 and 3.4). The average CV of the mean intensity values was 14.9% for C18 micro tips, and 15.6% for WCX micro tips. The average %CV corresponding to spot to spot variations for both the SPE micro tips was between 3-8%, and these significantly lower %CVs indicate good spot uniformity, reproducibility of the extractions and minimal experimental error.

Table 3.3. Statistical calculations of the degree of precision for peak *m/z* and signal intensity of the features marked in Figure 3.9 (C18 micro tip, n=8).

Mean *m/z*	% CV	Mean relative peak intensity	% CV
1163.0	0.032	45.94	29.90
1772.1	0.003	19.64	11.92
1969.8	0.041	30.32	16.59
2138.1	0.039	21.77	16.82
2250.3	0.057	47.02	11.02
2489.4	0.048	29.60	10.34
2791.3	0.035	28.47	13.53
2979.6	0.051	69.42	5.62
3050.6	0.034	34.95	7.91
3291.1	0.050	37.00	6.79
3361.4	0.033	100.00	0.00
3613.2	0.067	51.74	9.83
3748.8	0.031	21.54	14.73
4061.0	0.064	20.62	16.16
4123.5	0.058	35.12	10.20
4587.2	0.0045	12.47	19.38
5000.8	0.051	55.73	33.98
8128.2	0.020	20.62	34.62

In all cases, sample-handling operations were carried out manually, and thus, it is expected that the use of a robotic station could improve these figures. Compared to the average CV of the signal intensities, the CVs at both ends of the mass spectrum were larger, possibly originating from the lower S/N ratio of the signals in these regions (Figures 3.8 and 3.9). Overall, the ranges in CV of the mean intensity values were comparable or better than those observed in previous studies[70, 97], indicating that the design of the particle-embedded micro tips affords sample preparation with reproducible solution flow paths, and low pressure buildup within the tip, ensuring sufficient reproducibility for MALDI MS-based biomarker discovery studies.

Table 3.4. Statistical calculations of the degree of precision for peak *m/z* and signal intensity of the features marked in Figure 3.9 (WCX micro tip, n = 8).

Mean *m/z*	% CV	Mean relative peak intensity	% CV
1970.5	0.032	20.43	14.48
2250.3	0.047	25.49	20.43
2460.7	0.038	25.95	18.49
2506.7	0.032	25.27	15.56
2550.9	0.048	16.91	17.39
2577.6	0.049	15.14	16.94
2653.5	0.045	13.41	18.01
2790.4	0.029	41.66	16.13
2862.4	0.040	25.48	9.61
2978.7	0.036	92.14	7.99
3045.1	0.038	29.46	9.00
3289.4	0.025	45.44	6.20
3360.2	0.033	97.74	4.8
3610.8	0.035	41.87	13.43
3747.3	0.034	16.14	22.00
4125.4	0.032	11.19	20.57
4851.9	0.032	9.65	28.49
4999.9	0.024	56.97	20.65

3.5. Conclusions

Particle-embedded SPE micro tips were evaluated and characterized for their efficiency in purification, concentration, desalting and selective isolation of peptide subgroups and small proteins from control human serum. The mass spectrometric analysis of a simple protein digest with these SPE micro tips demonstrated that different embedded materials generated complementary information from identical model samples. Simple handling and minimum backpressure during sample loading and elution allowed serum profiling with good reproducibility by MALDI TOF MS. In summary, the methods

presented here provide a convenient, robust and rapid approach for protein profiling, which is expected to facilitate future biomarker discovery studies from serum proteomes.

CHAPTER 4. IN-LINE PNEUMATICALLY-ASSISTED (PA)-AP-MALDI MS FOR IMPROVING ION TRANSFER EFFICIENCY

4.1. Abstract

In this chapter, a proof-of-principle study of a new AP-MALDI ion source utilizing a coaxial gas flow is presented. Efforts to improve the sensitivity of AP-MALDI by using pneumatic assistance are discussed in detail, concluding with results that demonstrate the suitability of the newly developed pneumatically-assisted (PA)-AP-MALDI device for standard peptides and small drug molecules.

4.2. Introduction

With the pioneering work of Laiko and co-workers, an external ion source for performing conventional MALDI-MS under atmospheric conditions was introduced[80, 172]. Since then, AP-MALDI, has emerged as a powerful approach for analyzing a variety of target analytes such as peptides[173], oligosaccharides[174], RNA[175], telomers[176], fruit tissues[177] and metabolites[178].

The capability of operating at AP gives AP-MALDI several intrinsic advantages and some limitations when compared with conventional vacuum MALDI (vMALDI). As discussed in Chapter 1 and 2, AP-MALDI ion sources can be rapidly exchanged with standard electrospray ionization (ESI) sources, allowing AP-MALDI to be coupled to a diverse array of instruments including orthogonal-acceleration time-of-flight (oaTOF)[80, 179, 180], quadrupolar ion trap(IT)[79, 82, 173, 181], and Fourier transform-ion cyclotron

resonance (FT-ICR)[182] mass spectrometers. Operation at AP also provides increased possibilities for more easily interfacing with various extraction and separation techniques such as single-drop micro-extraction[83, 183], one-step reverse micellar micro-extraction (RMME)[184], two dimensional ultra-thin layer chromatography[185], and ion mobility[186] for rapid analysis of complex samples with high throughput. Lastly, AP-MALDI ions have lower effective temperatures than those generated by vMALDI[187] due to their thermalization by collisional cooling[188]. This feature of AP-MALDI has enabled its use for analyzing labile biomolecules such as conotoxins[179], phosphopeptides[82], and proteases[132] with minimal fragmentation. A side effect of the extensive collisional cooling of ions in AP-MALDI is that matrix-analyte and matrix-matrix interactions are also preserved, resulting in increased background signals[94].

One of the main disadvantages of producing ions under AP is the difficulty in efficiently transmitting them into the first differentially pumped stages of the mass spectrometer, which can be considered the main factor limiting the sensitivity of this technique. In order to overcome this challenge, Laiko and coworkers implemented a configuration where nitrogen gas was flowed towards the AP interface of the mass analyzer and orthogonally to the ion's path[79]. With this approach, limits of detection (LOD) in the range of 60-150 fmol were obtained for standard peptides, but the sensitivity was highly dependent upon the position of the sampling probe with respect to the mass spectrometer inlet, gas flow-rate, and the gas nozzle position. Subsequently to this work, Tan et al. showed three-fold sensitivity improvements by using a "pulse delay focusing" (PDF) approach where the voltage on the target plate was switched off several microseconds after the laser was fired. The ions generated after each laser pulse were

thus made to follow the gas flow path converging towards the capillary inlet, without the influence of an electric field[86, 189]. The features of the PDF technology are described in detail in Chapter 2 of this thesis. Several other approaches have been presented for improving AP-MALDI ion transmission, de-clustering and overall sensitivity. Miller and co-workers[85] showed that by using a countercurrent of heated N_2 carrier gas = a 100-fold increase in the sensitivity for a standard peptide mixture could be achieved. This gain was primarily attributed to improved de-clustering of analyte-matrix ions. Recently Hsieh, et al. evaluated self-assembled monolayer surfaces (SAMs) as substrates to improve AP-MALDI MS analysis of peptides[190].

In a different approach involving sample pretreatment (Chapter 2), an on-chip sample preconcentration and focusing strategy coupled to AP-MALDI showed enhanced sensitivity, with signal-to-noise ratio (S/N) gains of 200-900 for peptide standards[64]. The improved sensitivity was attributed to the on-chip preconcentration effect, which enabled deposit larger sample volumes on the MALDI plate, and the subsequent elution onto tightly focused spots.

In the work presented in this chapter, an instrument development approach was explored with the aim of improving AP-MALDI sensitivity. To that end, use of a coaxial gas as an ion carrier to improve ion transmission of peptides and drugs was studied. The main difference between the presented work and previously published approaches is the direction of the gas flow with respect to the analyte plume and mass spectrometer inlet, which is shown to have a significant effect on matrix noise reduction. A custom perforated target plate and target plate holder were designed to allow this in-line gas flow.

4.3. Experimental

4.3.1. Chemicals

Angiotensin I peptide standard, α-cyano-4-hydroxycinnamic acid (CHCA), HPLC grade acetonitrile (ACN), trifluoroacetic acid (TFA), hydroquinine, and chloroquine were purchased from Sigma-Aldrich (St. Louis, MO, USA). Gas cylinders containing N_2 (99.998%), He (99.999%), and SF_6 (99.8%) were purchased from Airgas (Airgas South, Atlanta, GA, USA). All aqueous solutions were prepared with pure water from a Nanopure Diamond laboratory water system (18 MΩ/cm, Barnstead International, Dubuque, IA, USA).

4.3.2. In-Line Pneumatically-assisted-AP-MALDI Source Design

A schematic of the new in-line PA-AP-MALDI ion source is shown in Figure 4.1a. A commercially available AP-MALDI source (model 611, MassTech, Inc., Columbia, MD, USA), equipped with a nitrogen laser (337 nm, max. repetition rate of 10 Hz, pulse width 4 ns) and a PDF module was mounted on an LCQ DECA XP+ quadrupole-ion trap (IT) mass spectrometer (Thermo Finnigan, San Jose, CA, USA). A detailed description of the commercial AP-MALDI ion source and the PDF module is presented in Chapter 2.

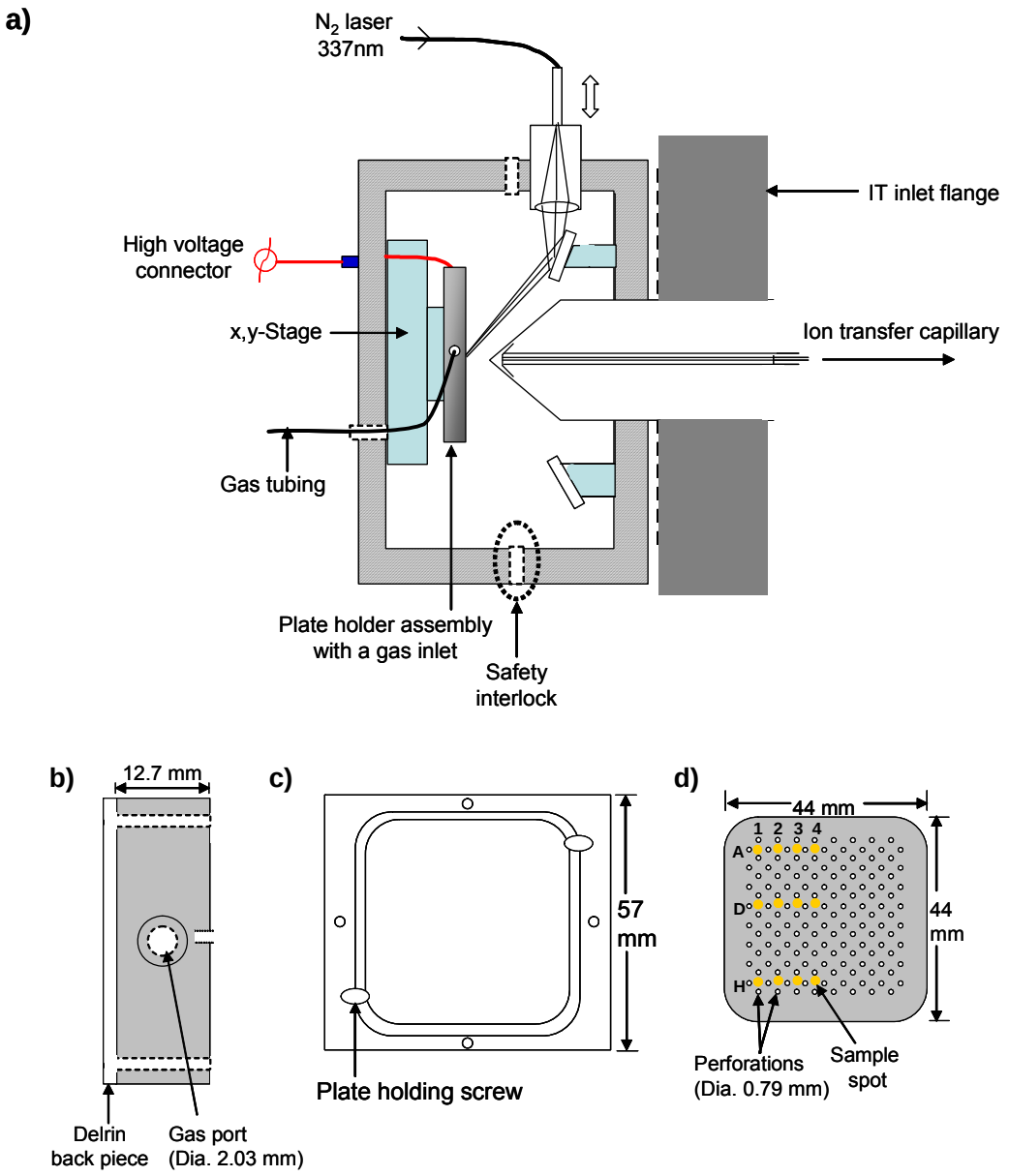

Figure 4.1. Schematic diagram of (a) the in-line PA-AP-MALDI ion source mounted on the IT mass spectrometer, (b) side view of the gas chamber showing the gas inlet, (c) front view of the target plate holder with two plate holding screws, and (d) view of the perforated target plate showing four typical sample spots (yellow) on rows A, D and H.

The original plate holder mounted on an XY stage was replaced by two stainless steel parts – a gas chamber and a plate holder. The gas chamber (Figure 4.1b, 57 mm x 57 mm x 12.7 mm) was furnished with a gas port on one side and a high voltage connector.

Gas enters the chamber via a Teflon tube connected to the gas port by a Swagelok fitting. The diameter of the gas port was 2.03 mm and the depth of the chamber was 11.09 mm. The plate holder (Figure 4.1c) was mounted on the gas chamber using four screws. When mounted, the gas chamber was sealed, allowing the gas to flow only through the perforated target plate. The modified target plate (44 mm x 44 mm) was held onto the plate holder using two washer screws and had 144 perforations of 0.79 mm id each (Figure 4.1d). The spacing between two adjacent perforations was 4.3 mm. Each sample spot was surrounded by four equally spaced perforations as shown in Figure 1d. The new design comprising the gas chamber, the plate holder and the perforated target plate allowed the pneumatic flow to be coaxial with the mass spectrometer inlet.

4.3.3. AP-MALDI Sample Preparation

A 2 μM angiotensin I peptide standard solution and a matrix solution containing 10 mg CHCA/mL were prepared in 50% ACN/0.1% TFA. Equal volumes of the peptide standard and matrix solution were premixed and 1 μL of the mixture was spotted on the perforated target plate and allowed to air dry. Four spots containing 1 pmol/spot of the peptide were deposited at adjacent positions in rows A (top), D (middle) and H (bottom). Each spot was labeled by its position on a given row (i.e. the first spot on row A is referred to as spot A1, etc.). In the case of hydroquinine and chloroquine standards, equal volumes of a 30 μM stock solution were premixed with 1 mg/mL of CHCA matrix solution and spotted on the target plate resulting in 15 pmol of the standard compound per spot.

4.3.4. PA-AP-MALDI-IT MS Set-up

The perforated target plate was mounted securely on the plate holder and the AP-MALDI source was closed to defeat the mass spectrometer's safety interlock. The target plate voltage was set to 2.5 KV, found to be optimum. The target layout stored in the ion source software (MassTech inc.) was custom modified by adjusting the sample plate geometry and target position offset parameters. The sample spacing parameters were set to 4.5 mm (x) and 9.0 mm (y) while a spiral motion velocity of 2 mm/ min and a between-run spacing of 0.08 mm were used throughout all experiments.

The optimum ion transfer capillary and tube lens offset voltages were 13 V and 55 V, respectively, with an inlet capillary temperature of 300 °C. Nitrogen gas was heated using an in-line air circulation heater and a temperature controller (Omega, Stamford, CT, USA). The skimmer-multipole 1 voltage difference was set to 60 V to enhance de-clustering of matrix-analyte adducts by low-energy collisions. Other ion optic voltages were as follows: multipole 1 offset: -2.50 V, intermultipole lens voltage: -20 V, multipole: 2 offset -10.00 V, and entrance lens: -50 V. The optimum PDF module pulse delays were 12 μs for angiotensin I and 2 μs for hydroquinine and chloroquine standards. Automatic gain control (AGC) was turned off, and the ion injection time was fixed to 300 ms for angiotensin I and 1000 ms for the smaller analytes. Spectral data were acquired for 2 minutes, and averaged over the entire acquisition time (approximately 50 scans). Averaged spectra were smoothed with a 7-point Boxcar filter and exported to Origin 7.5 (OriginLab Corp., MA, USA) for baseline correction. All experiments were performed in triplicate.

4.4. Results and Discussion

4.4.1. Effects of Carrier Gas Flow-rates and Transient Extraction High Voltage on PA-AP-MALDI Ion Transfer Efficiency

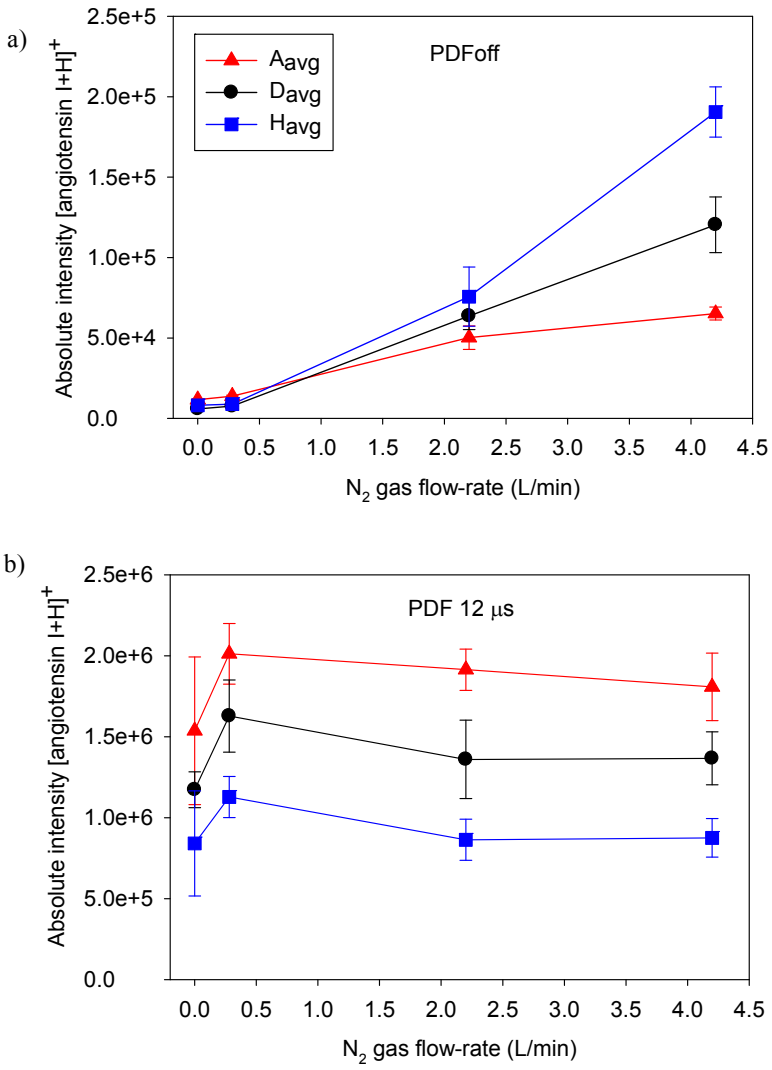

Figure 4.2. A plot of absolute signal intensity of the protonated angiotensin I ion ($[M+H]^+$, m/z = 1296) as a function of N_2 gas flow-rate with PDF pulse delay turned (a) off and (b) on, at 12 µs. The signal was obtained from 1 pmol of the standard peptide deposited per spot on rows A, D and H, each containing a total of 4 spots per row. Each data point is an average from three replicate analyses. Error bars indicate spot-to-spot variations in the absolute signal intensity of the protonated peptide.

As illustrated in Figure 4.1, the modified target plate assembly comprising a gas chamber, a hollow plate holder and a perforated target plate allowed the gas to flow from the back of the plate towards the mass spectrometer inlet. The effect of the coaxial gas flow of nitrogen (N_2) gas on ion transmission in PA-AP-MALDI was investigated at various gas flow-rates using 1 pmol angiotensin I/spot as shown in Figure 4.2. The experiments where the PDF module was off showed an almost linear increase in the absolute signal intensity of the protonated angiotensin I ion (*m/z* = 1296) as the gas flow was increased from 0.3 to 4.2 L/min ($R^2 = 0.95$ for A_{avg}, $R^2 = 1.0$ for D_{avg}, and $R^2 = 1.0$ for H_{avg}) as shown in Figure 4.2a. The average % increase in the absolute signal obtained from peptide spots on rows A, D and H were 20%, 800% and 1900% at the flow-rates of 0.3 L/min, 2.2 L/min and at 4.2 L/min, respectively. However, upon turning the PDF module on, the highest % increase in the absolute signal intensity (20%) was observed at the lowest gas flow-rate of 0.3 L/min (Figure 4.2b).

This observation can be attributed to the fact that when the PDF is off, the increase in ion intensity is primarily due to the increase in gas flow. However, when the PDF is on, the transient high voltage electric field was the predominant factor influencing total ion transmission. In these experiments, the electric field was pulsed but the gas flow was continuous. Hence, we believe that the PDF-focused ion packets near the mass spectrometer inlet were disturbed by the turbulence caused by the gas at higher flow-rates, reducing ion transmission. Therefore, the most optimal experimental conditions for analyzing peptides with highest sensitivity would be at lower coaxial gas flow-rates and at an optimal PDF setting. In instances where the relatively expensive PDF

module is not available, in-line PA-AP-MALDI operated at higher gas flow-rates would be preferable over conventional AP-MALDI for better sensitivity.

4.4.2. De-clustering Effect of N_2 in PA-AP-MALDI

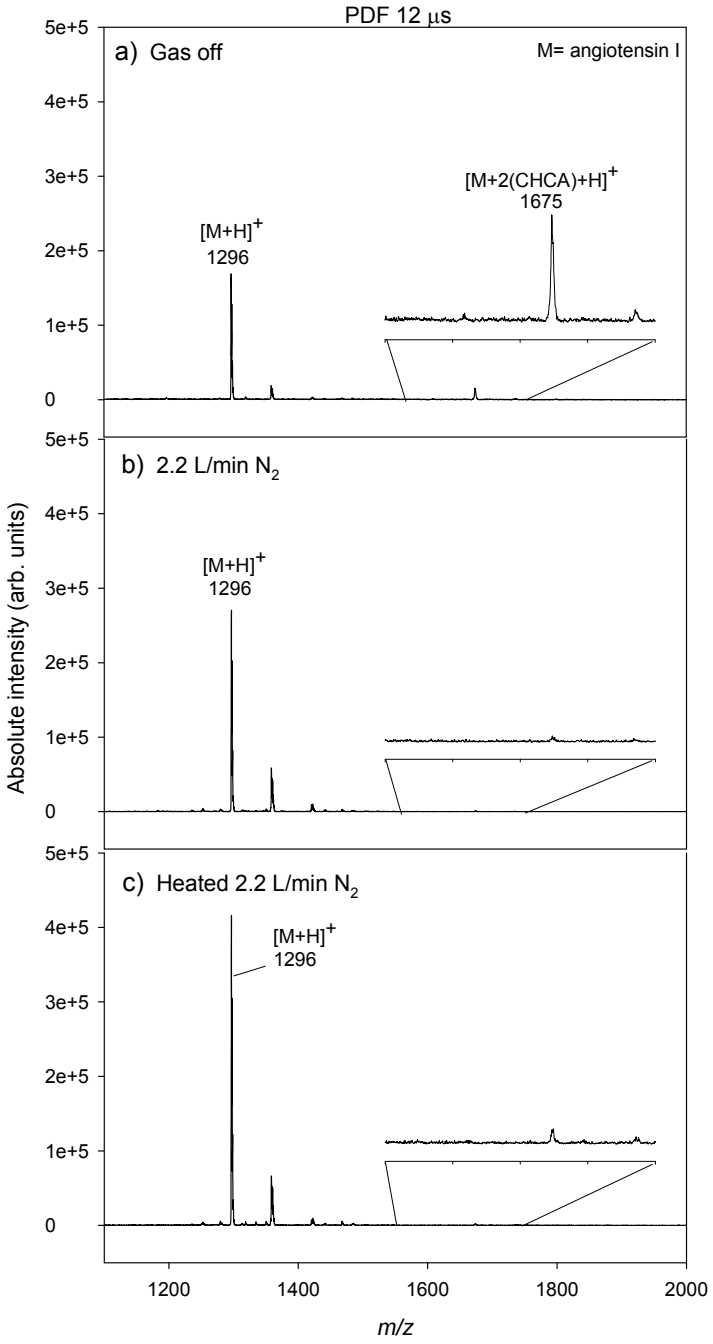

Figure 4.3. Representative PA-AP-MALDI mass spectra of 1 pmol angiotensin I/spot obtained (a) without N_2 gas flow, (b) with 2.2 L/min ambient N_2, and (c) with 2.2 L/min N_2 heated to 60 ºC. The PDF module was set to 12 μs pulse delay and the in-source

de-clustering voltage turned off. The inset in each panel shows a close-up of the *m/z* 1500-2000 region.

In mass spectrometers equipped with an atmospheric pressure interface, the kinetic energy of ions can be increased by increasing the potential drop between the ion transfer capillary and the skimmer[191]. The de-clustering effect observed by skimmer-capillary collision-induced dissociation was similar to the effect observed upon using the coaxial N_2 gas flow. Figure 4.3 shows a comparison of the AP-MALDI mass spectra obtained from 1 pmol angiotensin I/spot with the PDF on and set to a 12 μs pulse delay, with no gas (4.3a), with 2.2 L/min of room temperature N_2 gas (4.3b) or heated gas (4.3c) flowing from the back of the perforated plate. The de-clustering voltage was turned off during the experiments to avoid factor confounding. As seen earlier, the signal intensity of the $[M+H]^+$ angiotensin I ion increased when coaxial unheated and heated N_2 gas was used. Similarly another peak observed at *m/z* 1358 showed improvement in the signal intensity upon using ambient temperature and heated carrier gas flow. This peak was assigned to the $[(\text{angiotensin I}-H)+ Na+K^+]^+$ ion. The S/N ratios calculated for the protonated peptide ion peak were 128, 458 and 504 when no gas, unheated and heated gas flow was employed, respectively. The peak corresponding to the protonated angiotensin I-CHCA matrix adduct at *m/z* 1675 $[M+2(CHCA)+H]^+$ was dramatically reduced upon flowing 2.2 L/min of N_2 gas (insets 4.3a-c). It was expected that using heated gas would de-cluster the analyte-matrix adduct ions more efficiently than using ambient temperature gas molecules due to the more highly-energetic ion-gas molecule collisions. However, no significant improvement in the de-clustering of the peptide-matrix adduct was observed at elevated gas temperature, possibly due to the relatively

low maximum temperature (60 ºC at the outlet) that could be achieved at this gas flow-rate with the heater used.

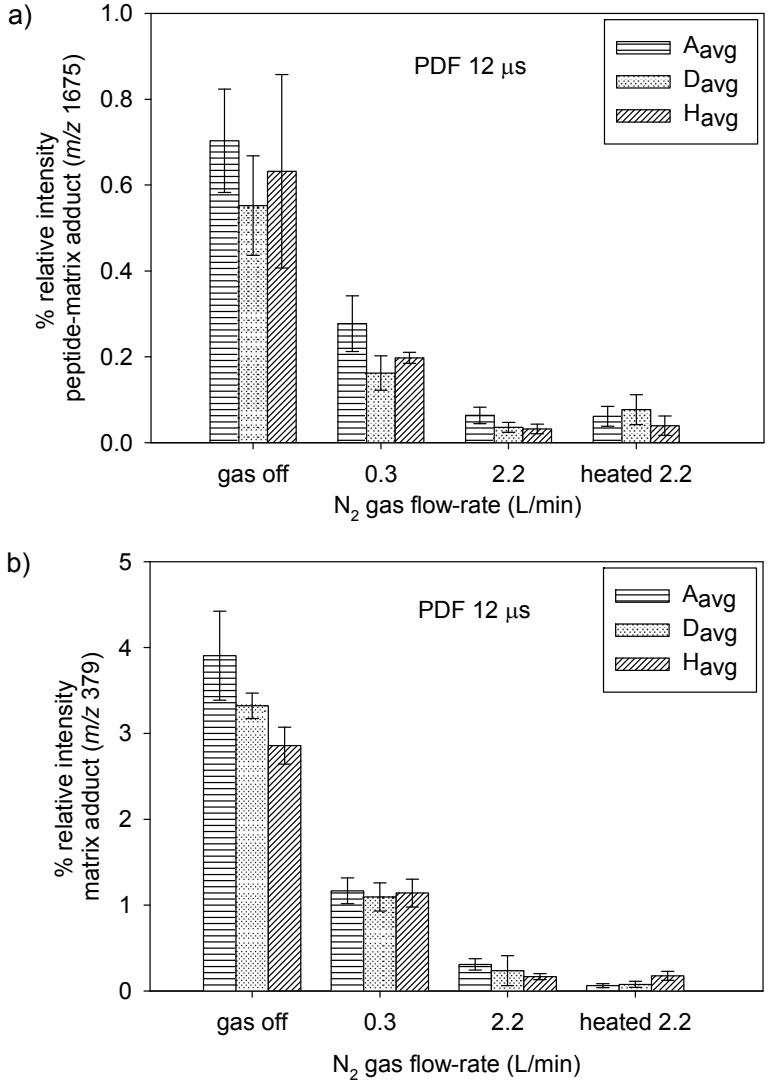

Figure 4.4. Average % relative intensity of (a) the protonated matrix-peptide adduct ion at *m/z* 1675 and (b) the CHCA matrix cluster ion at *m/z* 379 as a function of gas flow-rate and temperature.

The carrier gas de-clustering effect on peptide-ion clusters is shown in Figure 4.4a for target plate rows A, D and H. It was observed that the average cluster ion % relative intensity decreased from 0.63 % to 0.21% at 0.3 L/min. At 2.2 L/min, the signal intensity was further decreased to 0.04% and 0.05% when using heated and unheated N_2 gas,

respectively. The trend was also observed for the $[2(CHCA)+H]^+$ matrix adduct ion monitored at *m/z* 379. The average % peak intensity for this ion decreased from 3.3 % to 1.1%, 0.23% and 0.08% when using 0.3 L/min, and 2.2 L/min of ambient temperature gas, and 2.2 L/min of 60 ºC gas (Figure 4.4b). Although the temperate of the heated gas was not sufficient to de-cluster the peptide-matrix adduct in the high mass range (*m/z* 1675) with a greater efficiency, it exhibited improved de-clustering of the smaller matrix adduct with *m/z* of 379.

4.4.3. Limit of Detection of PA-AP-MALDI

The PA-AP-MALDI mass spectra shown in Figure 4.5 were obtained at different gas flow-rates when the PDF mode was turned off (4.5a-d) and on with 12 μs pulse delay (4.5e-h). The relative intensities of the peaks corresponding to matrix and matrix-salt adducts at *m/z* 172 $[CHCA\text{-}H_2O+H]^+$, 190 $[CHCA+H]^+$, 379 $[2(CHCA)+H]^+$, and at 439 $[CHCA+(CHCA\text{-}H)+Na+K]^+$ were more intense when the gas flow was off. Comparison of the matrix peak intensities in the spectra obtained without coaxial N_2 gas flow and those with gas (3a vs. 3b-d and 3e vs. 3f-h) clearly shows that the in-line gas flow not only entrained the protonated peptide ions, as seen in the earlier experiments, but also deflected or help fragment the low molecular weight CHCA matrix ions causing a reduction in baseline noise. As a result, a significant increase in the S/N ratio of the protonated angiotensin I peak, from 82 to 290 in PDF off mode and from 1245 to 2112 in PDF on mode, was observed when pneumatic gas-assistance was used. The limit of detection (LOD) for angiotensin I was significantly improved from 73 to 20 fmol/μL

when the PDF was off and from 5 to 3 fmol/μL when it was turned on, at the optimal coaxial N_2 gas flow-rates of 4.2 L/min and 0.3 L/min, respectively.

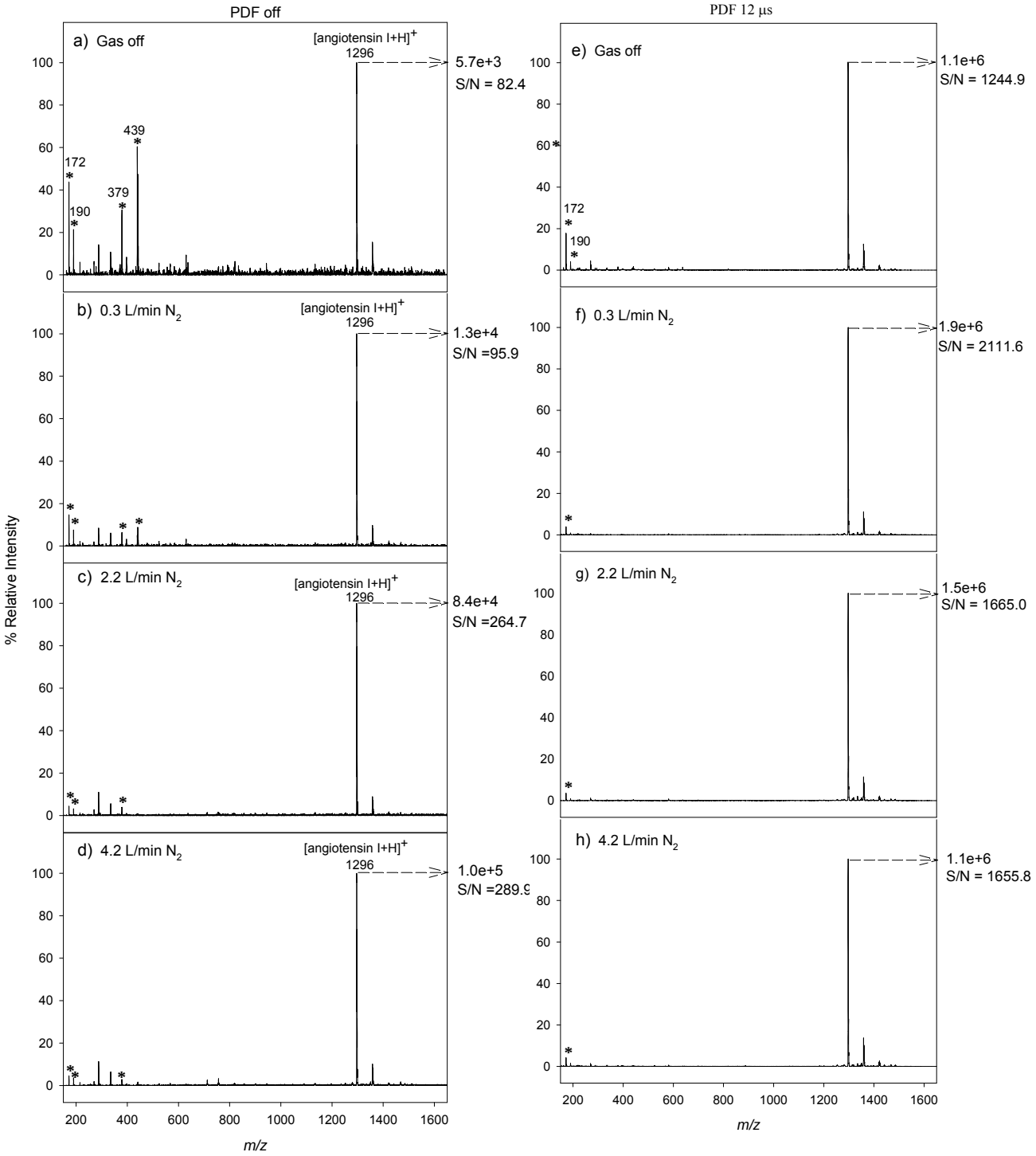

Figure 4.5. Mass spectra of 1 pmol angiotensin/spot obtained with N_2 gas turned off (a and e), and on with the gas flow-rate adjusted to 0.3 L/min (b and f), 2.2 L/min (c and g), or 4.2 L/min (d and h), under PDF off (a-d) and PDF on (e-h) conditions. Known matrix peaks in the low mass range are denoted by asterisks. Absolute intensity of the base peak in each spectrum is shown to the right as indicated by the arrow.

4.4.4. Investigation of Other Potential Carrier Gases for PA-AP-MALDI

The use of other gases such as helium (He) and sulfur hexafluoride (SF_6) for PA-AP-MALDI was also evaluated, and the sensitivity obtained using these gases compared to that observed using N_2. Due to the lower electrical breakdown voltages of He, discharges were observed during experiments in which high rates of this gas flowed through the 2.5 kV target plate. The maximum flow-rate that could be used without inducing an electrical discharge was 0.6 L/min. For this flow-rate, the average % increase in ion signal intensity when using N_2 and He without PDF focusing was 64% and 32%, respectively (Figure 4.6a). The gains were reduced to 28% and 15% when the PDF mode was utilized (Figure 4.6b), but the differences between gases did not seem to be significant. In general, ion transmission efficiency when using N_2 as the carrier gas seemed to be higher than with He. This observation was attributed to the lower ionic mobility of most ions in N_2 than in He, which leads to a more pronounced effect of electrical field lines not converging towards the instrument's inlet, resulting in more loses when the sampling plate potential is constantly held on (PDF off).

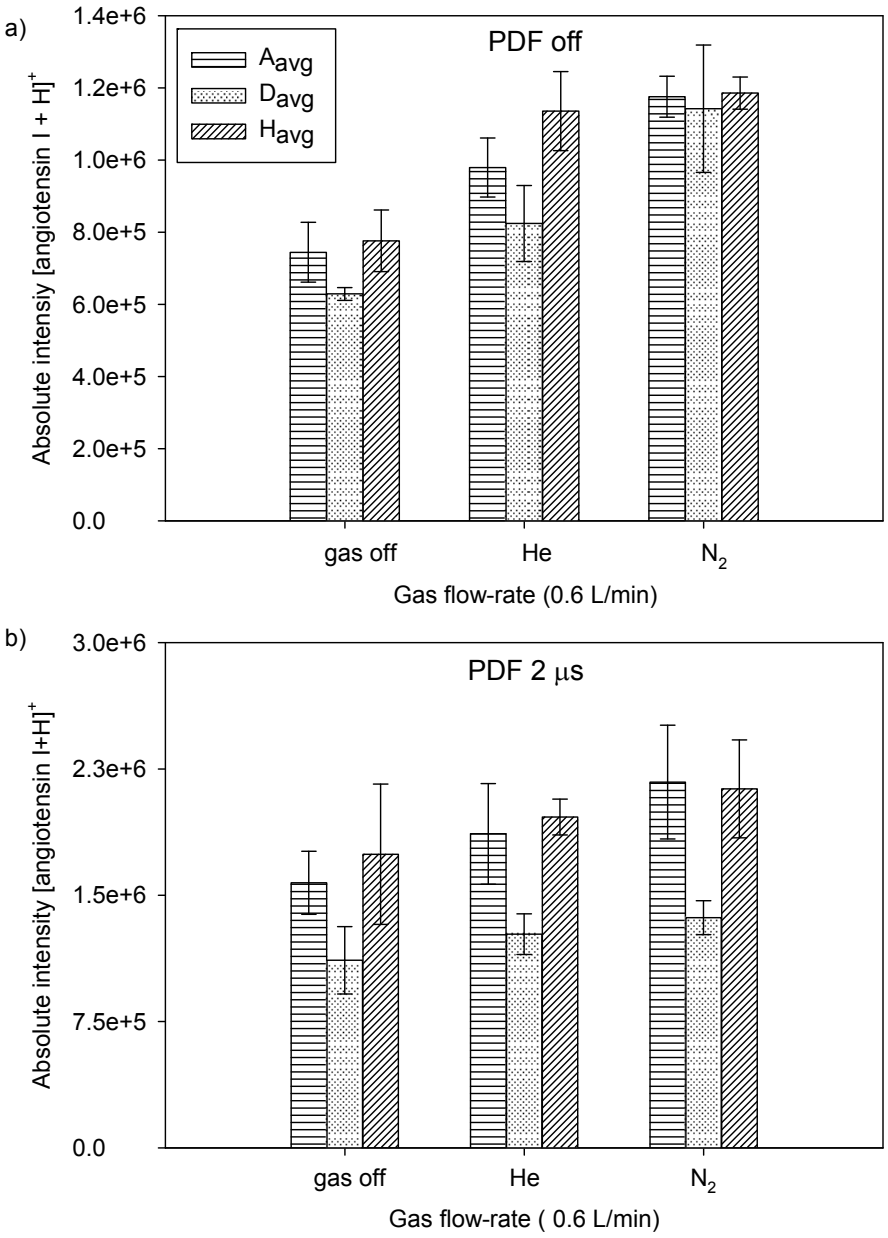

Figure 4.6. Comparison of the ion transmission efficiencies observed for He and N_2 gas for the monoisotopic protonated angiotensin I ion using a 0.6 L/min carrier gas flow-rate and (a) PDF off and, (b) PDF on with 2 μs pulse delay. AP-MALDI mass spectra were acquired from 1 pmol of the peptide standard spotted on rows A, D and H on the target plate.

In addition to improving the ion transmission, several research groups have also explored the possibility of improving MALDI signal intensity by removing photoelectrons from the MALDI plume[192]. It has been postulated that the photoelectrons

generated by laser irradiation of metal targets during MALDI process[45, 192] neutralize positively charged species in the MALDI plume by recombination[57]. SF_6, a well known electron scavenger gas[193], was tested as coaxial carrier gas in order to explore the possibility of removing these photoelectrons produced during PA-AP-MALDI MS. Experiments were performed using 1 pmol of angiotensin I standard per spot and 2.2 L/min of SF_6 gas. The absolute signal intensities were observed to decrease significantly when SF_6 was used (Figure 4.7c), concomitantly with the appearance of a low intensity peak at *m/z* 1278 arising from dehydration of the protonated peptide ion. It was speculated that since the mass of an SF_6 molecule is higher than that of N_2 and other atmospheric gases, inelastic ion-molecule collisions occurring during ion transit to the mass spectrometer inlet are more energetic than collisions occurring between the analyte ion and gases such as N_2 or He, resulting in fragmentation of the analyte ion.

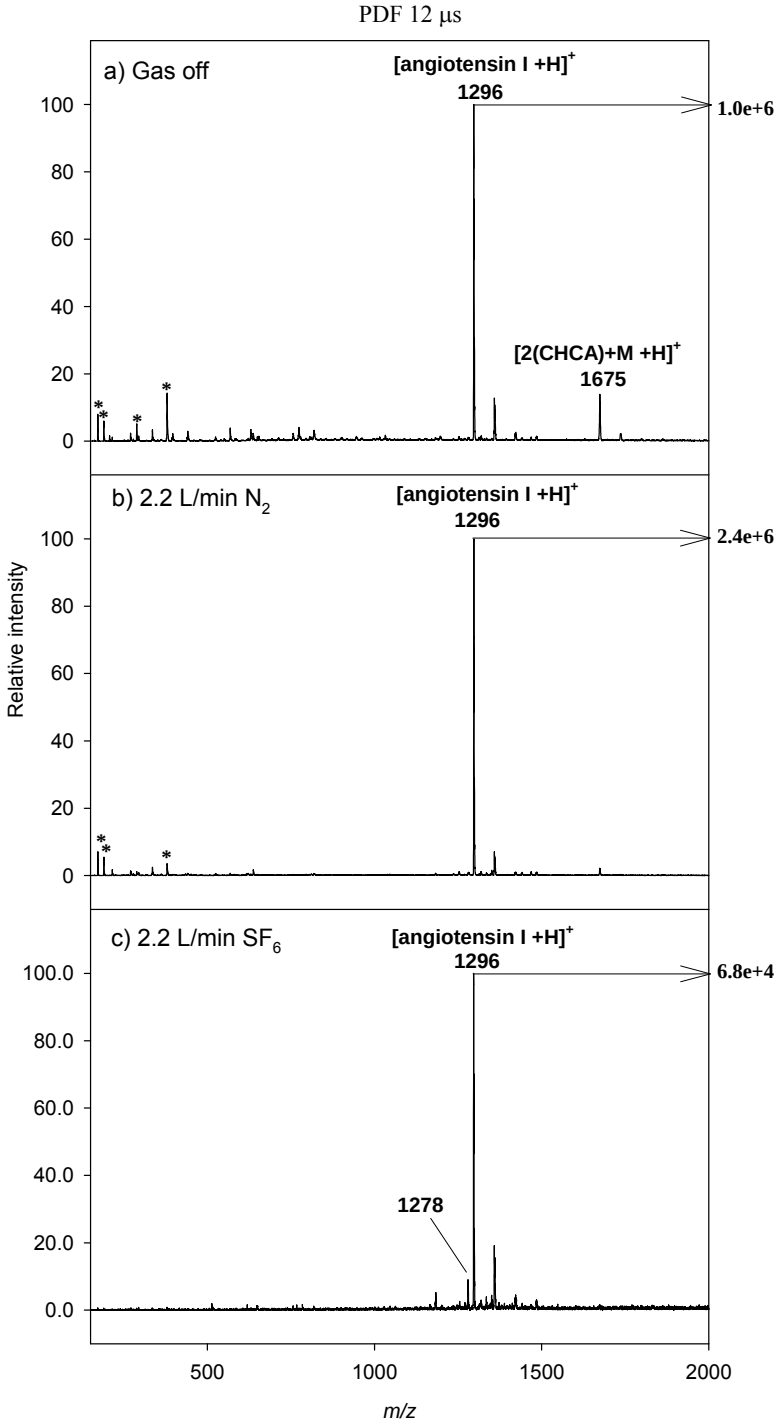

Figure 4.7. Comparison of spectra obtained with N_2 and SF_6 used as carrier gases in the PA-AP-MALDI set-up. The top, middle and bottom panels show mass spectra of 1 pmol angiotensin I collected with (a) gas flow off, (b) 2.2 L/min of N_2 and (c) 2.2 L/min SF_6.

4.4.5. Evaluation of PA-AP-MALDI for Analyzing Small Drug Molecules

Due to the reduction in background noise observed in the low mass range for in-line PA-AP-MALDI mass spectra, it was anticipated that PA-AP-MALDI MS could be particularly advantageous for the analysis of low molecular weight molecules (< 500 Da) whose signal is typically obscured by matrix peaks in vMALDI. Therefore, experiments designed to further evaluate the applicability of in-line PA-AP-MALDI for analyzing two relatively labile antimalarial drugs, chloroquine and hydroquinine, were performed. For these experiments, the in-source de-clustering voltage was kept off and only ambient temperature N_2 was used to avoid unwanted fragmentation of protonated molecules.

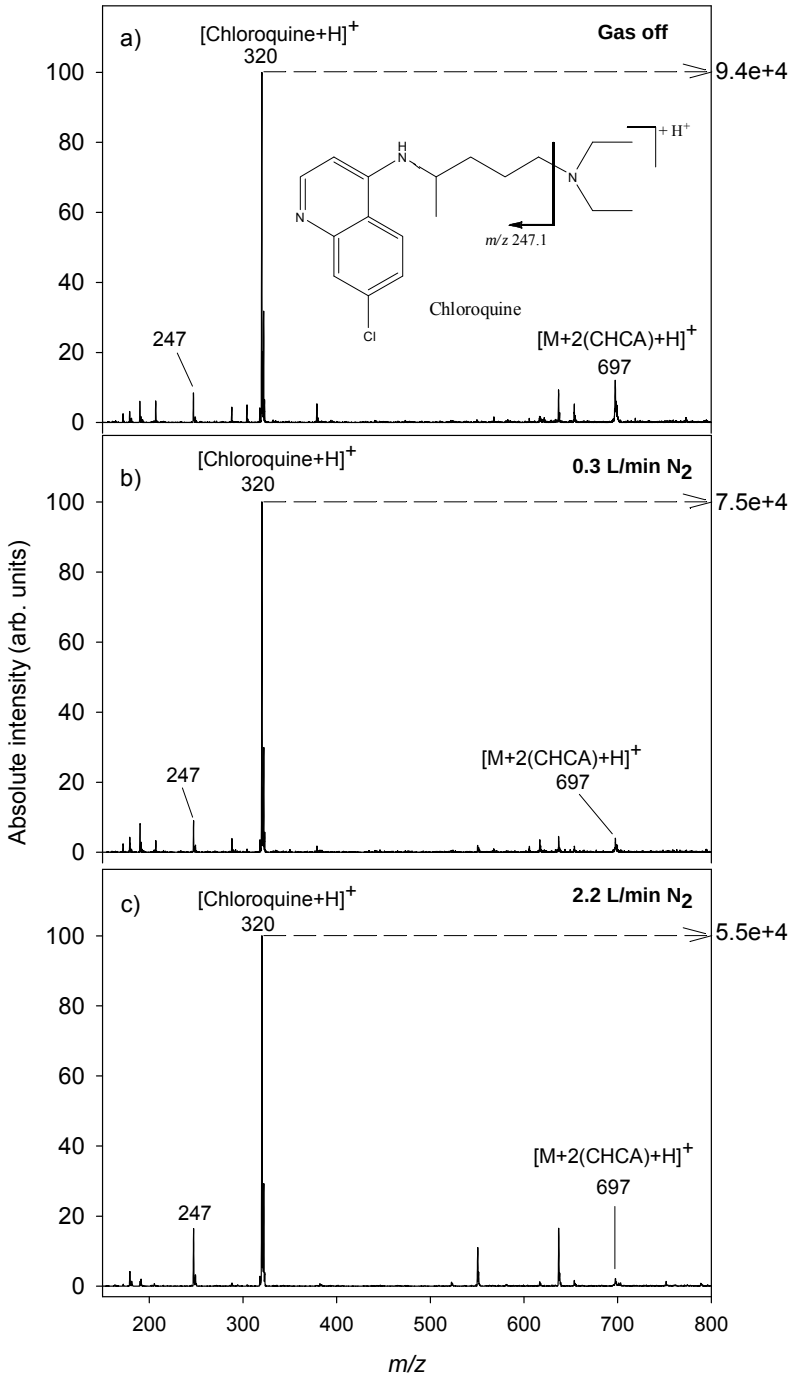

Figure 4.8. PA-AP-MALDI MS mass spectra of 15 pmol/spot of chloroquine standard acquired with (a) N_2 gas flow off, (b) 0.3 L/min and (c) 2.2 L/min N_2 gas.

Under these mild ionization conditions, mass spectra with good S/N ratio were obtained by PA-AP MALDI for both analytes (Figure 4.8 and Figure 4.9), indicating that

this method has significant potential for small molecule mass spectrometry applications. Despite all precautions taken, it was observed that protonated chloroquine still fragmented to a certain extent which increased with increasing carrier gas flow (Figure 4.8 b-c), suggesting an increase in ion internal energy at higher flow rates.

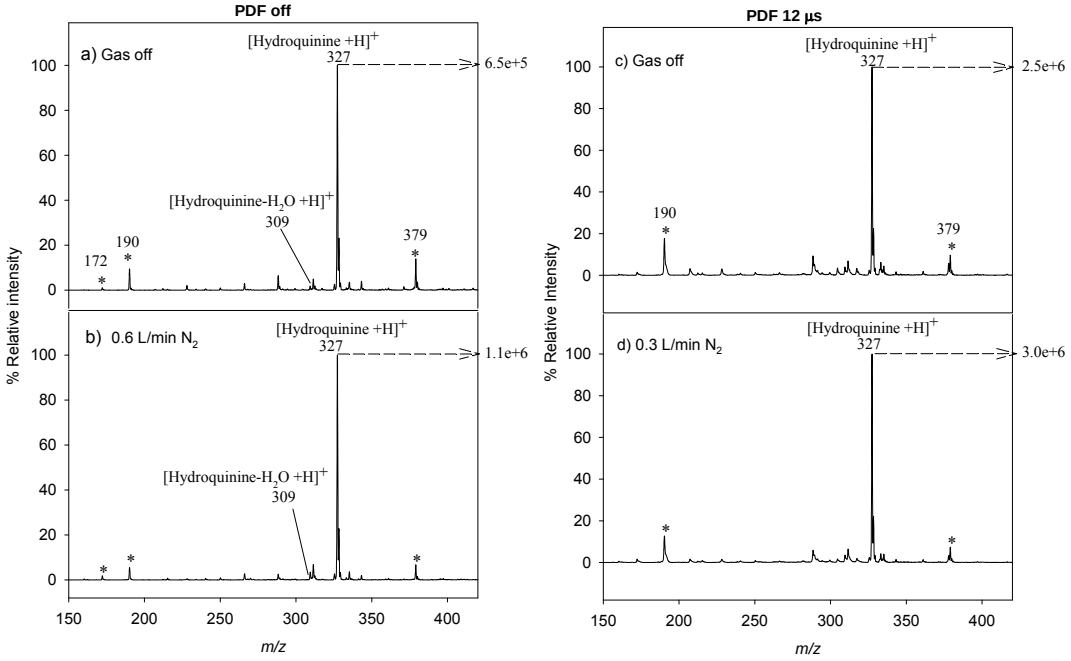

Figure 4.9. PA-AP-MALDI mass spectra obtained from hydroquinine standard (15 pmol/spot). The panels on the right show spectra obtained in PDF off mode with (a) no gas and (b) with 0.6 L/min N_2. The panels on the left show the mass spectra collected in PDF on mode (2 µs pulse delay) with (c) no gas and (d) 0.3 L/min of N_2 gas flowing from the back of the plate.

Hydroquinine, which showed little to no fragmentation, was selected for further characterization experiments. The PA-AP-MALDI MS spectra obtained from 15 pmol hydroquinine/spot (Figure 4.9a) showed an increase in absolute peak intensity of 43% at 0.6 L/min of N_2 carrier gas flow when the PDF was off (Figure 4.9b) and 20% at 0.3 L/min when the PDF module was on (Figure 4.9d). The differences in the optimal flow-

rates for the two different PDF settings were similar to what had been observed for angiotensin I where the presence of a continuous or transient electric field had a strong effect on the improvement in ion transmission efficiency of a given carrier gas. The coaxial gas flow could also cause loss of water from the protonated hydroquinine molecule depending on the flow employed. The signal intensity of the [hydroquinine-H_2O+H]$^+$ fragment ion at *m/z* 309 increased by 3-fold as the gas flow was increased from 0.3 to 2.2 L/min (data not shown), indicating a marked increase in internal energy deposition. High carrier gas flows were therefore avoided altogether for small molecule analysis to ensure optimal ion transmission with minimal ion activation.

4.5. Conclusions

PA-AP-MALDI ion transmission efficiency was found to be strongly dependent on coaxial gas flow magnitude, nature of the carrier gas, and applied electric field between the target plate and the mass spectrometer inlet. Nitrogen showed the best ion transport efficiency with sensitivity gains of up to 1900% and 20% for a peptide standard when the target plate voltage was either continuous or pulsed, respectively. This was attributed to the ability of the in-line gas flow used in this source to modify the ion's trajectories during their transit towards the instrument's inlet. The higher S/N ratios afforded by the improvement in ion transport efficiency yielded femtomole detection limits due to low or almost negligible background noise, suggesting that this ionization source could be beneficial in analyzing dilute peptide mixtures. With the increased sensitivity of PA-AP-MALDI, angiotensin I limits of detection of 20 or 3 fmols were obtained for continuous or pulsed target plate voltage, respectively. The performance of

PA-AP-MALDI for analyzing low molecular weight compounds depended on the lability of the analyte as well as on the nature of the carrier gas. To that end, it was found that very low gas flow-rates (0.3 to 0.6 L/min) were preferable due to increased fragmentation at higher gas flows.

Further improvements in S/N ratio gains could be achieved by optimizing design parameters of the current ion source configuration, such as the distance between the neighboring perforations, the size of each individual perforation, the distance between the target plate and the mass spectrometer inlet, and by synchronizing a pulsed gas flow with the AP-MALDI laser pulse and voltage step. Computational fluid dynamic modeling should also help to further rationalize the observed dependence of ion transmission with the various experimental variables.

PART II: DART IONIZATION OF TEREPENES

CHAPTER 5. DIRECT ANALYSIS IN REAL TIME (DART) MASS SPECTROMETRIC ANALYSIS OF JUVENILE HORMONE III AND ITS TERPENE PRECURSORS

5.1. Abstract

In this chapter, results on the DART- orthogonal (oa)TOF MS analysis of mosquito juvenile hormone (JH) III and its various terpene precursors are presented. The chapter begins with a brief overview on the role of JH III in insect physiology, followed by a description of DART ionization. The high-throughput capacity of DART-oaTOF for identification of several terpene alcohols and their aldehyde products by accurate mass measurements is explored. Further, a design of experiment (DOE)-based optimization approach is presented to examine the effect of different DART experimental variables on the observed DART-oaTOF sensitivity. The chapter concludes with results from an investigation regarding the in-source collision induced dissociation (CID) capability of oaTOF to distinguish between two stereoisomers of an important JH precursor.

5.2. Introduction

Juvenile hormone (JH) III is the key hormone regulating previtellogenic ovarian development in mosquitoes[194, 195]. Reproducible and sensitive detection of JH and related chemical species is crucial for better understanding mosquito biochemistry and for developing safer insecticides that target JH as a way of controlling transmission of diseases such as malaria, yellow fever, and western encephalitis[196, 197]. JH is synthesized and released from the *corpora allata*, a pair of endocrine glands with neural connections

to the brain[195, 198, 199]. The early steps of JH III biosynthesis follow the mevalonate pathway, with the formation of five-carbon (5C) isoprenoid units from acetate via mevalonic acid, with the subsequent head to tail condensation of three 5C units to form farnesyl diphosphate (FPP)[200]. In the late steps, FPP is hydrolyzed by a pyrophosphatase[201] to form farnesol, followed by successive oxidations to farnesal and farnesoic acid (FA) by an alcohol dehydrogenase[202], and an aldehyde dehydrogenase[203]. In mosquitoes, the last two biosynthetic steps involve methylation of FA by an *O*-S-adenosylmethinine(SAM)-dependent methyltransferase (JHAMT)[204] to form methyl farnesoate (MF) that is subsequently epoxidated to JH III by a P450 monooxygenase[205]. The amount of these compounds in small insects, such as mosquitoes, is usually in the low picomole range, which makes it challenging to detect them by most typical analytical techniques[206-208].

The most commonly used analytical methods for identification and detection of JH III and its precursors include NMR, IR, and gas chromatography (GC)-mass spectrometry [195, 209, 210], the latter two being the tools of choice for distinguishing between different farnesol isomers[211]. Due to the volatile nature of JH III and its precursors, electron ionization (EI) or chemical ionization (CI) are commonly used following GC separation, with the main drawback of EI being the extensive fragmentation observed[211]. Although fragment ions are useful for identification purposes in low resolving power instruments MS experiments, unwanted fragmentation also complicates the mass spectrum and reduces sensitivity. In addition, GC separations are time consuming, with memory effects and stationary phase bleeding being some of the most common practical

issues. Such issues motivated us to investigate the application of ambient ionization techniques for direct mass spectrometric analysis of this family of related compounds.

5.2.1. DART Ionization

DART has gained popularity as one of the leading ambient pressure ionization method because it offers relative simplicity for obtaining useful data with shorter assay turn-around times, without chromatography or extensive sample preparation[88, 212]. The versatility of DART in ionizing a wide range of chemicals without the need of extensive sample preparation has motivated MS practitioners to apply the technique to various fields such as forensic drug discovery[88, 213, 214], reaction monitoring[214], counterfeit drugs rapid screening[212, 215, 216], contaminated pet-food analysis[217], detection of restricted phthalic acid esters (PAE) in toys[218], fragrance analysis[219], bacterial strain classification based on fatty acid methyl ester fingerprinting[220], and rapid human serum fingerprinting without sample cleanup[221].

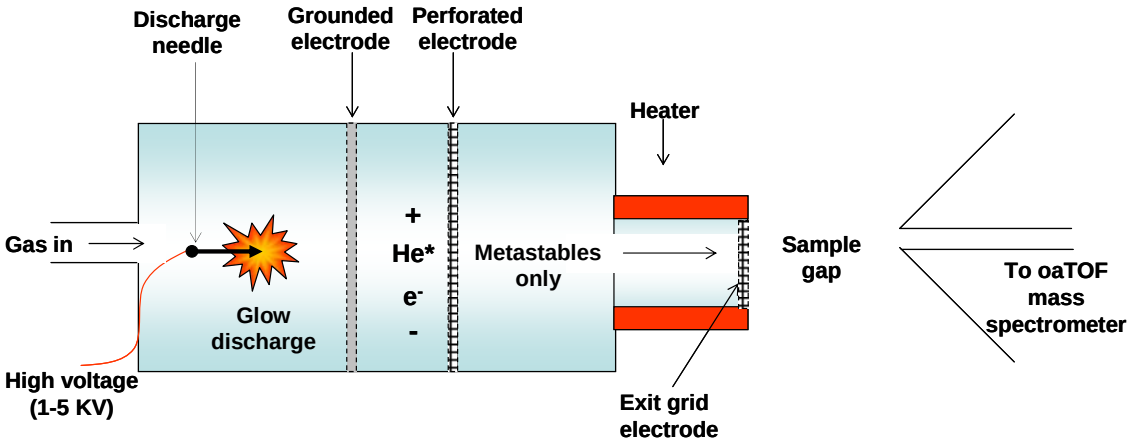

Figure 5.1. Schematics of the DART ion source couple to an oaTOF mass spectrometer.

The DART ion source contains of a chamber at the core of which is a point-to-plate glow discharge supported by a helium (He) gas stream (Figure 5.2). DART ionization involves formation of metastable He atoms (He^*, 2^3S_1, 19.8 eV) by a series of complex processes such as electron impact and ion-electron recombination within the glow discharge[88]. Nitrogen (N_2) gas can be used instead of He, in which case low-energy excited N_2 species are generated by vibronic excitation[88]. Ions and electrons generated concomitantly with metastable gas are filtered out by perforated disk electrodes positioned downstream, and an exit electrode positioned at the DART source exit prevents ion-ion recombination reactions (Figure 5.1). A built-in heater can be used to heat up the gas stream containing metastables up to 450 °C before exiting the source.

Cody et al. suggested involvement of different ionization mechanisms and that all reactions begin with initial Penning ionization of a neutral gas by gas metastables[88]. Penning ionization[222] of ambient water by He* generating water clusters as shown in reaction 5.1 has been confirmed by the presence of water cluster ions (n= 1 to 14) in DART mass spectra[88]. The protonated water clusters are then suggested to undergo proton transfer reactions with gaseous analyte molecules (M) to form protonated analyte species (reaction 5.2).

$$He^*(g) + nH_2O(g) \rightarrow [(H_2O_{n-1})H]^+ + He \cdots\cdots\cdots\cdots\cdots\cdots\cdots\cdots\cdots\cdots (5.1)$$

$$[(H_2O_{n-1})H]^+ + M \rightarrow [M+H]^+ + n-1(H_2O) \cdots\cdots\cdots\cdots\cdots\cdots\cdots\cdots\cdots\cdots (5.2)$$

A second mechanism is proposed to involve direct Penning ionization of analyte (M) by He^* to form molecular ion $[M]^{\cdot+}$ (reaction 5.3)[88]. In the negative ion mode, four

main mechanisms, namely electron capture, dissociative electron capture, proton transfer and anion attachment have been suggested by Song et al.[223].

$$He^{*}(g) + M(g) \rightarrow M^{\cdot +}(g) + e^{-} \quad \cdots\cdots\cdots\cdots\cdots\cdots\cdots\cdots\cdots\cdots (5.3)$$

Following ionization, the ions are transferred into the first differentially pumped region of a mass spectrometer such as an orthogonal (oa)TOF[213, 220, 224-227], or a triple quadrupole[219] instrument under the combined influence of the DART gas streaming toward the mass spectrometer inlet, suction from the API orifice and weak extraction field applied to the source exit grid. A recent study showed that various factors such as He gas flow-rates, thermal gradient produced by the gas streams, sample positioning, and DART exit grid voltage influenced the ion transmission in DART, affecting the overall sensitivity of DART-MS analysis of a solid sample[228]. Therefore, optimization of DART--MS methods is essential for achieving improved sensitivity and detection limits.

In a first study, we reported the first use of DART MS for confirming the biochemical role of an $NADP^{+}$-dependent farnesol-dehydrogenase enzyme in *Aedes aegypti*[202]. Follow up work involved an extensive full factorial design optimization process for improving DART-MS analysis of farnesol, JH III, methyl farnesoate (MF), and farnesoic acid (FA), which helped us better understand the physicochemical processes involved in ion generation. The utility of the optimized DART-MS approach was further evaluated for distinguishing between (2Z, 6Z)- and (2E, 6E)-isomers of farnesol via in-source collision-induced dissociation (CID)

5.3. Experimental

5.3.1. Chemicals

HPLC grade methanol was purchased from EMD chemicals Inc. (Gibbstown, NJ, USA). DIP-it sampler glass capillaries were purchased from IonSense Inc. (Danvers, MA, USA), and a PEEK tubing (360 μm O.D., 50 μm I.D.) was obtained from Health & Science (Oak Harbor, WA, U.S.A.). JH III, (*E*,*E*)-farnesol, geraniol, and poly(ethylene glycol) 600 were procured from Sigma-Aldrich (St. Louis, MO, USA). (*Z*,*Z*)-farnesol, (E,E,E)- geranylgeraniol, methyl farnesoate (MF), and (*E*,*E*)-farnesoic acid were purchased from Echelon (Salt Lake City, UT). 2-decanol and citronellol were obtained from Acros Organics (Morris plains, NJ, USA). The purity of all chemicals was higher than 85% as confirmed using HPLC or gas chromatography (GC).

5.3.2. Enzymatic Terpene Alcohol Oxidation

In vitro enzymatic oxidation reactions were performed in the group of Dr. Fernando G. Noriega (Florida International University, Miami, FL, USA). Briefly, various terpene alcohols including farnesol, nerol, geraniol, and geranylgeraniol (GG-OH) standards were incubated with recombinant enzyme, farnesol dehydrogenase for 1h at 30°C in four centrifuge vials. Acetonitrile was added to stop reactions and the mixtures were vortexed. Supernatants obtained by centrifugation of the reaction mixtures were dried. Each dried extract containing approximately 20 μg of expected oxidized product (aldehydes) of the respective terpene alcohols was dissolved in 30 μL of HPLC grade methanol, prior to the DART-oaTOF MS analysis.

5.3.3. Sample Preparation for DART-oaTOF optimization, LOD, and In-source CID Experiments

All standard solutions were prepared in HPLC grade methanol. For optimization studies, a 4 mM farnesol working solution was prepared by diluting 4M neat farnesol. Serial dilutions of farnesol, JH III, MF, and FA containing 0.1-5 pmol/μL of the standards were prepared for LOD studies. One hundred μg of (2Z,6Z)-farnesol and (2E,6E)-farnesol were dissolved in methanol to prepare 4 mM stock solution. The respective stock solutions were diluted to prepare 2 μM working solutions of the two isomers for in-source CID experiments.

5.3.4. DART-oaTOF Set-up

A commercial DART ion source (IonSense Inc., Saugus, MA, USA) was interfaced with an oaTOF mass spectrometer (AccuTOF^{TM}) from JEOL USA, Inc. (Peabody, MA, USA). A detailed description of the commercial DART-AccuTOF instrument can be found elsewhere[229]. The gap between the DART source exit and the oaTOF cone inlet was approximately 12 mm. The DART discharge needle voltage of +3600 V and perforated electrode voltage of +150V were kept constant for all experiments. For the initial DART-oaTOF analysis of the terpene alcohol oxidized products, the DART exit grid voltage was set to 150 V, DART gas heater was kept at 100°C, and He gas flow-rate was held at 3 L/min. During optimization studies, the DART exit grid voltage was varied between 50 – 200 V, while the DART gas temperature and flow-rate ranged from 50-200 °C, and 0.55-2 L/min, respectively.

The oa-TOF mass spectrometer settings were as follows: Inlet orifice 1 temperature = 80 °C, Orifice 1 voltage = +20 V, orifice 2 = +5 V, ring electrode = 5 V, ion guide peak voltage = 300 V, and detector voltage = −2750 V. Data was acquired in the 50-600 *m/z* range. Total ion chronograms (TICs) were acquired for 6 min, by first collecting a background signal, then introducing PEG 600 internal standard for few seconds followed by the different oxidized products of terpene alcohols, one at a time in the ionization stream until the signal decreased to the background level. For optimization studies and in-source CID experiments, each TIC was acquired for 0.5 min and for LOD experiments, TICs of the individual standards containing 5 replicates per run were collected for 2 min. The data were processed by first extracting the mass spectra from respective TICs and the profile spectra were the centrioded and calibrated using the pre-calibrated PEG 600 mass spectra acquired in the same run.

5.3.5. DART-oaTOF Sample Introduction Method

Two sample introduction methods, namely, 'manual sample injection', and 'continuous sample infusion' were tested and used alternatively during the various studies. In the manual sample injection method, 2 μL of a given working solution were pipette-deposited on the tip of the DIP-it sampler, which was secured by a home-built sampling arm at a fixed vertical position (Figure 5.2a). For a single sample introduction event, the sampling arm was rapidly lowered so that its tip came in contact with the He stream from the DART ion source outlet, producing a transient signal.

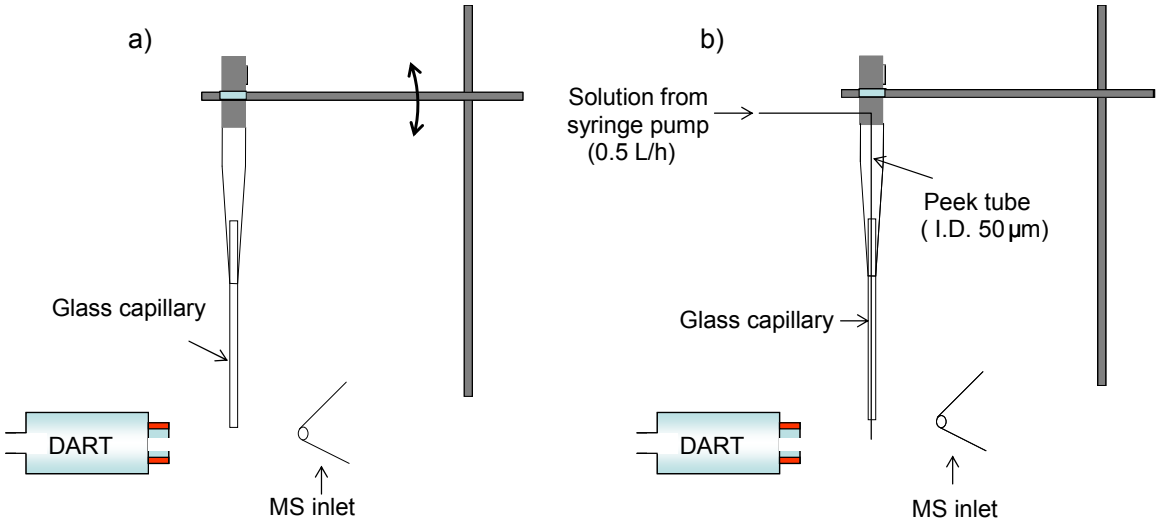

Figure 5.2. Sample introduction methods used in the DART-oaTOF experimental set up. (a) Manual sample injection, and (b) continuous sample infusion method.

In the continuous sample infusion method, the working solution was flowed at 0.55 L/min through a piece of PEEK tubing (360 µm O.D., 50 µM I.D.). One end of the PEEK tube was connected to a syringe pump delivering the fluid, and the other end was permanently positioned into the He gas stream with the aid of an open-ended DIP-it sampler capillary (Figure 5.2b). Manual sample injection was implemented for analyzing oxidized terpene alcohol products and for performing LOD studies where high-throughput analysis was desired. Continuous sample infusion was the method of choice for in-source CID analysis of farnesol isomers and for performing optimization studies for improving reproducibility and enabling to statistically estimate the effects of various experimental factors.

5.3.6. Design of Experiment Optimization

The DOE tool (DOE ++, Reliasoft Corp., Tucson, AZ, USA) was used to generate a randomized list of experiments to identify DART factors that significantly affected

sensitivity. The investigated factors were He gas temperature (factor A), gas flow-rate (factor B), and exit grid voltage (factor C). Each of these factors was assigned four settings (levels) which were as follows: factor A = 50 °C, 100 °C, 150 °C, and 200 °C; factor B = 0.55 L/min, 1.0 L/min, 1.5 L/min, and 2.0 L/min; factor C: 50 V, 100 V, 150 V, and 200 V. The general full factorial model developed consisted of 64 unique setting combinations for which five replicates were run, resulting in a total of 320 runs. For each run, the absolute signal intensity of the $[M+H]^+$ farnesol ion at *m/z* 205.19 was measured. The data was subjected to analysis of variance (ANOVA) by means of the DOE software, in which degrees of freedom, partial sum of squares, partial mean squares, F-ratios, and *p*-values were determined. Following full factorial designs, a response surface methodology (RSM) design was implemented to generate 39 individual runs to fine-tune the optimal settings for the most significant DART factors.

5.3.7. Limit of Detection (LOD) Experiments

All LOD experiments were performed using the optimized DART-oaTOF method. Two μL of diluted farnesol, JH III, MF and FA solutions were spotted on DIP-it samplers and analyzed using the manual sample injection method as described before. Each run comprised of five replicates.

5.3.8. In-source CID Experiments

The (2Z,6Z)- and (2E,6E)-isomers of farnesol were subjected to in-source CID at various orifice 1 fragmentation voltages (20-80 V). Breakdown plots of fragment ions

commonly observed in the in-source CID mass spectra of both isomers were plotted and their fragmentation profiles compared.

5.4. Results and Discussion

5.4.1. DART-oaTOF MS Analysis of Oxidized Terpene Alcohols

Figure 5.3 shows DART-oaTOF MS results obtained to confirm the products generated during an enzymatic oxidation process occurring during the synthesis of JH III in *Aedes aegypti*. Four sample extracts containing farnesol (extract 1), nerol (extract 2), geraniol (extract 3), and geranylgeraniol (GG-OH, extract 4) incubated with recombinant dehydrogenase enzyme were subjected to accurate mass measurements using DART-oaTOF[202]. The mass spectrum obtained from extract 1 (Figure 5.3a) showed a base peak at *m/z* 221.1900 corresponding to monoisotopic protonated farnesal $[farnesal+H]^+$, an aldehyde of farnesol, while the second peak at *m/z* 203.1801 corresponded to protonated farnesal with loss of one water molecule ($[farnesal-H_2O+H]^+$). The second most intense peak at 205.1955 corresponded to $[farnesol-H_2O+H]^+$ originating from unreacted farnesol in the extract. The experimental mass accuracies for $[farnesal+H]^+$, $[farnesal-H_2O+H]^+$, and $[farnesol-H_2O+H]^+$ ions were 0.2 ppm, 3.2 ppm and 2.1 ppm, respectively (Table 5.1). Mass spectra obtained from subsequent extracts containing other terpene alcohols as starting materials showed low intensity protonated monoisotopic peaks corresponding to the respective aldehydes, namely, neral at *m/z* 153.1273 (Figure 5.3b, extract 2), geranial at *m/z* 135.1171 (Figure 5.3c, extract 3), and geranylgeranial (GG-COH) at *m/z* 289.2500 (Figure 5.3d, extract 4).

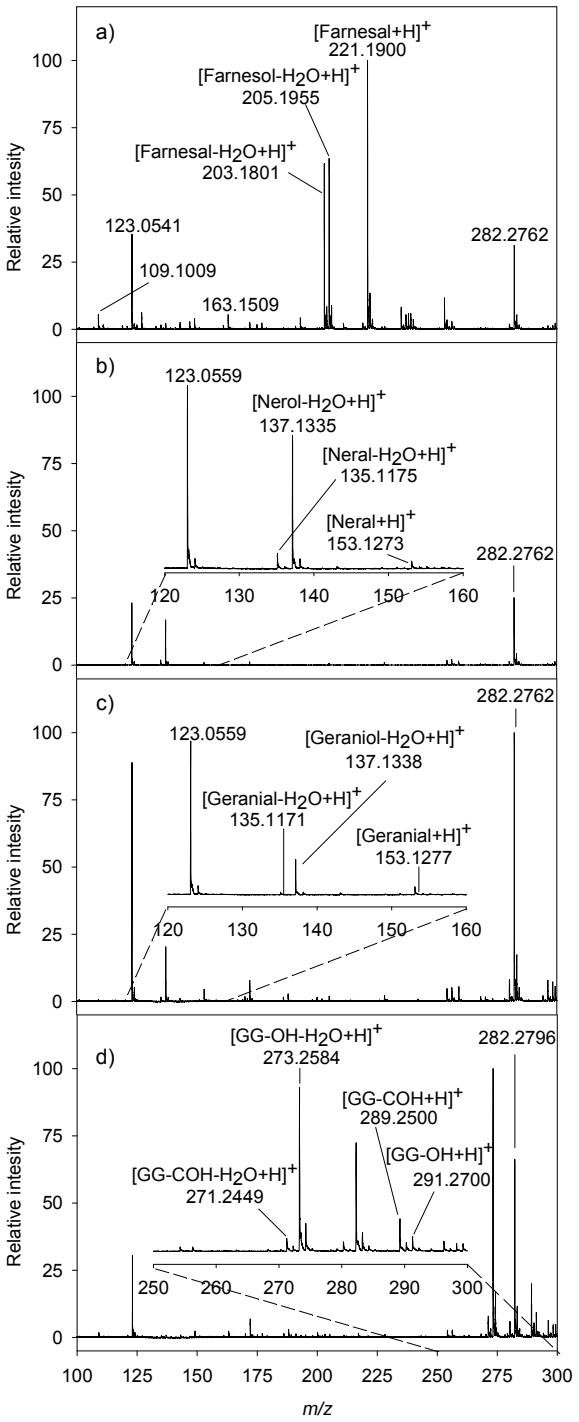

Figure 5.3. DART-oaTOF mass spectra obtained from extracts containing enzymatically oxidized products of (a) farnesol, (b) nerol (c) geraniol, and (d) geranylgeraniol (GG-OH), respectively.

Peaks corresponding to the loss of a H_2O molecule from the respective alcohols were also detected at *m/z* 137. 1335 for neral (extract 2), *m/z* 137.1336 for geraniol (extract 3) and at *m/z* 273.2584 for GG-OH (extract 4), as shown in Figures 5.3b-d. Unambiguous identities of the unoxidized terpene alcohols and their respective aldehydes were confirmed by accurate mass measurements. Despite the success in analyzing the products from these in-vitro enzymatic reactions, analysis of these metabolites at the sub-picomol to femtomol levels from more complex mixtures motivated us to pursue more in depth optimization studies described below.

Table 5.1. Mass accuracies of DART-oaTOF MS analysis of extracts containing oxidized products of various terpene alcohols

Analyte (M)	Type of ion	Theoretical mass	Experimental *m/z*	Mass accuracy (mmu)	Mass accuracy (ppm)
Farnesal (extract 1)	$[M+H]^+$	221.1899	221.1899	0.05	0.23
Farnesal (extract 1)	$[M-H_2O+H]^+$	203.1794	203.1801	0.66	3.25
Farnesol (extract 1)	$[M-H_2O+H]^+$	205.1951	205.1955	0.43	2.10
Neral (extract 2)	$[M+H]^+$	153.1274	153.1273	0.11	0.72
Neral (extract 2)	$[M-H_2O+H]^+$	135.1168	135.1175	0.68	5.03
Nerol (extract 2)	$[M-H_2O+H]^+$	137.1325	137.1335	1.05	7.66
Geranial (extract 3)	$[M+H]^+$	135.1168	135.1171	2.30	1.70
Geranial (extract 3)	$[M-H_2O+H]^+$	153.1274	153.1277	0.29	1.89
Geraniol (extract 3)	$[M-H_2O+H]^+$	137.1325	137.1336	1.09	7.95
Geranylgeranial (extract 4)	$[M+H]^+$	289.2526	289.2500	2.57	8.88
Geranylgeranial (extract 4)	$[M-H_2O+H]^+$	271.2420	271.2449	2.89	10.54
Geranylgeraniol (extract 4)	$[M+H]^+$	291.282	291.2700	1.75	6.00
Geranylgeraniol (extract 4)	$[M-H_2O+H]^+$	273.2677	273.2584	0.70	2.56

5.4.2. DOE Optimization of DART-oaTOF Method

As with any ambient ionization techniques, the sensitivity of DART is a function of the efficiency of ion transmission from the ambient pressure region into the vacuum regions of the mass spectrometer. Various factors including sample ionization, DART exit to mass spectrometer inlet distance, He gas flow-rate, gas temperature, and DART exit grid voltage affect ion transmission in DART[228]. In the present DART-oaTOF set-up, where the sample was positioned equidistantly in the 12 mm gap between the DART exit

and the oa-TOF inlet, the effects of the DART parameters on the DART MS sensitivity we investigated using a 4 mM farnesol working solution.

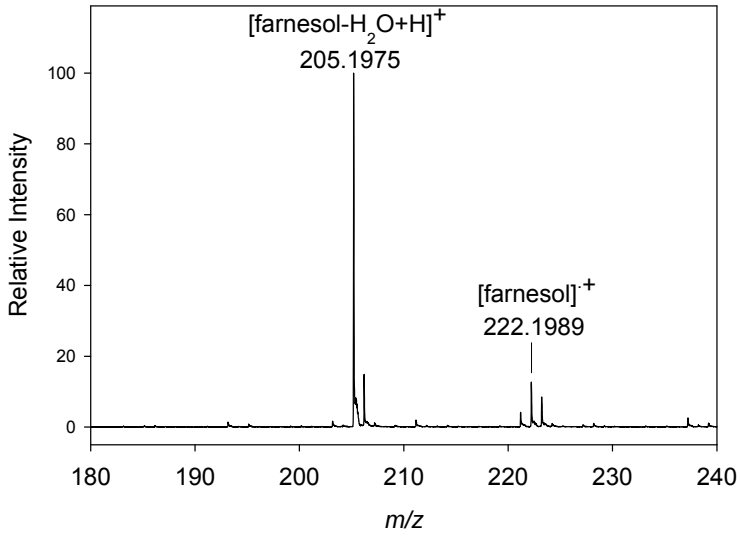

Figure 5.4. DART-oaTOF mass spectrum of 4 mM farnesol solution obtained using the manual sampling injection method.

Typical DART-oaTOF mass spectra of the 4 mM farnesol solution sample used for optimization purposes showed a base peak at *m/z* 205.1975 corresponding to $[\text{farnesol-H}_2\text{O+H}]^+$ along with a low intensity peak at *m/z* 222.1989 corresponding to farnesol molecular ion $[M]^{\cdot+}$ (Figure 5.4). The presence of the molecular ion was attributed to a direct Penning ionization process[222] in which long-lived He* reacts directly with analyte molecules (M) whose ionization energy is below 19.8 eV, forming a positively charged molecular ion $[M^{\cdot+}]$ with release of an electron (reaction 5.3). It is likely that the first ionization potential of farnesol is lower than 19.8 eV, as with other common organic molecules[230-232]. A second possible molecular ion formation reaction in DART was recently suggested by Cody[233] in which He^* first reacts with ambient O_2 to

form $O_2^{+\cdot}$ ions which subsequently react with analyte molecules (M) to generate to generate $M^{\cdot+}$ in a charge exchange reaction (reaction 5.4, and 5.5)

$$He^{*} + O_2 \rightarrow O_2^{\cdot+} + e^{-} + He \cdots\cdots\cdots\cdots\cdots\cdots\cdots\cdots (5.4)$$

$$O_2^{\cdot+} + M(g) \rightarrow M^{\cdot+} + O_2 \cdots\cdots\cdots\cdots\cdots\cdots\cdots\cdots (5.5)$$

It has been reported that certain DART parameters favor molecular ion formation by direct or indirect Penning ionization pathways over the more commonly observed protonated ions. Distances of up to 15 mm between the DART ion source nozzle and the mass spectrometer inlet, exit grid voltages of about 650 V, and placing the sample closer to the DART exit are known to favor $M^{\cdot+}$ ion formation. In the present DART-oaTOF set-up, the sample was placed equidistant to the DART exit and the mass spectrometer inlet, while the grid voltage was below 250 V, and the DART exit to MS entrance distance was 12 mm, which explains the predominance of protonated analyte species. Cody[233] also suggested that the use of a glass sampling probe, such as the DIP-it sampler used in the present study, may favor molecular ion formation by reducing the relative abundance of NO^{+}, and increasing the abundance of $O_2^{\cdot+}$ species under ambient conditions. These observations suggest that the DART MS experimental conditions can be manipulated to generate specific types of ions for analyzing polar and nonpolar compounds alike. Additionally, the presence of a molecular ion can be used as an additional diagnostic tool for identification of a compound by DART MS. Initial optimization experiments performed using the manual sample injection method suffered from large variations in the signal intensities, with % coefficient of variance (CV)

ranging from 20% - 60% (Figure 5.5a). In order to circumvent this problem and to maximize confidence in the DOE optimization results, a new sample introduction method referred to as a continuous sample infusion was developed. A comparison of the TICs obtained using both methods clearly showed that the manual sample injection reproducibility for these highly volatile compounds was quite low, (Figure 5.5a), whereas the continuous sample infusion method showed a more steady and reproducible signal with % CV between 5 – 15% (Figure 5.5b).

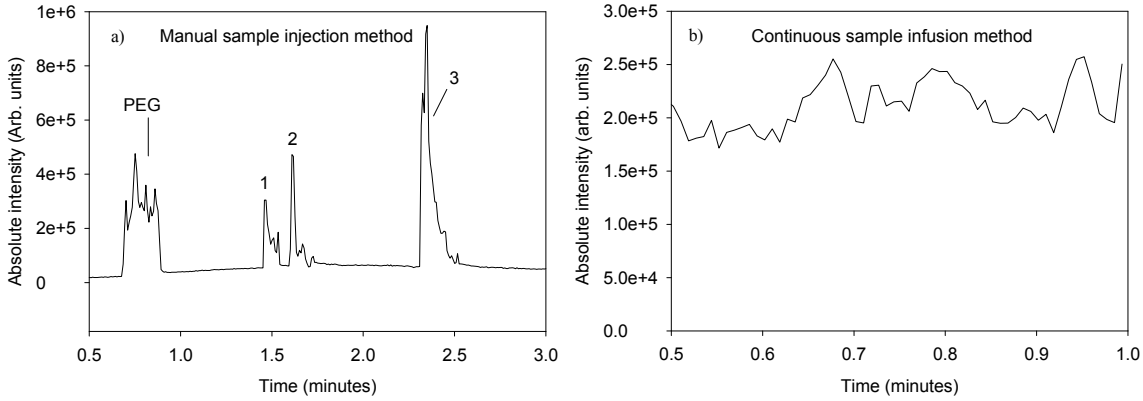

Figure 5.5. Total ion chronograms (TICs) of a 4 mM farnesol solution introduced in the DART-oaTOF gap using (a) manual sample injection, and (b) continuous sample infusion. Observed spikes in the TIC in (a) correspond to the introduction of PEG 600 internal standard followed by farnesol solution in triplicate.

The ANOVA results from the DOE optimization study are shown in Table 5.2, their significance is shown by the corresponding *p*-values. These suggested that He gas temperature (A-factor, *p*-value: 1.36×10^{-203}) was the most significant factor, followed by gas flow-rate (B-factor, *p*-value: 3.16×10^{-78}), and the combination of the two factors (A:B, *p*-value: 1.63×10^{-10}), as compared to DART grid voltage (C-factor, *p-value*: 0.8105).

Table 5.2. Analysis of Variance (ANOVA) table showing significant DART variables (in red) affecting DART-oaTOF sensitivity. Default *p*- value = 0.1. AB indicates the interaction between gas temperature and gas flow-rate.

Source of variations	Degrees of freedom	Sum of squares (partial)	Mean squares (partial)	F-ratio	*p*-value
Model	63	7.97E+09	1.21E+08	170.0634	2.64E-177
A: temperature	3	7.28E+09	2.43E+09	3261.3299	1.36E-203
B: flow-rate	3	5.92E+08	1.97E+08	265.2302	3.16E-78
C: grid voltage	3	7.16E+05	2.39E+05	0.3207	0.8104
AB	9	5.40E+07	6.00E+06	8.0615	1.63E-10
BC	9	8.82E+06	9.80E+05	1.316	0.2287
AC	9	9.32E+06	1.04E+06	1.3906	0.1925
ABC	27	2.59+E07	9.58E+05	1.2867	0.1621
Residual	256	1.91E+08	7.44E+05		
Pure error	256	1.91E+08	7.44E+05		
Total	319	8.16E09			

The *p*-values represent a probability which reflects the measure of evidence against the null hypothesis[234]. Small *p*-values correspond to strong evidence and vice versa. In the present study, in order to test whether certain DART variables affect the signal intensity more significantly than others, a null hypothesis of equality between sensitivity under two different conditions needs to be rejected. The experimentally observed differences could show an unequal response between two conditions, leading to rejection of the null hypothesis. However, the observed differences might not be due to the inequality of the variables, but might be due to measurement variance. If a *p*-value is below 0.1 (a pre-defined level of significance limit), then the probability that the observed difference is by chance is below 10%. The pre-defined limit is needed to make a decision on either rejecting or accepting the null hypothesis. If the *p*- value is less than 0.1, the null hypothesis can be rejected. In other words, if the *p*-value for a given factor is above 0.1, then the factor is considered insignificant.

From the ANOVA table shown below, *p*-values of factors A, B, and A:B were below 0.1, rendering these factors significant (last column, Table 5.2)., while the high value of factor C (0.8 > 0.1) suggested that the effect of DART grid voltage on the observed signal intensity was insignificant.

A plot of average [farnesol-H_2O+H]$^+$ signal intensity at various gas flow-rates and temperatures, and at a constant grid voltage (200 V) showed that higher gas temperatures and flow-rates enhanced sensitivity (Figure 5.6a). One possible explanation to this effect is that at elevated gas temperatures, the analyte evaporation rate increases with a concomitant increase in the ion yield. Higher gas flow-rates should be beneficial in terms of more efficient ion transport before diffusional losses become predominant. The effect of DART exit grid voltage on the signal intensity was not significant, where increasing the grid voltage from 50-200 V showed an increase in the signal intensity by approximately 10% (Figure 5.6b).

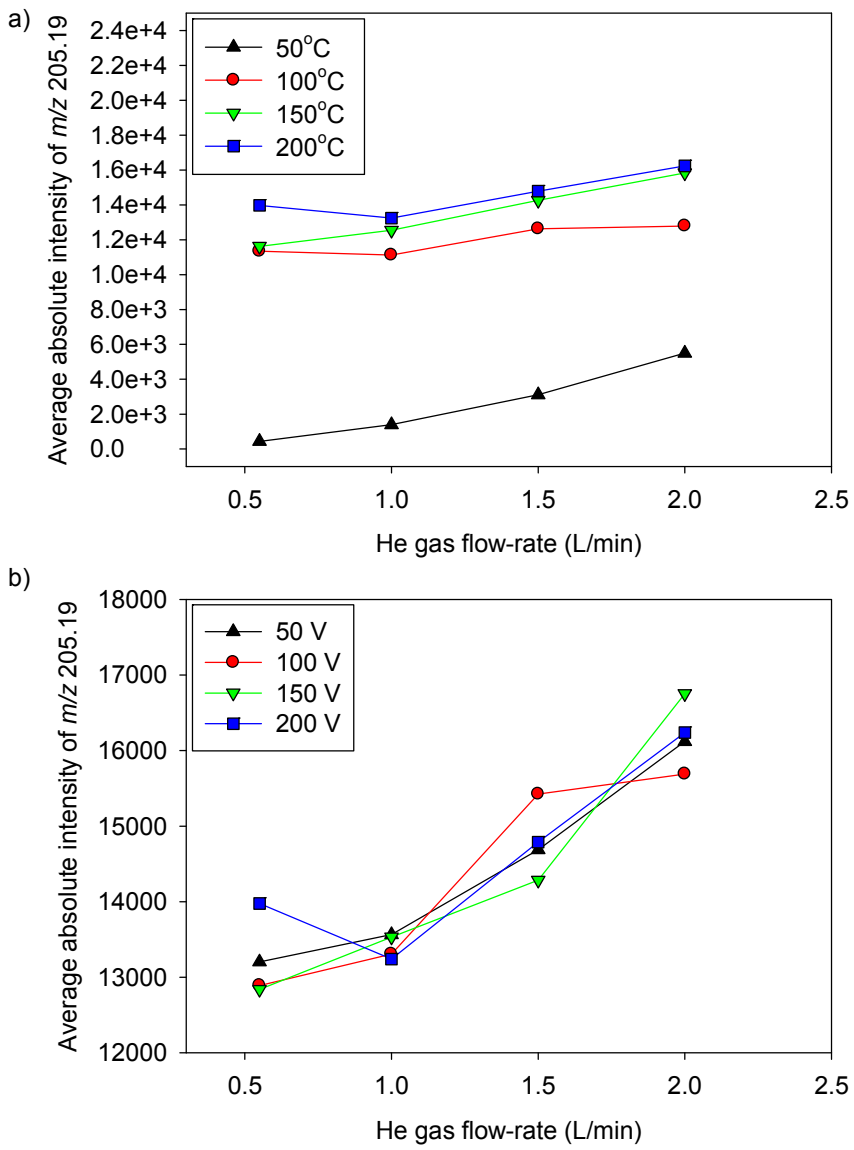

Figure 5.6. Effect of the most significant DART variables on sensitivity. Interaction plots showing absolute intensity of the *m/z* 205.19 ion as a function of He gas flow-rates at (b) various gas temperatures and at a constant grid voltage of 200 V, and at (c) various grid voltages at and at a constant gas temperature of 200 °C

In early DART work, the stated function of the grid voltage was to prevent ion-ion recombinations[88], however it also creates a weak extraction electric field across the sampling gap between source exit and orifice 1 of oaTOF, enabling ions closer to the orifice to be transmitted. This was evident from the observed small increase in signal,

when varying grid potential from 50-200 V at low flow-rates. However, the improvement in ion transmission efficiency caused by carrier gas flow increase superseded the ion transmission enhancement caused by this weak electric field.

DOE studies indicated that the optimal response was obtained within the following settings: DART gas temperature = between 150-200 °C, gas flow-rate = 2 L/min, and exit grid = between 150-200 V. Further optimization of these variables via response surface methodology (RSM) using a Box-Behnken model concluded that the following optimum settings should be chosen: He gas temperature = 200 °C, gas flow-rate = 2 L/min, and exit grid voltage = 180 V.

5.4.3. Limit of Detection of the Optimized DART-oaTOF Method

Figure 5.7 shows DART-oaTOF mass spectra obtained from a 0.1 pmol/μL solution of farnesol, 1 pmol/μL solution of JH III, and 4 pmol/μL of both, MF and FA. Mass spectra of all analytes (M) showed base peaks corresponding to protonated $[M+H]^+$ ions, except for farnesol, in which with the water loss ion was the dominant peak. The experimentally obtained mass accuracies of the analytes were as follows: 0.6 ppm for $[\text{farnesol-}H_2O+H]^+$ (*m/z* 205.1952), 0.8 ppm for $[\text{JH III}+H]^+$ (*m/z* 267.1957), 1.8 ppm for $[MF+H]^+$ (*m/z* 251.2001) and 5.8 ppm for $[FA+H]^+$ (*m/z* 273.1863).

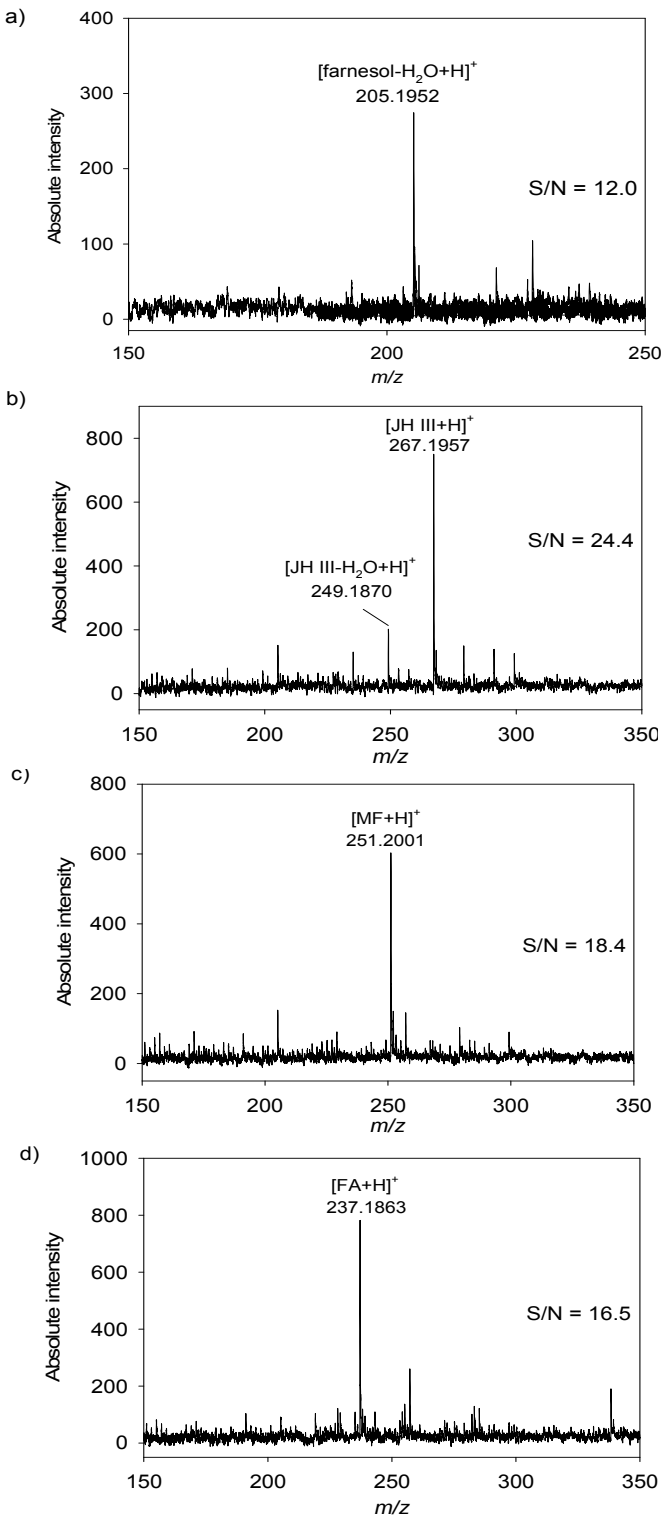

Figure 5.7. DART-oaTOF mass spectra of (a) 0.1 pmol/µL of farnesol, (b) 1 pmol/µL of juvenile hormone (JH) III, and 4 pmol/µL of (c) methyl farnesoate (MF), and (d) farnesoic acid (FA), respectively.

The experimentally calculated signal-to-noise (S/N) ratios for these analytes were 12 for farnesol (0.1 pmol/μL), 24.4 for JH III (1 pmol/μL), 18.4 for MF (4 pmol/μL), and 16.5 for FA (4 pmol/μL), as shown in Figure 5.7. The detection limits calculated from these S/N ratios were as follows: 25 fmol/μL for farnesol, 123 fmol/μL for JH III, 650 fmol/μL for MF, and 730 fmol/ μL for FA.

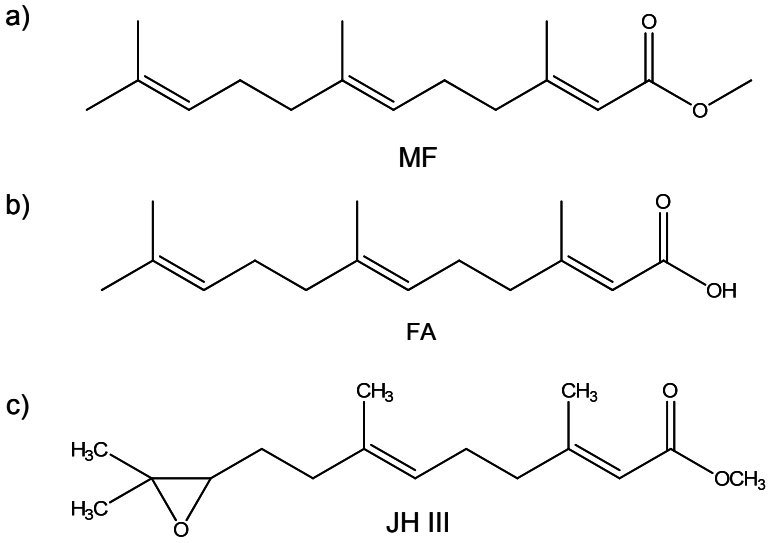

Figure 5.8. Structures of (a) MF, (b) FA, and (c) JH III.

The observed differences in detection limits follow expected differences in ionization efficiencies of the species under investigation. A higher ionization efficiency of JH III compared to MF and FA can be rationalized based on the corresponding molecular structures (Figure 5.8). Unlike MF (Figure 5.8a) and FA (Figure 5.8b), JH III (Figure 5.8c) contains an epoxy group that can serve as an additional proton binding site, contributing to a higher basicity of this molecule.

In *Aedes aegypti* mosquitoes, the highest amount of JH III produced in *corpora allata* glands is about 30-50 fmol/hour[206]. Previous studies have shown that *corpora*

allata glands stimulated with FA produced up to 1 pmol of JH III in 5 hours[207]. Therefore, the sensitivity afforded by the optimized DART-oaTOF method is expected to allow for the detection of changes of isoprenoid pools from *corpora allata* cultured *in vitro*, with a sample throughput of three samples per minute.

In an attempt to further improve the detection limits DART was coupled to a hybrid quadrupole time-of-flight (Q-TOF) mass spectrometer (MicroOTOF-Q I, Bruker Daltonics Inc., Billerica, MA, U.S.A.) for performing single reaction monitoring (SRM) experiments. In order to maintain a stable vacuum, and to further improve the sensitivity, a gas ion separator (Vapur interface, IonSense Inc., Saugus, MA, U.S.A.) was added to the front end of the Q-TOF mass spectrometer.

Despite the fact that all compounds were detectable with this approach, extensive memory effects were observed when using the Q-TOF set-up. This persistent contamination probably originates due to deposition of sample residues in the interior surfaces of the glass ion transfer capillary and the ion funnel optics in the front end of the instrument. As a result of this contamination, intense background farnesol fragment ions dominated blank SRM spectra, even after careful cleaning of all surfaces in close proximity with the ion beam. Experiments using this approach were thus discontinued.

5.4.4. Distinguishing between Farnesol Isomers by DART In-source CID MS

In addition to accurate mass measurements, in-source CID can also produce useful information for structural determination purposes. Along this line of thought, DART in combination with CID experiments was used for distinguishing between two farnesol isomers. Studies of enzymatic oxidation of farnesol in some insects such as

Manduca sexta have showed high specificity for one particular isomer[203]. Furthermore, only one farnesol stereoisomer showed biological activity in nutria[235]. Therefore, distinguishing between active and inactive isomers is important from the biological point of view. The fragmentation profiles of farnesol isomers obtained by CID MS could serve as fingerprints for identifying the stereochemistry of endogenous farnesol in *Aedes agypti*. Similar studies undertaken by Lee et al.[235] to determine the configurations of four farnesol isomers using EI and CI was only partially successful as the CI mass spectra of the isomers only showed small differences in fragmentation patterns. To that end, we explored in-source CID DART-generated ions as an alternative strategy.

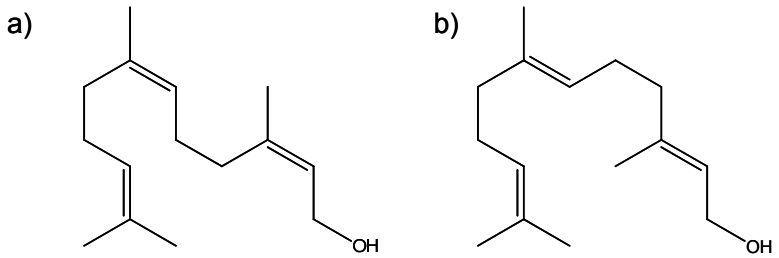

Figure 5.9. Farnesol isomers

Two µM (2Z,6Z)- and (2E,6E)-farnesol isomer (Figure 5.9) working solutions were subjected to in-source CID at various orifice 1 voltages. The in-source CID mass spectra of both isomers showed several common fragments at *m/z* 81, 95,109,121,135, and 149, along with the base peak at *m/z* 205.19, arising from neutral loss of one water molecule from the protonated farnesol ion when the orifice 1 voltage was held at 40 V (Figure 5.10a-b). When screened against the NIST EI MS reference database the DART-oaTOF CID spectrum of farnesol showed similarities in its spectral features when

compared to its EI spectrum{, #335; , #40}. The EI mass spectra of most aliphatic alcohols show alkene ions as the dominant species by loss of H_2O. Therefore, it was suggested that these alkene ions rather than their alkanols be considered to analyze the EI fragment ions[237]. The EI MS spectra of aliphatic alkenes show fragment ions with losses of ethene ($-C_nH_{2n}$) units[238]. A similar fragmentation pathway was considered to explain the observed farnesol fragment ions in CID spectra (Figure 5.10). After the formation of the protonated farnesol alkene by loss a H_2O molecule ($[farnesol-H_2O+H]^+$, *m/z* 205.10), the alkene could undergo further fragmentation by losses of ethene units. The fragment ions thus formed were as follows: *m/z* 163.15 ($-C_3H_6$), 149.13 ($-C_4H_8$), 135.11 ($-C_5H_{10}$), 121.10 ($-C_6H_{12}$), 107.08 ($-C_7H_{14}$), and *m/z* 93.06 ($-C_8H_{16}$). Further investigation, by deuterium labeling studies should be pursued to support the previous hypothesis.

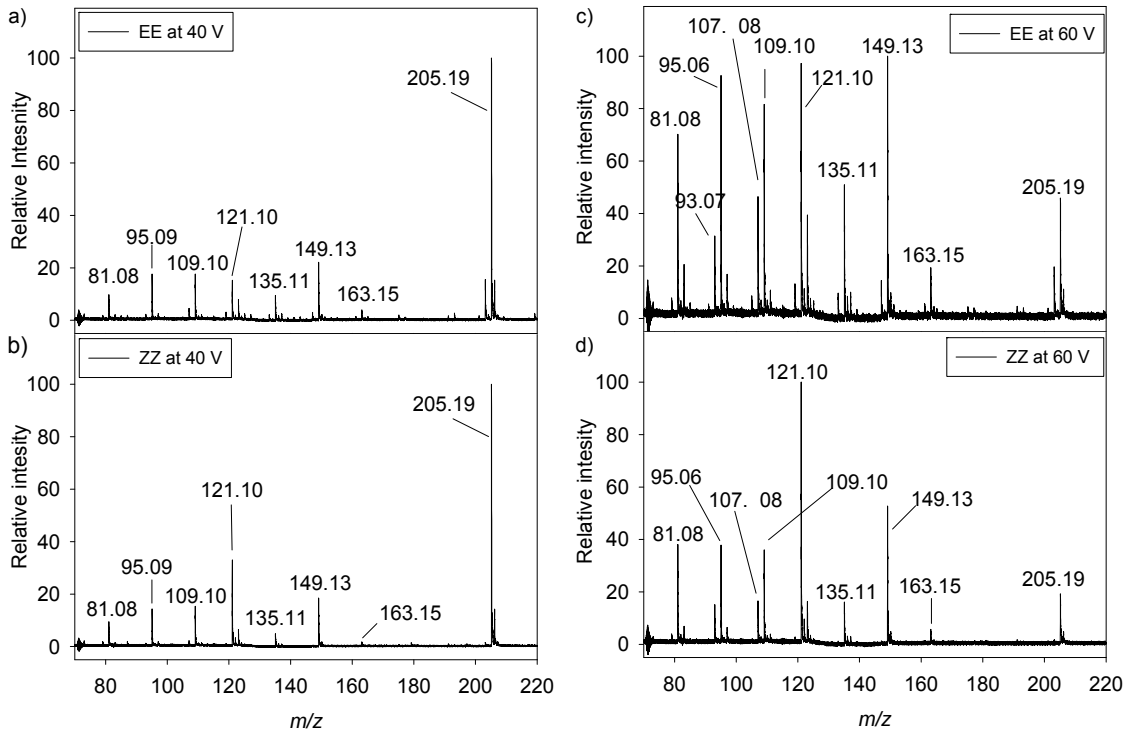

Figure 5.10. In-source collision-induced dissociation (CID) mass spectra of (2Z,6Z)- and (2E,6E)- farnesol isomers at (a,c) 40 V, and at (b,d) 60 V orifice 1 voltages using the DART-oaTOF set-up

As the acceleration voltage was increased from 40 V to 60 V, intense fragment ion signals dominated the CID spectra of both isomers (Figure 5.10c-d). The relative intensity ratios of several fragment ions such as 95:121, 109:121, and 121:149 differed significantly for the two isomers at a given orifice 1 voltage as shown in Figure 5.11. The relative intensity ratios of fragments 95:121 and 121:149 were appreciably different for the two isomers at all orifice 1 voltages, except for 80 V and 100 V (Figure 5.11a and 5.11c). On the other hand, dramatic differences in the ratio of 109:121 were observed at these high voltages (Figure 5.11b). These variations correlate with the different configurations of carbon-carbon double bond at C-2 of the two farnesol isomers.

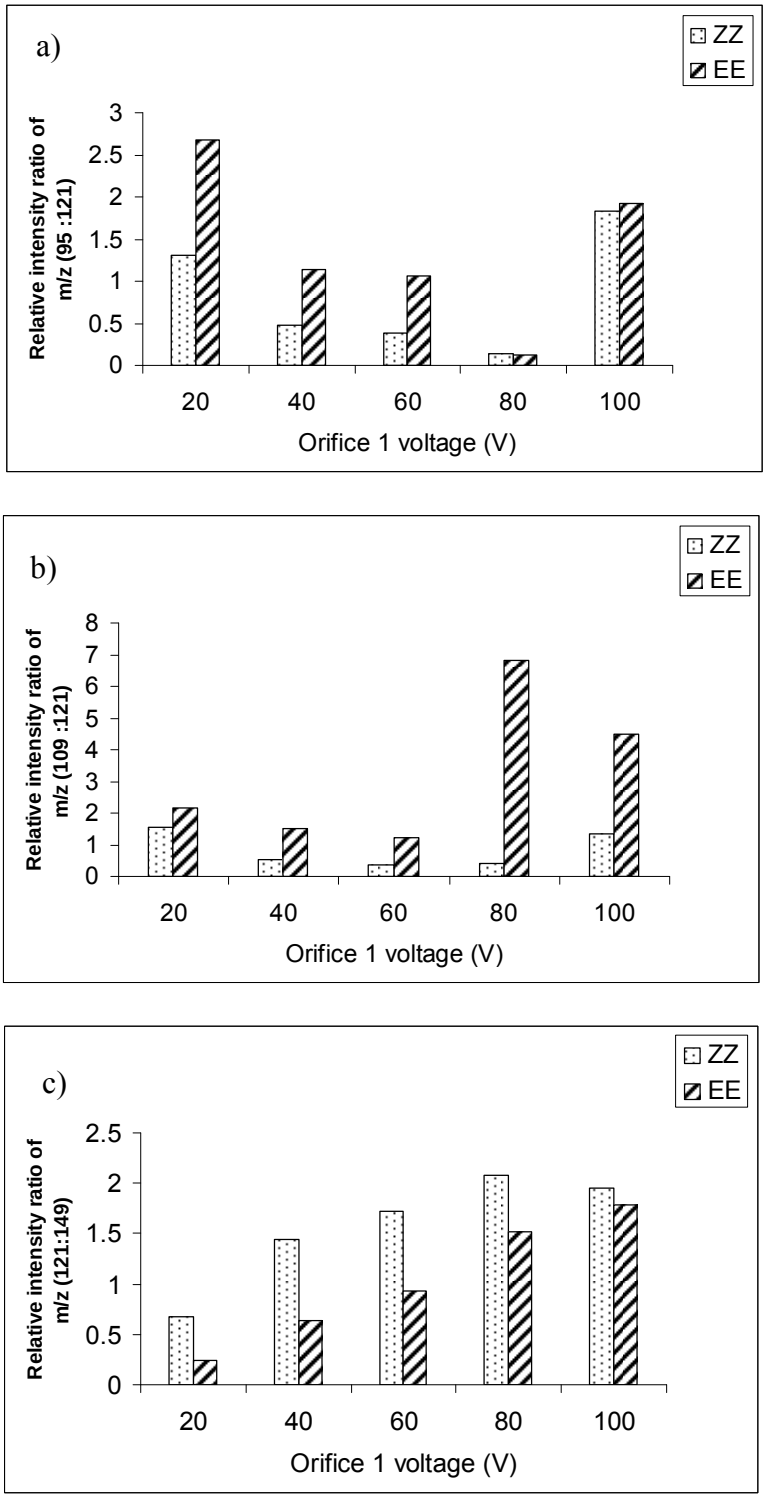

Figure 5.11. Relative intensity ratios for various pairs of fragment ions (a) 95:121, (b) 109:121, and (c) 121:149 as a function of orifice 1 voltage for (2Z,6Z)- and (2E,6E)-farnesol.

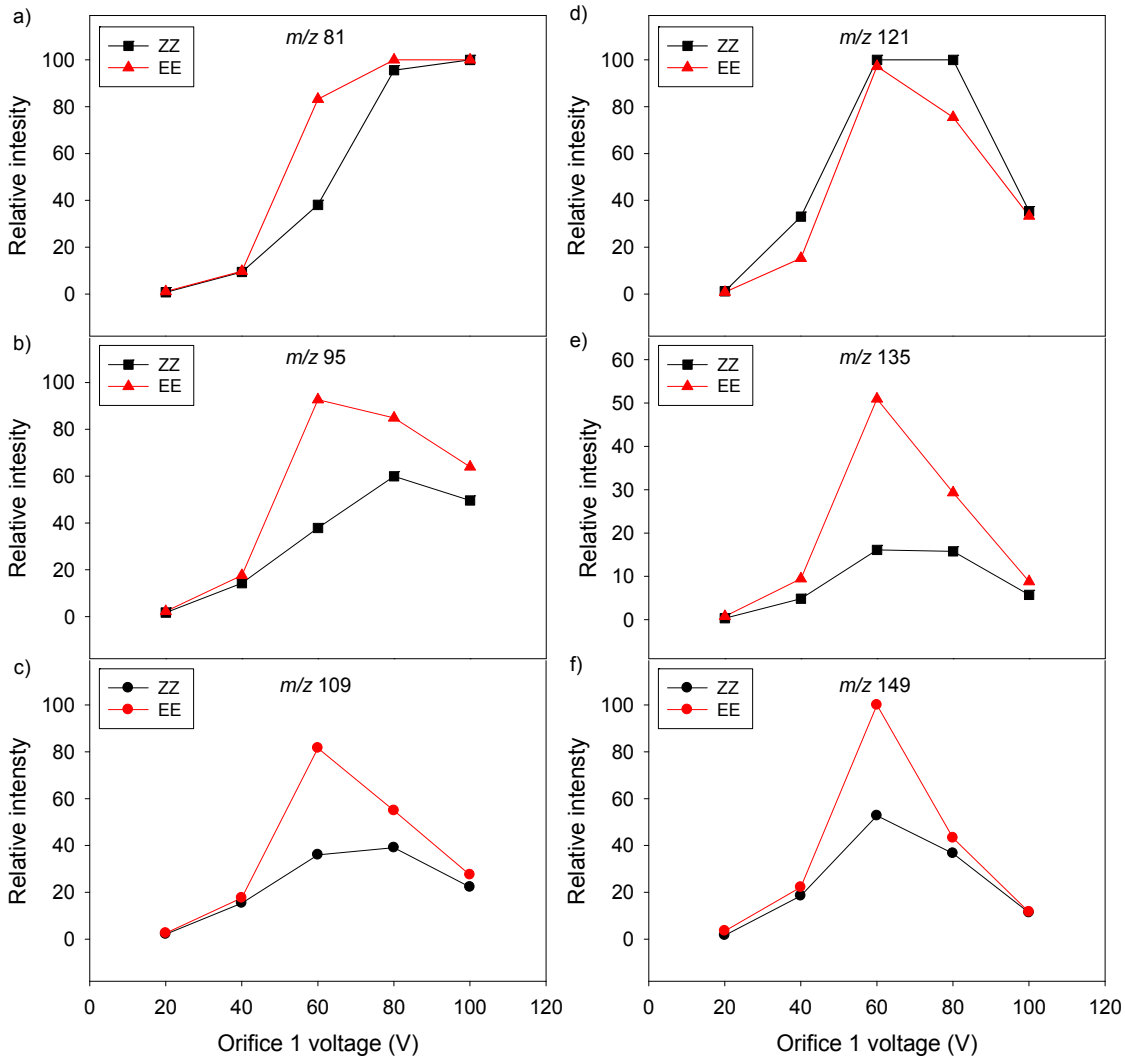

Figure 5.12. Breakdown plots of the commonly observed fragment ions at *m/z* (a) 85, (b) 95, (c) 121, (d) 109, (e) 135, and (f) 149 in the in-source CID mass spectra of (2Z,6Z)- and (2E,6E)-farnesol isomers. Relative intensity of each fragment ion was plotted as a function of orifice 1 voltage.

Furthermore, breakdown plots for both isomers were compared to study the differences in the fragmentation profiles of some of the commonly observed fragments in respective CID mass spectra (Figure 5.11a-f). These breakdown plots with characteristic fragmentation patterns could be used as standards to identify an unknown farnesol isomer. However, in order to implement this strategy to identify a particular isomer from

a racemic mixture, separations of these isomers by GC prior to the MS analysis would be essential.

Encouraging results from these experiments highlighted the potential of in-source CID of DART ions for discriminating stereoisomers. Except for fragment ion at *m/*z 121 (Figure 5.11d), the breakdown plots of all fragment ions showed differences in the fragmentation patterns for the (2Z,6Z)- and (2E,6E)-farnesol isomers. Overall, the relative fragmentation efficiency of the EE-isomer was found to be greater than that of ZZ-farnesol at orifice 1 voltages between 40 V and 80 V. These breakdown plots with characteristic fragmentation patterns could be used as standards to identify an unknown farnesol isomer.

5.5. Conclusions

An in depth characterization and optimization of DART parameters allowed for the development of a high-sensitivity DART-oaTOF MS approach for the rapid analysis of mosquito terpenoids. The examination of DART-oaTOF mass spectra of farnesol revealed the presence of a molecular ion along with the corresponding protonated species, indicating the presence of competing ionization mechanisms. With the optimized DART-MS method, LOD ranging from sub-picomole to femtomole were achieved for JH III and its precursors. With such detection limits, and mass accuracies below 5 ppm, it could be possible to selectively detect endogenous levels of these biologically significant molecules. Additionally, we have shown that in principle it is possible to distinguish between farnesol isomers based on differences in the in-source CID fragmentation profiles. This particular application of DART-oaTOF can be useful to study enzymes

responsible for the preferential production of one isomer over the other in the enzymatic pathway of JH III biosynthesis.

CHAPTER 6. CONCLUSIONS AND FUTURE OUTLOOK

6.1. Abstract

This Chapter presents a summary of the results of my work with AP-MALDI and DART, followed by a brief discussion of the strengths and limitations of the various research methodologies selected to achieve the goals. The chapter concludes with a discussion of possible future directions to extend this work.

6.2. Improving AP-MALDI Sensitivity

6.2.1. Summary of Accomplished Task in Developing Enhanced Sensitivity AP-MALDI Approaches

Since the first report on AP-MALDI in 2000[80], its softer ionization capabilities have been widely explored for the analysis of fragile biomolecules[81, 82, 84]. At the same time, its less-than-optimal sensitivity is now apparent, and with a few exceptions[85, 86], the field has remained relatively open for new research. To that extent, the first part of this dissertation was geared towards exploring new methods to enhance AP-MALDI sensitivity for analyzing biomolecules such as neuropeptides and protein digests. Two different approaches were investigated for this purpose, starting with an on-chip sample purification strategy, and followed by designing an in-line PA-AP-MALDI ion source.

The use of preconcentration chips improved AP-MALDI sensitivity by two orders of magnitude, enabling AP-MALDI-IT MS analysis of pico to nanomolar concentrations of derivatized protein digests and neuropeptides obtained from a mosquito head extract samples[239].

The strength of the on-chip preconcentration/focusing approach resides in the characteristic wettability gradient offered by the focusing targets, which enabled deposition of larger (5-20 μL) sample volumes for preconcentration as compared to conventional AP-MALDI targets with 1-2 μL sample loading capacity. Secondly, with these chips it was possible to use a 10-fold lower MALDI matrix concentrations, culminating in improved S/N ratios with negligible matrix background noise. Furthermore, this approach offered a viable option for solid-phase extraction of size limited samples. This is a significant feature, since most of the currently available purification techniques, such as molecular weight cut-off centrifuge filters[96], or SPE magnetic beads[148] require sample dilutions and larger starting volumes. Lastly, no major modifications were needed in the ion source design in order to couple on-chip preconcentration/focusing to AP-MALDI.

It was observed that the focusing targets' dynamic range was limited to sub-picomoles per loading site, and that depositing higher analyte amounts resulted in saturation. Another limitation of these substrates surfaced when initial attempts to preconcentrate and focus neuropeptides from crude mosquito head extracts were unsuccessful. Non-specific surface adsorption of sample proteins significantly altered surface wettabiliy. This problem was overcome by removing these interfering proteins using on-tip SPE micro tips[64] prior to the on-chip preconcentration step. Although a stepwise purification was needed for the crude extracts, this approach was substantially faster than other multiple-step routine fractionation methods used prior to the MS neuropeptides analysis[121].

The second approach to improve AP-MALDI sensitivity was directed toward development of an in-line PA-AP-MALDI source for more efficient ion transmission. This new in-line PA-AP-MALDI demonstrated enhanced sensitivity along with a reduction in the matrix background and analyte-matrix adduction as a consequence of the de-clustering effect of the carrier gas. Although this effect has been reported previously[85] using countercurrent gas flow, the co-axial direction employed in the present design resulted in better detection limits. The effectiveness of this strategy was especially evident in the presence of a static ion extraction field. Applicability of the in-line PA-AP-MALDI technique to small molecule analysis was limited by the increase in observed fragmentation.

6.2.2. Proposed Future Directions

Considerably more work needs to be done in order to overcome the observed limitations of the on-chip preconcentration/focusing and in-line PA-AP-MALDI methods for improving their performances. To that end, the following studies are recommended for future research:

1. Inherent to SAMs is the contamination of their surface by non-specific adsorption which alters its hydrophobic or hydrophilic properties[240]. Therefore, it is recommended that various types of SAMs resistant to protein adsorption be investigated. Zwitterionic SAMs[241], SAMs presenting poly(ethylene) glycol moieties[242] or derivatized terminal groups[243] could be explored as potential candidates.

2. The layer of surface-bound water on hydrophobic SAM is known to stimulate protein adsorption[124]. During on-chip focusing of peptides, surrounding humidity influenced the focusing ability of the targets. Therefore, future investigation of humidity-resistant SAMs is recommended. To that end, densely packed monolayers of alkanethiols can be evaluated, since the robust molecular architecture provided by these SAMs on a copper substrate has shown excellent resistance to surrounding moisture[244, 245].

3. The encouraging results with in-line PA-AP-MALDI showed that the carrier gas entrained bigger peptide molecules with a concomitant reduction in the matrix signal in the lower mass range. It was postulated that the co-axial gas flow deviated small molecules from their trajectories. However, no concrete evidence could be obtained to support this hypothesis. Therefore, it is recommended that future research be undertaken to simulate co-axial gas flow, and ion trajectories of small and large molecules under AP conditions.

4. Neutralization of positively charged MALDI ions by photoelectrons emitted by metal targets upon laser irradiation[55] was suggested to lower MALDI sensitivity[43, 57, 192]. SF_6, a well known electron scavenging gas[193] was evaluated to improve PA-AP-MALDI sensitivity by removing available photoelectrons for the neutralization reaction. On the contrary, inelastic collisions between analyte and heavy SF_6 molecules produced extensive

fragmentation of the analyte. Therefore, it would be worth exploring the effects of another scavenger gas, O_2[246], which is much lighter than SF_6.

5. A study by Frankevich et al.[192] showed that replacing metal targets with non-metal substrates dramatically improved MALDI sensitivity, reinforcing the the role of photoelectrons in the MALDI process. Therefore, similar studies could be conducted to explore the possibility of further improving the performance of in-line PA-AP-MALDI.

6. Finally, the possibility of performing AP-MALDI in combination with Venturi devices[247-250] or flared API capillary inlets used for ESI[249, 251] for improving ion transmission could be pursued.

6.3. DART Ionization of Terpenes

6.3.1. Summary of Accomplished Tasks

DART-MS was a very powerful technique for ionization and identification of JH III and its terpene precursors by accurate mass measurements[202]. Experiments were performed to characterize and optimize the effects that varying DART parameters had on the overall sensitivity observed for the detection of a terpene alcohol. It was observed that the He gas temperature and flow-rate had the largest effect. The optimized DART-oaTOF method showed LODs close to endogenous levels with the added advantage of high-sample throughputs. Although obtaining useful DART data was rapid, large experimental variations were apparent due to irreproducibility in the sample introduction method. This

problem was circumvented by implementing a more robust, and steady method of sampling, with a caveat, that with the use of this method, the high-throughput feature of DART ionization was compromised.

6.3.2. Proposed Future Directions

Further work in the following area is recommended:

1. It is recommended that the optimized DART-oaTOF method be applied to real-world *corpora allata* sample extracts in order to test its applicability as a rapid screening and profiling tool.

2. Critical proof-of-principle in-source CID experiments demonstrated the capability of DART-oaTOF to distinguish between ZZ- and EE-farnesol isomers. As a next step, it is recommended that this method be implemented to identify the stereochemistry of endogenous farnesol.

REFERENCES

(1) Vastola, F. J.; Mumma, R. O.; Pirone, A. J. 'Analysis of organic salts by laser ionization',*Org.Mass Spectrom.* **1970**, *3*, 101-104.

(2) Karas, M.; Hillenkamp, F. 'Laser desorption ionization of proteins with molecular masses exceeding 10000 daltons',*Anal. Chem.* **1988**, *60*, 2299-2301.

(3) Hunt, D. F. 'New ionization techniques in mass spectrometry',*Int. J. Mass Spectrom. Ion Phys.* **1982**, *45*, 111-123.

(4) Beckey, H. D. 'Field desorption mass spectrometry: A technique for the study of thermally unstable sunstances of low volatility',*J.Mass Spectrom. Ion Phys.* **1969**, *2*, 500-530.

(5) Beckey, H. D.; Schulten, H. R. 'Field desorption mass-spectrometry .2. New analytical methods',*Angew. Chem. Int.Edt.* **1975**, *14*, 403-415.

(6) Rollgen, F. W.; Giessmann, U.; Heinen, H. J.; Reddy, S. J. 'Field-ion emitters for field desorption of salts',*Int. J. Mass Spectrom.* **1977**, *24*, 235-238.

(7) Posthumus, M. A.; Kistemaker, P. G.; Meuzelaar, H. L. C.; Tennoeverdebrauw, M. C. 'Laser desorption-mass spectrometry of polar non-volatile bio-organic molecules',*Anal. Chem.* **1978**, *50*, 985-991.

(8) Cotter, R. J.; Tabet, J. C. 'Laser desorption mass-spectrometry - mechanisms and applications',*Int. J. Mass Spectrom.* **1983**, *53*, 151-166.

(9) Rollgen, F. W. 'Field desorption mass spectrometry',*Trend.Anal.Chem.* **1982**, *1*, 304-307.

(10) Antonov, V. S.; Letokhov, V. S.; Shibanov, A. N. 'Nonthermal desorption of molecular-ions of polyatomic-molecules induced by UV laser-radiation',*Appl. Phys.* **1981**, *25*, 71-76.

(11) Beuhler, R. J.; Flanigan, E.; Greene, L. J.; Friedman, L. 'Proton transfer mass spectrometry of peptides. A rapid heating technique for underivatized peptides containing arginine',*J. Am. Chem. Soc.* **1974**, *96*, 3990-3999.

(12) Zakett, D.; Schoen, A. E.; Cooks, R. G.; Hemberger, P. H. 'Laser-desorption mass-spectrometry mass-spectrometry and the mechanism of desorption ionization',*J.Am.Chem.Soc.* **1981**, *103*, 1295-1297.

(13) Conzemius, R. J.; Capellen, J. M. 'A review of the applications to solids of the laser ion-source in mass-spectrometry',*Int. J. Mass Spectrom.* **1980**, *34*, 197-271.

(14) Furstenau, N.; Hillenkamp, F. 'Laser-induced cluster-ions from thin foils of metals and semiconductors',*Int. J. Mass Spectrom.* **1981**, *37*, 135-151.

(15) Hardin, E. D.; Vestal, M. L. 'Laser ionization mass-spectrometry of non-volatile samples',*Anal. Chem.* **1981**, *53*, 1492-1497.

(16) Hillenkamp, F. 'Laser desorption techniques of non-volatile organic-substances',*Int. J. Mass Spectrom.* **1982**, *45*, 305-313.

(17) Linder, B.; Seydel, U. 'Laser desorption mass spectrometry of nonvolatile under shockwave conditions',*Anal. Chem.* **1985**, *57*, 895-899.

(18) Wilkins, C. L.; Weil, D. A.; Yang, C. L. C.; Ijames, C. F. 'High mass analysis by laser desorption fourier-transform mass-spectrometry',*Anal. Chem.* **1985**, *57*, 520-524.

(19) Stoll, R.; Rollgen, F. W. 'Laser desorption mass spectrometry of thermally labile compounds using a continuous wave CO_2 laser',*Org.Mass Spectrom.* **1979**, *14*, 642-645.

(20) Lindner, B.; Seydel, U. 'Laser desorption mass-spectrometry of nonvolatiles under shock-wave conditions',*Anal. Chem.* **1985**, *57*, 895-899.

(21) Vanderpeyl, G. J. O.; Isa, K.; Haverkamp, J.; Kistemaker, P. G. 'Thermal aspects of laser desorption mass-spectrometry (LDMS)',*Int. J. Mass Spectrom.* **1983**, *47*, 11-14.

(22) Karas, M.; Bachmann, D.; Bahr, U.; Hillenkamp, F. 'Matrix-assisted ultraviolet-laser desorption of nonvolatile compounds',*Int. J. Mass Spectrom.* **1987**, *78*, 53-68.

(23) Tanaka, K.; Ido, Y.; Akita, S.; Yoshida, Y.; Yoshida, T. 'Detection of high mass molecules by laser desorption time-of-flight mass spectrometry',*Proc.Second Japan-China Joint Symp. Mass Spectrom.* **1987**, 185-187.

(24) Tanaka, K.; Waki, H.; Ido, Y.; Akita, S.; Yoshida, Y. 'Protein and polymer analyses up to *m/z* 100000 by laser ionization time-of-flight mass spectrometry',*Rapid.Commun.Mass Spectrom.* **1988**, *2*, 151-153.

(25) Karas, M.; Bachmann, D.; Hillenkamp, F. 'Influence of the wavelength in high-irradiance ultraviolet-laser desorption mass-spectrometry of organic-molecules',*Anal. Chem.* **1985**, *57*, 2935-2939.

(26) Rousell, D. J.; Dutta, S. M.; Little, M. W.; Murray, K. K. 'Matrix-free infrared soft laser desorption/ionization',*J.Mass Spectrom.* **2004**, *39*, 1182-1189.

(27) Beavis, R. C.; Chait, B. T. 'Cinnamic acid derivatives as matrices for ultraviolet laser desorption mass spectrometry of proteins',*Rapid.Commun.Mass Spectrom.* **1989**, *3*, 432-435.

(28) Beavis, R. C.; Chait, B. T. 'Matrix-assisted laser-desorption mass spectrometry using 355 nm radiation',*Rapid.Commun.Mass Spectrom.* **1989**, *3*, 436-439.

(29) Beavis, R. C.; Chaudhary, T.; Chait, B. T. 'Alpha -cyano-4-hydroxycinnamic acid as a matrix for matrix-assisted laser desorption mass spectrometry',*Org.Mass Spectrom.* **1992**, *27*, 156-158.

(30) Wu, K. J.; Steding, A.; Becker, C. H. 'Matrix-assisted laser desorption time-of-flight mass-spectrometry of oligonucleotides using 3-hydroxypicolinic acid as an ultraviolet-sensitive matrix',*Rapid Commun.Mass Spectrom.* **1993**, *7*, 142-146.

(31) Strupat, K.; Karas, M.; Hillenkamp, F. '2,5-dihydroxybenzoic acid - a new matrix for laser desorption ionization mass-spectrometry',*Int. J. Mass Spectrom.* **1991**, *111*, 89-102.

(32) Cornett, D. S.; Duncan, M. A.; Amster, I. J. 'Matrix-assisted laser desorption at visible wavelengths using a 2-component matrix',*Org.Mass Spectrom.* **1992**, *27*, 831-832.

(33) Overberg, A.; Karas, M.; Bahr, U.; Kaufmann, R.; Hillenkamp, F. 'Matrix-assisted infrared-laser (2.94-mu-M) desorption ionization mass-spectrometry of large biomolecules',*Rapid Commun.Mass Spectrom.* **1990**, *4*, 293-296.

(34) Overberg, A.; Karas, M.; Hillenkamp, F. 'Matrix-assisted laser desorption of large biomolecules with a tea-CO_2-laser',*Rapid Commun.Mass Spectrom.* **1991**, *5*, 128-131.

(35) Nordhoff, E.; Ingendoh, A.; Cramer, R.; Overberg, A.; Stahl, B.; Karas, M.; Hillenkamp, F.; Crain, P. F. 'Matrix-assisted laser desorption/ionization mass spectrometry of nucleic acids with wavelengths in the ultraviolet and infrared',*Rapid.Commun.Mass Spectrom.* **1992**, *6*, 771-776.

(36) Berkenkamp, S.; Karas, M.; Hillenkamp, F. 'Ice as a matrix for ir-matrix-assisted laser desorption/ionization: Mass spectra from a protein single crystal',*Proc.Natl. Acad. Sci. U S A* **1996**, *93*, 7003-7007.

(37) Armstrong, D. W.; Zhang, L.-K.; He, L.; Gross, M. 'Ionic liquids as matrixes for matrix-assisted laser desorption/ionization mass spectrometry',*Anal. Chem.* **2001**, *73*, 3679-3686.

(38) McLean, J. A.; Stumpo, K. A.; Russell, D. H. 'Size-selected (2-10 nm) gold nanoparticles for matrix assisted laser desorption ionization of peptides',*J.Am.Chem.Soc.* **2005**, *127*, 5304-5305.

(39) Cooks, R. G.; Busch, K. L. 'Matrix effects, internal energies and MS/MS spectra of molecular-ions sputtered from surfaces',*Int. J. Mass Spectrom.* **1983**, *53*, 111-124.

(40) Beavis, R. C.; Chait, B. T. 'Velocity distributions of intact high mass polypeptide molecule ions produced by matrix assisted laser desorption',*Chem. phys. Lett.* **1991**, *181*, 479-484.

(41) Vertes, A.; Gijbels, R.; Levine, R. D. 'Homogeneous bottleneck model of matrix-assisted ultraviolet-laser desorption of large molecules',*Rapid Commun.Mass Spectrom.* **1990**, *4*, 228-233.

(42) Zhigilei, L. V.; Garrison, B. J. 'Molecular dynamics simulation study of the fluence dependence of particle yield and plume composition in laser desorption and ablation of organic solids',*App. Phys. Lett.* **1999**, *74*, 1341-1343.

(43) Knochenmuss, R.; Stortelder, A.; Breuker, K.; Zenobi, R. 'Secondary ion-molecule reactions in matrix-assisted laser desorption/ionization',*J. Mass Spectrom.* **2000**, *35*, 1237-1245.

(44) Knochenmuss, R.; Vertes, A. 'Time-delayed 2-pulse studies of MALDI matrix ionization mechanisms',*J.Phys.Chem.B* **2000**, *104*, 5406-5410.

(45) Knochenmuss, R.; Zenobi, R. 'MALDI ionization: The role of in-plume processes',*Chem. Rev.* **2003**, *103*, 441-452.

(46) Carr, S. R.; Cassidy, C. J. 'Gas-phase basicities of histidine and lysine and their selected di- and tripeptides.',*J. Am. Soc. Mass Spectrom.* **1996**, *7*, 1203-1210.

(47) Zhang, X.; Cassidy, C. J. 'Apparent gas-phase acidities of multiply protonated peptide ions: Ubiquitin, insulin B and renin substrate.',*J. Am. Soc. Mass Spectrom.* **1996**, *7*, 1211-1218.

(48) Gross, D. S.; Williams, E. R. 'Structure of gramicidin s $(M+H+K)^{2+}$ ions (x= Li, Na, K) probed by proton transfer reactions',*J. Am. Chem. Soc.* **1996**, *118*, 202-204.

(49) Mormann, M.; Bashir, S.; Derrick, P. J.; Kuck, D. 'Gas-phase basicities of the isomeric dihydroxybenzoic acids and gas-phase acidities of their radical cations',*J. Am. Soc. Mass. Spectrom.* **2000**, *11*, 544-552.

(50) Burton, R. D.; Watson, C. H.; Eyler, J. R.; Lang, G. L.; Powell, D. H.; Avery, M. Y. 'Proton affinities of eight matrices used for matrix-assisted laser desorption/ionization',*Rapid Commun.Mass Spectrom.* **1997**, *11*, 443-446.

(51) Breuker, K.; Knochenmuss, R.; Zenobi, R. 'Gas-phase basicities of deprotonated matrix-assisted laser desorption/ionization matrix molecules',*Int. J. Mass Spectrom.* **1999**, *184*, 25-38.

(52) Stevenson, E.; Breuker, K.; Zenobi, R. 'Internal energies of analyte ions generated from different matrix-assisted laser desorption/ionization matrices',*J.Mass Spectrom.* **2000**, *35*, 1035-1041.

(53) Klassen, J. S.; Anderson, S. G.; Blades, A. T.; Kebarle, P. 'Reaction enthalpies for M(+)l=M(+)+l, where M(+)=Na^+ and K^+ and l equals acetamide, N-methylacetamide, N,N-dimethylacetamide, glycine, and glycylglycine, from determinations of the collision-induced dissociation thresholds',*J.Phys.Chem* **1996**, *100*, 14218-14227.

(54) Hoyau, S.; Norrman, K.; McMahon, T. B.; Ohanessian, G. 'A quantitative basis for a scale of Na+ affinities of organic and small biological molecules in the gas phase',*J.Am.Chem.Soc.* **1999**, *121*, 8864-8875.

(55) Frankevich, V.; Knochenmuss, R.; Zenobi, R. 'The origin of electrons in MALDI and their use for sympathetic cooling of negative ions in FTICR',*Int. J. Mass Spectrom.* **2002**, *220*, 11-19.

(56) Zhang, J.; Frankevich, V.; Knochenmuss, R.; Friess, S. D.; Zenobi, R. 'Reduction of Cu(II) in matrix-assisted laser desorption/ionization mass spectrometry',*J.Am.Chem.Soc.Mass Spectrom.* **2003**, *14*, 42-50.

(57) Karas, M.; Gluckmann, M.; Schafer, J. 'Ionization in matrix-assisted laser desorption/ionization: Singly charged molecular ions are the lucky survivors',*J.Mass Spectrom.* **2000**, *35*, 1-12.

(58) Fournier, I.; Brunot, A.; Tabet, J. C.; Bolbach, G. 'Delayed extraction experiments using a repulsive potential before ion extraction: Evidence of clusters as ion precursors in UV-MALDI. Part I: Dynamical effects with the matrix 2,5-dihydroxybenzoic acid',*Int. J. Mass Spectrom.* **2002**, *213*, 203-215.

(59) Zhigilei, L. V.; Garrison, B. J. 'Velocity distributions of analyte molecules in matrix-assisted laser desorption from computer simulations',*Rapid Commun.Mass Spectrom.* **1998**, *12*, 1273-1277.

(60) Krutchinsky, A. N.; Chait, B. T. 'On the nature of the chemical noise in MALDI mass spectra',*J.Am.Chem.Soc.Mass Spectrom.* **2002**, *13*, 129-134.

(61) Dekker, L. J.; Dalebout, J. C.; Siccama, I.; Jenster, G.; Smitt, P. A. S.; Luider, T. M. 'A new method to analyze matrix-assisted laser desorption/ionization time-of-flight peptide profiling mass spectra',*Rapid Commun.Mass Spectrom.* **2005**, *19*, 865-870.

(62) Markus, K.; Schafer, H.; Klaus, S.; Bunse, C.; Swart, R.; Meyer, H. E. 'A new fast method for nanoLC-MALDI-TOF/TOF-MS analysis using monolithic columns for peptide preconcentration and separation in proteomic studies',*J. Proteome Res.* **2007**, *6*, 636-643.

(63) Dunn, J. D.; Watson, J. T.; Bruening, M. L. 'Detection of phosphopeptides using Fe(III)-nitrilotriacetate complexes immobilized on a MALDI plate',*Anal. Chem.* **2006**, *78*, 1574-1580.

(64) Navare, A.; Zhou, M.; McDonald, J.; Noriega, F. G.; Sullards, M. C.; Fernandez, F. M. 'Serum biomarker profiling by solid-phase extraction with particle-embedded micro tips and matrix-assisted laser desorption/ionization mass spectrometry',*Rapid Commun.Mass Spectrom.* **2008**, *22*, 997-1008.

(65) Aerni, H. R.; Cornett, D. S.; Caprioli, R. M. 'Automated acoustic matrix deposition for MALDI sample preparation',*Anal. Chem.* **2006**, *78*, 827-834.

(66) Hillenkamp, F.; Karas, M.; Beavis, R. C.; Chait, B. T. 'Matrix-assisted laser desorption ionization mass-spectrometry of biopolymers',*Anal. Chem.* **1991**, *63*, A1193-A1202.

(67) Trimpin, S.; Weidner, S. M.; Falkenhagen, J.; McEwen, C. N. 'Fractionation and solvent-free MALDI-MS analysis of polymers using liquid adsorption chromatography at critical conditions in combination with a multisample on-target homogenization/transfer sample preparation method',*Anal. Chem.* **2007**, *79*, 7565-7570.

(68) de Noo, M. E.; Tollenaar, R. A. E. M.; Ozalp, A.; Kuppen, P. J. K.; Bladergroen, M. R.; Eilers, P. H. C.; Deelder, A. M. 'Reliability of human serum protein profiles generated with C8 magnetic beads assisted MALDI-TOF mass spectrometry',*Analytical Chemistry* **2005**, *77*, 7232-7241.

(69) Zhang, L.; Orlando, R. 'Solid-phase extraction MALDI-MS: Extended ion-pairing surfaces for the on-target cleanup of protein samples',*Anal. Chem.* **1999**, *71*, 4753-4757.

(70) Callesen, A. K.; Mohammed, S.; Bunkenborg, J.; Kruse, T. A.; Cold, S.; Mogensen, O.; Christensen, R. D.; Vach, W.; Jorgensen, P. E.; Jensen, O. N. 'Serum protein profiling by miniaturized solid-phase extraction and matrix-assisted laser desorption/ionization mass spectrometry',*Rapid Commun.Mass Spectrom.* **2005**, *19*, 1578-1586.

(71) Warren, M. E.; Brockman, A. H.; Orlando, R. 'On-probe solid-phase extraction MALDI-MS using ion-pairing interactions for the cleanup of peptides and proteins',*Anal. Chem.* **1998**, *70*, 3757-3761.

(72) Nagele, E.; Vollmer, m. 'Coupling of nanoflow liquid chromatography to matrix-assisted laser desorption/ionization mass spectrometry: Real-time liquid chromatography run mapping on a MALDI plate',*Rapid Commun.Mass Spectrom.* **29004**, *18*, 3008-3014.

(73) Harkins, J. B.; Katz, B. B.; Pastor, S. J.; Osucha, P.; Hafeman, D. G.; Witkowski, C. E.; Norris, J. L. 'Parallel electrophoretic depletion, fractionation, concentration,

and desalting of 96 complex biological samples for mass spectrometry',*Anal. Chem.* **2008**, *80*, 2734-2743.

(74) Evans-Nguyen, K. M.; Tao, S. C.; Zhu, H.; Cotter, R. J. 'Protein arrays on patterned porous gold substrates interrogated with mass spectrometry: Detection of peptides in plasma',*Anal. Chem.* **2008**, *80*, 1448-1458.

(75) Blackledge, J. A.; Alexander, A. J. 'Polyethylene membrane as a sample support for direct matrix-assisted laser-desorption ionization mass-spectrometric analysis of high-mass proteins',*Anal. Chem.* **1995**, *67*, 843-848.

(76) Tang, N.; Tornatore, P.; Weinberger, S. R. 'Current developments in SELDI affinity technology',*Mass Spectrom.Rev.* **2004**, *23*, 34-44.

(77) Kruse, R. A.; Li, X. L.; Bohn, P. W.; Sweedler, J. V. 'Experimental factors controlling analyte ion generation in laser desorption/ionization mass spectrometry on porous silicon',*Anal. Chem.* **2001**, *73*, 3639-3645.

(78) Su, C.-L.; Tseng, W.-L. 'Gold nanoparticles as assisted matrix for determining neutral small carbohydrates through laser desorption/ionization time-of-flight mass spectrometry',*Anal. Chem.* **2007**, *79*, 1626-1633.

(79) Laiko, V. V.; Moyer, S. C.; Cotter, R. J. 'Atmospheric pressure MALDI/ion trap mass spectrometry',*Anal. Chem.* **2000**, *72*, 5239-5243.

(80) Laiko, V. V.; Baldwin, M. A.; Burlingame, A. L. 'Atmospheric pressure matrix-assisted laser desorption/ionization mass spectrometry',*Anal. Chem.* **2000**, *72*, 652-657.

(81) Von Seggern, C. E.; Zarek, P. E.; Cotter, R. J. 'Fragmentation of sialylated carbohydrates using infrared atmospheric pressure MALDI ion trap mass spectrometry from cation-doped liquid matrixes',*Anal. Chem.* **2003**, *75*, 6523-6530.

(82) Moyer, S. C.; Cotter, R. J.; Woods, A. S. 'Fragmentation of phosphopeptides by atmospheric pressure MALDI and ESI/ ion trap mass spectrometry',*J. Am. Soc. Mass. Spectrom.* **2002**, *13*, 274-283.

(83) Shrivas, K.; Wu, H. F. 'Single drop microextraction as a concentrating probe for rapid screening of low molecular weight drugs from human urine in atmospheric-pressure matrix-assisted laser desorption/ionization mass spectrometry',*Rapid.Commun.Mass Spectrom.* **2007**, *21*, 3103-3108.

(84) Gudlavalleti, S. K.; Sundaram, A. K.; Razumovski, J.; Doroshenko, V. M. 'Application of atmospheric-pressure matrix-assisted laser desorption/ionization mass spectrometry for rapid identification of *neisseria* species.',*J.Biomol.Tech.* **2008**, *19*, 200-204.

(85) Miller, C. A.; Donghui, Y.; Perkins, P. D. 'An atmospheric pressure matrix-assisted laser desorption/ionization ion trap with enhanced sensitivity',*Rapid.Commun.Mass Spectrom.* **2003**, *17*, 860-868.

(86) Tan, P. V.; Laiko, V. V.; Doroshenko, V. M. 'Atmospheric pressure MALDI with pulsed dynamic focusing for high-efficiency transmission of ions into a mass spectrometer',*Anal. Chem.* **2004**, *76*, 2462-2469.

(87) Takats, Z.; Wiseman, J. M.; Gologan, B.; Cooks, R. G. 'Mass spectrometry sampling under ambient conditions with desorption electrospray ionization',*Science* **2004**, *306*, 471-473.

(88) Cody, R. B.; Laramee, J. A.; Durst, H. D. 'Versatile new ion source for the analysis of materials in open air under ambient conditions',*Anal. Chem.* **2005**, *77*, 2297-2302.

(89) Chen, H. W.; Talaty, N. N.; Takats, Z.; Cooks, R. G. 'Desorption electrospray ionization mass spectrometry for high-throughput analysis of pharmaceutical samples in the ambient environment',*Anal. Chem.* **2005**, *77*, 6915-6927.

(90) Venter, A.; Nefliu, M.; Cooks, R. G. 'Ambient desorption ionization mass spectrometry',*Trac-Tred Anal.Chem.* **2008**, *27*, 284-290.

(91) Harris, G. A.; Nyadong, L.; Fernandez, F. M. 'Recent developments in ambient ionization techniques for analytical mass spectrometry',*Analyst* **2008**, *133*, 1297-1301.

(92) Sampson, S. S.; Hawkridge, A. M.; Muddiman, D. C. 'Generation and detection of multiply-charged peptides and proteins by matrix-assisted laser desorption electrospray ionization (MALDESI) fourier transform ion cyclotron resonance mass spectrometry',*J. Am. Soc. Mass Spectrom.* **2006**, *17*, 1712-1716.

(93) Wolfender, J. L.; Chu, F. X.; Ball, H.; Wolfender, F.; Fainzilber, M.; Baldwin, M. A.; Burlingame, A. L. 'Identification of tyrosine sulfation in conus pennaceus conotoxins alpha-pnia and alpha-pnib: Further investigation of labile sulfo- and phosphopeptides by electrospray, matrix-assisted laser desorption/ionization (MALDI) and atmospheric pressure MALDI mass spectrometry',*J.Mass Spectrom.* **1999**, *34*, 447-454.

(94) Danell, R. M.; Glish, G. L.,*Proc. 49th ASMS conf. Mass Spectrometry and Allied Topics, Chicago, IL, 2001* **2001**.

(95) Doroshenko, V. M.; Laiko, V. V.; Taranenko, N. I.; Berkout, V. D.; Lee, H. S. 'Recent developments in atmospheric pressure MALDI mass spectrometry',*Int. J. Mass Spectrom.* **2002**, *221*, 39-58.

(96) Harper, R. G.; Workman, S. R.; Schuetzner, S.; Timperman, A. T.; Sutton, J. N. 'Low-molecular-weight human serum proteome using ultrafiltration, isoelectric focusing, and mass spectrometry',*Electrophoresis* **2004**, *25*, 1299-1306.

(97) Orvisky, E.; Drake, S. K.; Martin, B. M.; Abdel-Hamid, M.; Ressom, H. W.; Varghese, R. S.; An, Y.; Saha, D.; Hortin, G. L.; Loffredo, C. A.; Goldman, R. 'Enrichment of low molecular weight fraction of serum for MS analysis of peptides associated with hepatocellular carcinoma',*Proteomics* **2006**, *6*, 2895-2902.

(98) Vorderwulbecke, S.; Cleverley, S.; Weinberger, S.; Wiesner, A. 'Protein quantification by the SELDI-TOF-MS-based protein chip (R) system',*Mol.Cell.Proteomics* **2005**, *4*, S381-S381.

(99) Ekstrom, S.; Wallman, L.; Hok, D.; Marko-Varga, G.; Laurell, T. 'Miniaturized solid-phase extraction and sample preparation for MALDI MS using a microfabricated integrated selective enrichment target',*J Proteome Res* **2006**, *5*, 1071-1081.

(100) Moon, H.; Wheeler, A. R.; Garrell, R. L.; Loo, J. A.; Kim, C. J. 'An integrated digital microfluidic chip for multiplexed proteomic sample preparation and analysis by MALDI-MS',*Lab.Chip* **2006**, *6*, 1213-1219.

(101) Villanueva, J.; Philip, J.; Chaparro, C. A.; Li, Y.; Toledo-Crow, R.; DeNoyer, L.; Fleisher, M.; Robbins, R. J.; Tempst, P. 'Correcting common errors in identifying cancer-specific serum peptide signatures',*J Proteome Res* **2005**, *4*, 1060-1072.

(102) Turney, K.; Harrison, W. W. 'Liquid supports for ultraviolet atmospheric pressure matrix-assisted laser desorption/ionization',*Rapid Commun.Mass Spectrom.* **2004**, *18*, 629-635.

(103) Bennett, H. P.; Browne, C. A.; Solomon, S. 'Purification of the two major forms of rat pituitary corticotropin using only reversed-phase liquid chromatography',*Biocehmistry-US* **1981**, *20*, 4530-4538.

(104) Beardsley, R. L.; Reilly, J. P. 'Optimization of guanidination procedures for MALDI mass mapping',*Anal. Chem.* **2002**, *74*, 1884-1890.

(105) Keough, T.; Lacey, M. P.; Youngquist, R. S. 'Derivatization procedures to facilitate de novo sequencing of lysine-terminated tryptic peptides using postsource decay matrix-assisted laser desorption/ionization mass spectrometry',*Rapid Commun.Mass Spectrom.* **2000**, *14*, 2348-2356.

(106) Smirnov, I. P.; Zhu, X.; Taylor, T.; Huang, Y.; Ross, P.; Papayanopoulos, I. A.; Martin, S. A.; Pappin, D. J. 'Suppression of alpha-cyano-4-hydroxycinnamic acid matrix clusters and reduction of chemical noise in MALDI-TOF mass spectrometry',*Anal. Chem.* **2004**, *76*, 2958-2965.

(107) Zhu, X.; Papayannopoulos, I. A.; (Applied Biosystems, USA). Application: US, 2005, pp 10 pp.

(108) Kang, J. H.; Toita, R.; Oishi, J.; Niidome, T.; Katayama, Y. 'Effect of the addition of diammonium citrate to alpha-cyano-4-hydroxycinnamic acid (CHCA) matrix for the detection of phosphorylated peptide in phosphorylation reactions using cell and tissue lysates',*J.Am.Chem.Soc.Mass Spectrom.* **2007**, *18*, 1925-1931.

(109) Verbeck, G. F. I. V.; Beale, S. C. 'Isoelectric point analysis of proteins and peptides by capillary isoelectric focusing with two-wavelength laser-induced fluorescence detection',*Journal of Microcolumn Separations* **1999**, *11*, 708-715.

(110) 'Hopp & woods property calculator. Available at http://www.Innovagen.Se/custom-peptide-synthesis/peptide-property-calculator/peptide-property-calculator.Asp'.

(111) Hopp, T. P.; Woods, K. R. 'Prediction of protein antigenic determinants from amino acid sequences',*Proc. Natl. Acad. Sc.i U S A* **1981**, *78*, 3824-3828.

(112) Kataoka, H.; Toschi, A.; Li, J. P.; Carney, R. L.; Schooley, D. A.; Kramer, S. J. 'Idenification of an allatotropin from from adult manduca sexta',*Science* **1989**, *243*, 1481-1483.

(113) Kramer, S. J.; Toschi, A.; Miller, C. A.; Kataoka, H.; Quistad, G. B.; Li, J. P.; Carney, R. L.; Schooley, D. A. 'Identification of an allatostatin from the tobacco hornworm manduca sexta',*Proc. Natl. Acad. Sc.i U S A* **1991**, *88*, 9458-9462.

(114) Lorenz, M. W.; Kellner, R.; Hoffmann, K. H. 'A family of neuropeptides that inhibit juvenile hormone biosynthesis in the cricket, gryllus bimaculatus',*J. Biol. Chem.* **1995**, *270*, 21103-21108.

(115) Gilbert, L. I.; Granger, N. A.; Roe, R. M. 'The juvenile hormones: Historical facts and speculations on future research directions',*Insect. Biochem. Mol. Biol.* **2000**, *30*, 617-644.

(116) Woodhead, A. P.; Stay, B.; Seidel, S. L.; Khan, M. A.; Tobe, S. S. 'Primary structure of 4 allatostatins - neuropeptide inhibitors of juvenile-hormone synthesis',*Proc.Natl. Acad. Sci. U S A* **1989**, *86*, 5997-6001.

(117) Bendena, W. G.; Donly, B. C.; Tobe, S. S. 'Allatostatins: A growing family of neuropeptides with structural and functional diversity',*Ann. N. Y. Acad. Sci.i* **1999**, *897*, 311-329.

(118) Nassel, D. R. 'Neuropeptides in the nervous system of drosophila and other insects: Multiple roles as neuromodulators and neurohormones',*Prog. Neurobiol.* **2002**, *68*, 1-84.

(119) Petri, B.; Homberg, U.; Loesel, R.; Stengl, M. 'Evidence for a role of gaba and mas-allatotropin in photic entrainment of the circadian clock of the cockroach leucophaea maderae',*J. Exp. Biol.* **2002**, *205*, 1459-1469.

(120) Elekonich, M. M.; Horodyski, F. M. 'Insect allatotropins belong to a family of structurally-related myoactive peptides present in several invertebrate phyla',*Peptides* **2003**, *24*, 1623-1632.

(121) Li, Y.; Hernandez-Martinez, S.; Fernandez, F.; Mayoral, J. G.; Topalis, P.; Priestap, H.; Perez, M.; Navare, A.; Noriega, F. G. 'Biochemical, molecular, and functional characterization of PISCF-allatostatin, a regulator of juvenile hormone biosynthesis in the mosquito aedes aegypti',*J.Am.Soc.Mass Spectrom.* **2006**, *281*, 34048-34055.

(122) Hernandez-Martinez, S.; Li, Y.; Lanz-Mendoza, H.; Rodriguez, M. H.; Noriega, F. G. 'Immunostaining for allatotropin and allatostatin-a and -c in the mosquitoes aedes aegypti and anopheles albimanus',*Cell Tissue Res.* **2005**, *321*, 105-113.

(123) Hernandez-Martinez, S.; Mayoral, J. G.; Li, Y.; Noriega, F. G. 'Role of juvenile hormone and allatotropin on nutrient allocation, ovarian development and survivorship in mosquitoes',*J. Insect Physiol.* **2007**, *53*, 230-234.

(124) Kanari, Y.; Shoji, Y.; Ode, H.; Miyake, T.; Tanii, T.; Hoshino, T.; Ohdomari, I. 'Protein adsorption on self-assembled monolayers induced by surface water molecule',*Jpn. J. Appl. Phys.* **2007**, *46*, 6303-6308.

(125) Mayrhofer, C.; Krieger, S.; Raptakis, E.; Allmaier, G. 'Comparison of vacuum matrix-assisted laser desorption/ionization (MALDI) and atmospheric pressure MALDI (AP-MALDI) tandem mass spectrometry of 2-dimensional separated and trypsin-digested glomerular proteins for database search derived identification',*J. Proteome Res.* **2006**, *5*, 1967-1978.

(126) Dongre, A. R.; Jones, J. L.; Somogyi, A.; Wysocki, V. H. 'Influence of peptide composition, gas-phase basicity, and chemical modification on fragmentation efficiency: Evidence for the mobile proton model',*J.Am.Chem.Soc.* **1996**, *118*, 8365-8374.

(127) Bauer, M. D.; Sun, Y.; Keough, T.; Lacey, M. P. 'Sequencing of sulfonic acid derivatized peptides by electrospray mass spectrometry',*Rapid Commun.Mass Spectrom.* **2000**, *14*, 924-929.

(128) Keough, T.; Youngquist, R. S.; Lacey, M. P. 'A method for high-sensitivity peptide sequencing using postsource decay matrix-assisted laser desorption ionization mass spectrometry',*Proc. Natl. Acad. Sci. U S A* **1999**, *96*, 7131-7136.

(129) Keough, T.; Lacey, M. P.; Strife, R. J. 'Atmospheric pressure matrix-assisted laser desorption/ionization ion trap mass spectrometry of sulfonic acid derivatized tryptic peptides',*Rapid Commun.Mass Spectrom.* **2001**, *15*, 2227-2239.

(130) Keough, T.; Lacey, M. P.; Fieno, A. M.; Grant, R. A.; Sun, Y.; Bauer, M. D.; Begley, K. B. 'Tandem mass spectrometry methods for definitive protein identification in proteomics research',*Electrophoresis* **2000**, *21*, 2252-2265.

(131) Mehl, J. T.; Cummings, J. J.; Rohde, E.; Yates, N. N. 'Automated protein identification using atmospheric-pressure matrix-assisted laser desorption/ionization',*Rapid Commun.Mass Spectrom.* **2003**, *17*, 1600-1610.

(132) Grasso, G.; Rizzarelli, E.; Spoto, G. 'AP/MALDI-MS complete characterization of the proteolytic fragments produced by the interaction of insulin degrading enzyme with bovine insulin',*J. Mass Spectrom.* **2007**, *42*, 1590-1598.

(133) Frahm, J. L.; Howard, B. E.; Heber, S.; Muddiman, D. C. 'Accessible proteomics space and its implications for peak capacity for zero-, one- and two-dimensional separations coupled with FT-ICR and TOF mass spectrometry',*J. Mass Spectrom.* **2006**, *41*, 281-288.

(134) Kozak, K. R.; Su, F.; Whitelegge, J. P.; Faull, K.; Reddy, S.; Farias-Eisner, R. 'Characterization of serum biomarkers for detection of early stage ovarian cancer',*Proteomics* **2005**, *5*, 4589-4596.

(135) Ahmed, N.; Oliva, K. T.; Barker, G.; Hoffmann, P.; Reeve, S.; Smith, I. A.; Quinn, M. A.; Rice, G. E. 'Proteomic tracking of serum protein isoforms as screening biomarkers of ovarian cancer',*Proteomics* **2005**, *5*, 4625-4636.

(136) Purohit, S.; Podolsky, R.; Schatz, D.; Muir, A.; Hopkins, D.; Huang, Y. H.; She, J. X. 'Assessing the utility of SELDI-TOF and model averaging for serum proteomic biomarker discovery',*Proteomics* **2006**, *6*, 6405-6415.

(137) Roche, S.; Tiers, L.; Provansal, M.; Piva, M. T.; Lehmann, S. 'Interest of major serum protein removal for surface-enhanced laser desorption/ionization - time of flight (SELDI-TOF) proteomic blood profiling',*Proteome science* **2006**, *4*, 20.

(138) Shen, Y.; Kim, J.; Strittmatter, E. F.; Jacobs, J. M.; Camp, D. G., 2nd; Fang, R.; Tolie, N.; Moore, R. J.; Smith, R. D. 'Characterization of the human blood plasma proteome',*Proteomics* **2005**, *5*, 4034-4045.

(139) Tirumalai, R. S.; Chan, K. C.; Prieto, D. A.; Issaq, H. J.; Conrads, T. P.; Veenstra, T. D. 'Characterization of the low molecular weight human serum proteome',*Mol.Cell Proteomics* **2003**, *2*, 1096-1103.

(140) Villanueva, J.; Philip, J.; Entenberg, D.; Chaparro, C. A.; Tanwar, M. K.; Holland, E. C.; Tempst, P. 'Serum peptide profiling by magnetic particle-assisted, automated sample processing and MALDI-TOF mass spectrometry',*Anal. Chem.* **2004**, *76*, 1560-1570.

(141) Xiao, Z.; Luke, B. T.; Izmirlian, G.; Umar, A.; Lynch, P. M.; Phillips, R. K.; Patterson, S.; Conrads, T. P.; Veenstra, T. D.; Greenwald, P.; Hawk, E. T.; Ali, I.

U. 'Serum proteomic profiles suggest celecoxib-modulated targets and response predictors',*Cancer Res.* **2004**, *64*, 2904-2909.

(142) King, R.; Bonfiglio, R.; Fernandez-Metzler, C.; Miller-Stein, C.; Olah, T. 'Mechanistic investigation of ionization suppression in electrospray ionization',*J. Am. Soc. Mass. Spectrom.* **2000**, *11*, 942-950.

(143) Ledford, E. B., Jr.; Rempel, D. L.; Gross, M. L. 'Space charge effects in fourier transform mass spectrometry. Mass calibration',*Anal. Chem.* **1984**, *56*, 2744-2748.

(144) Zhao, J.; Simeone, D. M.; Heidt, D.; Anderson, M. A.; Lubman, D. M. 'Comparative serum glycoproteomics using lectin selected sialic acid glycoproteins with mass spectrometric analysis: Application to pancreatic cancer serum',*J Proteome Res.* **2006**, *5*, 1792-1802.

(145) Jacobs, J. M.; Adkins, J. N.; Qian, W. J.; Liu, T.; Shen, Y.; Camp, D. G., 2nd; Smith, R. D. 'Utilizing human blood plasma for proteomic biomarker discovery',*J. Proteome Res.* **2005**, *4*, 1073-1085.

(146) Pieper, R.; Gatlin, C. L.; Makusky, A. J.; Russo, P. S.; Schatz, C. R.; Miller, S. S.; Su, Q.; McGrath, A. M.; Estock, M. A.; Parmar, P. P.; Zhao, M.; Huang, S. T.; Zhou, J.; Wang, F.; Esquer-Blasco, R.; Anderson, N. L.; Taylor, J.; Steiner, S. 'The human serum proteome: Display of nearly 3700 chromatographically separated protein spots on two-dimensional electrophoresis gels and identification of 325 distinct proteins',*Proteomics* **2003**, *3*, 1345-1364.

(147) Mitchell, B. L.; Yasui, Y.; Lampe, J. W.; Gafken, P. R.; Lampe, P. D. 'Evaluation of matrix-assisted laser desorption/ionization-time of flight mass spectrometry proteomic profiling: Identification of alpha 2-HS glycoprotein B-chain as a biomarker of diet',*Proteomics* **2005**, *5*, 2238-2246.

(148) de Noo, M. E.; Tollenaar, R. A.; Ozalp, A.; Kuppen, P. J.; Bladergroen, M. R.; Eilers, P. H.; Deelder, A. M. 'Reliability of human serum protein profiles generated with C8 magnetic beads assisted MALDI-TOF mass spectrometry',*Anal. Chem.* **2005**, *77*, 7232-7241.

(149) Chertov, O.; Biragyn, A.; Kwak, L. W.; Simpson, J. T.; Boronina, T.; Hoang, V. M.; Prieto, D. A.; Conrads, T. P.; Veenstra, T. D.; Fisher, R. J. 'Organic solvent extraction of proteins and peptides from serum as an effective sample preparation for detection and identification of biomarkers by mass spectrometry',*Proteomics* **2004**, *4*, 1195-1203.

(150) Prahalad, A. K.; Hickey, R. J.; Huang, J.; Hoelz, D. J.; Dobrolecki, L.; Murthy, S.; Winata, T.; Hock, J. M. 'Serum proteome profiles identifies parathyroid hormone physiologic response',*Proteomics* **2006**, *6*, 3482-3493.

(151) Petricoin, E. F.; Ardekani, A. M.; Hitt, B. A.; Levine, P. J.; Fusaro, V. A.; Steinberg, S. M.; Mills, G. B.; Simone, C.; Fishman, D. A.; Kohn, E. C.; Liotta,

L. A. 'Use of proteomic patterns in serum to identify ovarian cancer',*Lancet* **2002**, *359*, 572-577.

(152) Petricoin, E. F.; Mills, G. B.; Kohn, E. C.; Liotta, L. A. 'Proteomic patterns in serum and identification of ovarian cancer - reply',*Lancet* **2002**, *360*, 170-171.

(153) Kozak, K. R.; Amneus, M. W.; Pusey, S. M.; Su, F.; Luong, M. N.; Luong, S. A.; Reddy, S. T.; Farias-Eisner, R. 'Identification of biomarkers for ovarian cancer using strong anion-exchange proteinchips: Potential use in diagnosis and prognosis',*Proc. Natl. Acad. Sc.i U S A* **2003**, *100*, 12343-12348.

(154) Baggerly, K. A.; Morris, J. S.; Coombes, K. R. 'Reproducibility of SELDI-TOF protein patterns in serum: Comparing datasets from different experiments',*Bioinformatics (Oxford, England)* **2004**, *20*, 777-785.

(155) Ekblad, L.; Baldetorp, B.; Ferno, M.; Olsson, H.; Bratt, C. 'In-source decay causes artifacts in SELDI-TOF MS spectra',*J Proteome Res* **2007**, *6*, 1609-1614.

(156) Muck, A.; Nesnerova, P.; Pichova, I.; Svatos, A. 'Fast prototyping of hydrophobic disposable polymer support arrays for matrix-assisted laser desorption/ionization-time of flight-mass spectrometry of proteins by atmospheric molding',*Electrophoresis* **2005**, *26*, 2835-2842.

(157) Dunn, J. D.; Watson, J. T.; Bruening, M. L. 'Detection of phosphopeptides using Fe(III)-nitrilotriacetate complexes immobilized on a MALDI plate',*Anal. Chem.* **2006**, *78*, 1574-1580.

(158) Gobom, J.; Nordhoff, E.; Mirgorodskaya, E.; Ekman, R.; Roepstorff, P. 'Sample purification and preparation technique based on nano-scale reversed-phase columns for the sensitive analysis of complex peptide mixtures by matrix-assisted laser desorption/ionization mass spectrometry',*J. Mass Spectrom.* **1999**, *34*, 105-116.

(159) 'Available at http://prospector.Ucsf.Edu/'.

(160) 'Available at http://www.Vivo.Colostate.Edu/molkit/hydropathy/index.Html
'.

(161) Gusev, A. I.; Wilkinson, W. R.; Proctor, A.; Hercules, D. M. 'Improvement of signal reproducibility and matrix/comatrix effects in maldi analysis',*Anal. Chem.* **1995**, *67*, 1034-1041.

(162) Cohen, S. L.; Chait, B. T. 'Influence of matrix solution conditions on the MALDI-MS analysis of peptides and proteins',*Anal. Chem.* **1996**, *68*, 31-37.

(163) Beavis, R. C.; Bridson, J. N. 'Epitaxial protein inclusion in sinapic acid crystals',*J. Phys.D Appl.Phys.* **1993**, *26*, 442-447.

(164) Chou, J. Z.; Kreek, M. J.; Chait, B. T. 'Matrix-assisted laser-desorption mass-spectrometry of biotransformation products of dynorphin-a in-vitro',*J.Am.Chem.Soc.Mass Spectrom.* **1994**, *5*, 10-16.

(165) Righetti, P. G. 'Real and imaginary artefacts in proteome analysis via two-dimensional maps',*J. Chromatogr. B* **2006**, *841*, 14-22.

(166) Posewitz, M. C.; Tempst, P. 'Immobilized gallium(III) affinity chromatography of phosphopeptides',*Anal. Chem.* **1999**, *71*, 2883-2892.

(167) Zhou, W.; Merrick, B. A.; Khaledi, M. G.; Tomer, K. B. 'Detection and sequencing of phosphopeptides affinity bound to immobilized metal ion beads by matrix-assisted laser desorption/ionization mass spectrometry',*J. Am. Soc. Mass. Spectrom.* **2000**, *11*, 273-282.

(168) Nawrocki, J.; Rigney, M. P.; McCormick, A.; Carr, P. W. 'Chemistry of zirconia and its use in chromatography',*J. Chromatogr. A* **1993**, *657*, 229-282.

(169) Nawrocki, J.; Dunlap, C.; McCormick, A.; Carr, P. W. 'Part I. Chromatography using ultra-stable metal oxide-based stationary phases for HPLC',*J. Chromatogr. A* **2004**, *1028*, 1-30.

(170) Hoth, D. C.; Rivera, J. G.; Colon, L. A. 'Metal oxide monolithic columns',*J. Chromatogr. A* **2005**, *1079*, 392-396.

(171) Kweon, H. K.; Hakansson, K. 'Selective zirconium dioxide-based enrichment of phosphorylated peptides for mass spectrometric analysis',*Anal. Chem.* **2006**, *78*, 1743-1749.

(172) Laiko, V. V.; Burlingame, A. L.; US, Ed.: US, 1999; Vol. US005965884A.

(173) Laiko, V. V.; Taranenko, N. I.; Berkout, V. D.; Yakshin, M. A.; Prasad, C. R.; Lee, H. S.; Doroshenko, V. M. 'Desorption/ionization of biomolecules from aqueous solutions at atmospheric pressure using an infrared laser at 3 micro m',*J.Am.Chem.Soc.Mass Spectrom.* **2002**, *13*, 354-361.

(174) Tan, P. V.; Taranenko, N. I.; Laiko, V. V.; Yakshin, M. A.; Prasad, C. R.; Doroshenko, V. M. 'Mass spectrometry of N-linked oligosaccharides using atmospheric pressure infrared laser ionization from solution',*J. Mass Spectrom.* **2004**, *39*, 913-921.

(175) Kellersberger, K. A.; Yu, E. T.; Merenbloom, S. I.; Fabris, D. 'Atmospheric pressure MALDI-FTMS of normal and chemically modified RNA',*J. Am. Soc. Mass. Spectrom.* **2005**, *16*, 199-207.

(176) Hanton, S. D.; Parees, D. M.; Zweigenbaum, J. 'The fragmentation of ethoxylated surfactants by AP-MALDI-QiT',*J. Am. Soc. Mass. Spectrom.* **2006**, *17*, 453-458.

(177) Li, Y.; Shrestha, B.; Vertes, A. 'Atmospheric pressure molecular imaging by infrared MALDI mass spectrometry',*Anal. Chem.* **2007**, *79*, 523-532.

(178) Li, Y.; Shrestha, B.; Vertes, A. 'Atmospheric pressure infrared MALDI imaging mass spectrometry for plant metabolomics',*Anal. Chem.* **2008**, *80*, 407-420.

(179) Wolfender, J. L.; Chu, F.; Ball, H.; Wolfender, F.; Fainzilber, M.; Baldwin, M. A.; Burlingame, A. L. 'Identification of tyrosine sulfation in conus pennaceus conotoxins alpha-pnia and alpha-pnib: Further investigation of labile sulfo- and phosphopeptides by electrospray, matrix-assisted laser desorption/ionization (MALDI) and atmospheric pressure MALDI mass spectrometry',*J. Mass Spectrom.* **1999**, *34*, 447-454.

(180) McLean, J. A.; Russell, W. K.; Russell, D. H. 'A high repetition rate (1 khz) microcrystal laser for high throughput atmospheric pressure MALDI-quadrupole-time-of-flight mass spectrometry',*Anal. Chem.* **2003**, *75*, 648-654.

(181) Galicia, M. C.; Vertes, A.; Callahan, J. H. 'Atmospheric pressure matrix-assisted laser desorption/ionization in transmission geometry',*Anal. Chem.* **2002**, *74*, 1891-1895.

(182) Koestler, M.; Kirsch, D.; Hester, A.; Leisner, A.; Guenther, S.; Spengler, B. 'A high-resolution scanning microprobe matrix-assisted laser desorption/ionization ion source for imaging analysis on an ion trap/fourier transform ion cyclotron resonance mass spectrometer',*Rapid.Commun.Mass Spectrom.* **2008**, *22*, 3275-3285.

(183) Shrivas, K.; Wu, H. F. 'A rapid, sensitive and effective quantitative method for simultaneous determination of cationic surfactant mixtures from river and municipal wastewater by direct combination of single-drop microextraction with AP-MALDI mass spectrometry',*J. Mass Spectrom.* **2007**, *42*, 1637-1644.

(184) Agrawal, K.; Wu, H. F.; Shrivas, K. 'Reverse micellar microextraction for rapid analysis of thiol-containing peptides and amino acids by atmospheric-pressure matrix-assisted laser desorption/ionization ion trap and matrix-assisted laser desorption/ionization time-of-flight mass spectrometry',*Rapid.Commun.Mass Spectrom.* **2008**, *22*, 1437-1444.

(185) Salo, P. K.; Salomies, H.; Harju, K.; Ketola, R. A.; Kotiaho, T.; Yli-Kauhaluoma, J.; Kostiainen, R. 'Analysis of small molecules by ultra thin-layer chromatography-atmospheric pressure matrix-assisted laser desorption/ionization mass spectrometry',*J. Am. Soc. Mass. Spectrom.* **2005**, *16*, 906-915.

(186) Steiner, W. E.; Clowers, B. H.; English, W. A.; Hill, H. H., Jr. 'Atmospheric pressure matrix-assisted laser desorption/ionization with analysis by ion mobility time-of-flight mass spectrometry',*Rapid.Commun.Mass Spectrom.* **2004**, *18*, 882-888.

(187) Gabelica, V.; Schulz, E.; Karas, M. 'Internal energy build-up in matrix-assisted laser desorption/ionization',*J.Mass Spectrom.* **2004**, *39*, 579-593.

(188) Konn, D. O.; Murrell, J.; Despeyroux, D.; Gaskell, S. J. 'Comparison of the effects of ionization mechanism, analyte concentration, and ion "Cool-times" On the internal energies of peptide ions produced by electrospray and atmospheric pressure matrix-assisted laser desorption ionization',*J.Am.Chem.Soc.Mass Spectrom.* **2005**, *16*, 743-751.

(189) Berkout, V. D.; Kryuchkov, S. I.; Doroshenko, V. M. 'Modeling of ion processes in atmospheric pressure matrix-assisted laser desorption/ionisation',*Rapid Commun.Mass Spectrom.* **2007**, *21*, 2046-2050.

(190) Hsieh, S.; Ku, H. Y.; Ke, Y. T.; Wu, H. F. 'Self-assembled-monolayer-modified silicon substrate to enhance the sensitivity of peptide detection for AP-MALDI mass spectrometry',*J. Mass Spectrom.* **2007**, *42*, 1628-1636.

(191) kambara, H.; Kanomata, I. 'Collisional dissociation in atmospheric pressure ionization mass spectrometry.',*Shitsuryo Bunseki* **1976**, *24*, 271-282.

(192) Frankevich, V. E.; Zhang, J.; Friess, S. D.; Dashtiev, M.; Zenobi, R. 'Role of electrons in laser desorption/ionization mass spectrometry',*Anal. Chem.* **2003**, *75*, 6063-6067.

(193) Christophorou, L. G.; Olthoff, J. K. 'Electron interactions with sf6',*J.Phys.Chem.Ref.Data* **2000**, *29*, 267-330.

(194) Hagedorn, H. H. 'The endocrinoogy of the adult female mosquito',*Adv. Disease Vector Res.* **1994**, *10*, 109-148.

(195) Baker, F. C.; Hagedorn, H. H.; Schooley, D. A.; Wheelock, G. 'Mosquito juvenile-hormone - identification and bioassay activity',*J.Insect Physiol.* **1983**, *29*, 465-470.

(196) Sparks, T. C. *Drug and chemical toxicology, safer insecticides: Development and use*, 1990.

(197) Mulla, M. S., Taichung, Taiwan 1991; Chinese J. Entomology; 81-91.

(198) Lococo, D. J.; Tobe, S. S. 'Neuroanatomy of the retrocerebral complex, in particular the pars intercerebralis and partes laterales in the cockroach diploptera-punctata eschscholtz (dictyoptera, blaberidae)',*Int. J. Insect Morphol.* **1984**, *13*, 65-76.

(199) Klowden, M. J. 'Endocrine aspects of mosquito reproduction',*Arch. Insect Biochem.* **1997**, *35*, 491-512.

(200) Belles, X.; Martin, D.; Piulachs, M. D. 'The mevalonate pathway and the synthesis of juvenile hormone in insects',*Annu. Rev. Entomol.* **2005**, *50*, 181-199.

(201) Cao, L.; Zhang, P.; Grant, D. F. 'An insect farnesyl phosphatase homologous to the N-terminal domain of soluble epoxide hydrolase',*Biochem. Biophys. Res. Commun.* **2009**, *380*, 188-192.

(202) Mayoral, J. G.; Nouzova, M.; Navare, A.; Noriega, F. G. 'NADP(+)-dependent farnesol dehydrogenase, a corpora allata enzyme involved in juvenile hormone synthesis',*Proc.Natl. Acad. Sci. U S A* **2009**, *106*, 21091-21096.

(203) Baker, F. C.; Mauchamp, B.; Tsai, L. W.; Schooley, D. A. 'Farnesol and farnesal dehydrogenase(s) in corpora allata of the tobacco hornworm moth, manduca-sexta',*J.Lipid Res.* **1983**, *24*, 1586-1594.

(204) Mayoral, J. G.; Nouzova, M.; Yoshiyama, M.; Shinod, T.; Hernandez-Martinez, S.; Dolghih, E.; Turjanski, A. G.; Roitberg, A. E.; Priestap, H.; Perez, M.; Mackenzie, L.; Li, Y. P.; Noriega, F. G. 'Molecular and functional characterization of a juvenile hormone acid methyltransferase expressed in the corpora allata of mosquitoes',*Insect Biochemistry and Molecular Biology* **2009**, *39*, 31-37.

(205) Helvig, C.; Koener, J. F.; Unnithan, G. C.; Feyereisen, R. 'CYP15A1, the cytochrome P450 that catalyzes epoxidation of methyl farnesoate to juvenile hormone III in cockroach corpora allata',*Proc. Natl. Acad. Sc.i U S A* **2004**, *101*, 4024-4029.

(206) Li, Y. P.; Hernandez-Martinez, S.; Unnithan, G. C.; Feyereisen, R.; Noriega, F. G. 'Activity of the corpora allata of adult female aedes aegypti: Effects of mating and feeding',*Insect Biochemistry and Molecular Biology* **2003**, *33*, 1307-1315.

(207) Li, Y.; Unnithan, G. C.; Veenstra, J. A.; Feyereisen, R.; Noriega, F. G. 'Stimulation of jh biosynthesis by the corpora allata of adult female aedes aegypti in vitro: Effect of farnesoic acid and aedes allatotropin',*J. Exp. Biol.* **2003**, *206*, 1825-1832.

(208) Mayoral, J. G.; Nouzova, M.; Yoshiyama, M.; Shinoda, T.; Hernandez-Martinez, S.; Dolghih, E.; Turjanski, A. G.; Roitberg, A. E.; Priestap, H.; Perez, M.; Mackenzie, L.; Li, Y.; Noriega, F. G. 'Molecular and functional characterization of a juvenile hormone acid methyltransferase expressed in the corpora allata of mosquitoes',*Insect Biochem. mol. Biol.* **2009**, *39*, 31-37.

(209) Bergot, B. J.; Ratcliff, M.; Schooley, D. A. 'Method for quantitative-determination of the 4 known juvenile hormones in insect tissue using gas chromatography-mass spectroscopy',*J.Chromatogr.* **1981**, *204*, 231-244.

(210) Teal, P. E.; Proveaux, A. T.; Heath, R. R. 'Analysis and quantitation of insect juvenile hormones using chemical ionization ion-trap mass spectrometry',*Anal. Biochem.* **2000**, *277*, 206-213.

(211) Lee, H.; Finckbeiner, S.; Yu, J. S.; Wiemer, D. F.; Eisner, T.; Attygalle, A. B. 'Characterization of (E,E)-farnesol and its fatty acid esters from anal scent glands of nutria (myocastor coypus) by gas chromatography-mass spectrometry and gas chromatography-infrared spectrometry',*J.Chromatogr. A* **2007**, *1165*, 136-143.

(212) Fernandez, F. M.; Hampton, C. Y.; Nyadong, L.; Navare, A.; Kwasnik, M. *In LC/TOF-MS for accurate mass analysis: Principles, tools, and applications for accurate mass analysis; ferrer, I., thurman, e. M., eds.*; Wiley Hoboken, NJ, 2009.

(213) Jones, R. W.; Cody, R. B.; McClelland, J. F. 'Differentiating writing inks using direct analysis in real time mass spectrometry',*J. Forensic Sci.* **2006**, *51*, 915-918.

(214) Petucci, C.; Diffendal, J.; Kaufman, D.; Mekonnen, B.; Terefenko, G.; Musselman, B. 'Direct analysis in real time for reaction monitoring in drug discovery',*Anal. Chem.* **2007**, *79*, 5064-5070.

(215) Newton, P. N.; Fernandez, F. M.; Plancon, A.; Mildenhall, D. C.; Green, M. D.; Ziyong, L.; Christophel, E. M.; Phanouvong, S.; Howells, S.; McIntosh, E.; Laurin, P.; Blum, N.; Hampton, C. Y.; Faure, K.; Nyadong, L.; Soong, C. W.; Santoso, B.; Zhiguang, W.; Newton, J.; Palmer, K. 'A collaborative epidemiological investigation into the criminal fake artesunate trade in south east asia',*PLoS Med.* **2008**, *5*, e32.

(216) Newton, P. N.; McGready, R.; Fernandez, F.; Green, M. D.; Sunjio, M.; Bruneton, C.; Phanouvong, S.; Millet, P.; Whitty, C. J.; Talisuna, A. O.; Proux, S.; Christophel, E. M.; Malenga, G.; Singhasivanon, P.; Bojang, K.; Kaur, H.; Palmer, K.; Day, N. P.; Greenwood, B. M.; Nosten, F.; White, N. J. 'Manslaughter by fake artesunate in asia--will africa be next?',*PLoS Med.* **2006**, *3*, e197.

(217) Vail, T.; Jones, P. R.; Sparkman, O. D. 'Rapid and unambiguous identification of melamine in contaminated pet food based on mass spectrometry with four degrees of confirmation',*J. Anal. Toxicol.* **2007**, *31*, 304-312.

(218) Rothenbacher, T.; Schwack, W. 'Rapid and nondestructive analysis of phthalic acid esters in toys made of poly(vinyl chloride) by direct analysis in real time single-quadrupole mass spectrometry',*Rapid.Commun.Mass Spectrom.* **2009**, *23*, 2829-2835.

(219) Haefliger, O. P.; Jeckelmann, N. 'Direct mass spectrometric analysis of flavors and fragrances in real applications using DART',*Rapid.Commun.Mass Spectrom.* **2007**, *21*, 1361-1366.

(220) Pierce, C. Y.; Barr, J. R.; Cody, R. B.; Massung, R. F.; Woolfitt, A. R.; Moura, H.; Thompson, H. A.; Fernandez, F. M. 'Ambient generation of fatty acid methyl ester ions from bacterial whole cells by direct analysis in real time (DART) mass spectrometry',*Chem. Commun. (Camb.)* **2007**, 807-809.

(221) Yu, S.; Crawford, E.; Tice, J.; Musselman, B.; Wu, J. T. 'Bioanalysis without sample cleanup or chromatography: The evaluation and initial implementation of direct analysis in real time ionization mass spectrometry for the quantification of drugs in biological matrixes',*Anal. Chem.* **2009**, *81*, 193-202.

(222) Penning, F. M. 'Ionisation by metastable atoms',*Naturwissenschaften* **1927**, *15*, 818-818.

(223) Song, L. G.; Dykstra, A. B.; Yao, H. F.; Bartmess, J. E. 'Ionization mechanism of negative ion-direct analysis in real time: A comparative study with negative ion-atmospheric pressure photoionization',*J.Am.Chem.Soc.Mass Spectrom.* **2009**, *20*, 42-50.

(224) Williams, J. P.; Patel, V. J.; Holland, R.; Scrivens, J. H. 'The use of recently described ionisation techniques for the rapid analysis of some common drugs and samples of biological origin',*Rapid.Commun.Mass Spectrom.* **2006**, *20*, 1447-1456.

(225) Newton, P. N.; Green, M. D.; Fernandez, F. M.; Day, N. P. J.; White, N. J. 'Counterfeit anti-infective drugs',*Lancet infect. Dis.* **2006**, *6*, 602-613.

(226) Morlock, G.; Schwack, W. 'Determination of isopropylthioxanthone (ITX) in milk, yoghurt and fat by HPTLC-FLD, HPTLC-ESI/MS and HPTLC-DART/MS',*Anal. Bioanal. Chem.* **2006**, *385*, 586-595.

(227) Morlock, G.; Ueda, Y. 'New coupling of planar chromatography with direct analysis in real time mass spectrometry',*J. Chromatogr.A* **2007**, *1143*, 243-251.

(228) Harris, G. A.; Fernandez, F. M. 'Simulations and experimental investigation of atmospheric transport in an ambient metastable-induced chemical ionization source',*Anal. Chem.* **2009**, *81*, 322-329.

(229) Zhou, M.; McDonald, J. F.; Fernandez, F. M. 'Optimization of a direct analysis in real time/time-of-flight mass spectrometry method for rapid serum metabolomic fingerprinting',*J. Am. Soc. Mass. Spectrom.* **2009**, *21*, 68-75.

(230) Keniti, H.; Nozoe, T.; Omura, I. 'Ionization potentials of some organic molecules. Iv: Troponoid compounds',*BCSJ* **1957**, *30*, 408-410.

(231) Kazakov, S. M.; Kaputerko, M. N.; Suchkov, V. A. 'Determination of first ionization potentials from spectra of electronic energy loss in the vapor of polyatmic compounds',*J. Appl. Spectrosc.* **1999**, *66*, 375-379.

(232) Hanebeck, W.; Gasteiger, J. 'Rapid empirical calculation of the 1st (N or pi) ionization-potential of organic-molecules',*J. Comput. Chem.* **1993**, *14*, 138-154.

(233) Cody, R. B. 'Observation of molecular ions and analysis of nonpolar compounds with the direct analysis in real time ion source',*Anal. Chem.* **2009**, *81*, 1101-1107.

(234) du Prel, J. B.; Hommel, G.; Rohrig, B.; Blettner, M. 'Confidence interval or P-value? Part 4 of a series on evaluation of scientific publications',*Detsch. Arztebl. Int.* **2009**, *106*, 335-339.

(235) Lee, H.; Finckbeiner, S.; Yu, J. S.; Wiemer, D. F.; Eisner, T.; Attygalle, A. B. 'Characterization of (E,E)-farnesol and its fatty acid esters from anal scent glands of nutria (myocastor coypus) by gas chromatography-mass spectrometry and gas chromatography-infrared spectrometry',*J. Chromatogr.A* **2007**, *1165*, 136-143.

(236) NIST MS number 352675 National Institute of Standards and Technology Mass Spectrometry Data Center, U.S. Secretary of Commerce. http://webbook.nist.gov/cgi/cbook.cgi?Name=farnesol&Units=SI&cMS=on

(237) Gross, J. H. *Mass spectrometry: A textbook*; Springer-Verlag Berlin Hidenberg New York, 2004.

(238) Carroll, D. I.; Dzidic, I.; Stillwell, R. N.; Haegele, K. D.; Horning, E. C. 'Atmospheric-pressure ionization mass-spectrometry - corona discharge ion-source for use in liquid chromatograph mass spectrometer-computer analytical system',*Anal. Chem.* **1975**, *47*, 2369-2373.

(239) Navare, A.; Nouzova, M.; Noriega, F. G.; Hernandez-Martinez, S.; Menzel, C.; Fernandez, F. M. 'On-chip solid-phase extraction pre-concentration/focusing substrates coupled to atmospheric pressure matrix-assisted laser desorption/ionization ion trap mass spectrometry for high sensitivity biomolecule analysis',*Rapid Commun.Mass Spectrom.* **2009**, *23*, 477-486.

(240) Wink, T.; vanZuilen, S. J.; Bult, A.; vanBennekom, W. P. 'Self-assembled monolayers for biosensors',*Analyst* **1997**, *122*, R43-R50.

(241) Holmlin, R. E.; Chen, X. X.; Chapman, R. G.; Takayama, S.; Whitesides, G. M. 'Zwitterionic sams that resist nonspecific adsorption of protein from aqueous buffer',*Langmuir* **2001**, *17*, 2841-2850.

(242) Ostuni, E.; Chapman, R. G.; Holmlin, R. E.; Takayama, S.; Whitesides, G. M. 'A survey of structure-property relationships of surfaces that resist the adsorption of protein',*Langmuir* **2001**, *17*, 5605-5620.

(243) Ostuni, E.; Chapman, R. G.; Liang, M. N.; Meluleni, G.; Pier, G.; Ingber, D. E.; Whitesides, G. M. 'Self-assembled monolayers that resist the adsorption of proteins and the adhesion of bacterial and mammalian cells',*Langmuir* **2001**, *17*, 6336-6343.

(244) Jennings, G. K.; Laibinis, P. E. 'Self-assembled monolayers of alkanethiols on copper provide corrosion resistance in aqueous environments',*Colloid. Surfaces A* **1996**, *116*, 105-114.

(245) Laibinis, P. E.; Jennings, G. K. 'Corrosion inhibition on copper using self-assembled monolayers and multilayers.',*Abstr. Pap. Am. Chem. S.* **1996**, *211*, 127-PMSE.

(246) Fujisaki, N.; Fujimoto, I.; Hatano, Y. 'Role of added olefins and oxygen in gas-phase radiolysis of butane',*J.Phys.Chem* **1972**, *76*, 1260-&.

(247) Zhou, L.; Yue, B. F.; Dearden, D. V.; Lee, E. D.; Rockwood, A. L.; Lee, M. L. 'Incorporation of a venturi device in electrospray ionization',*Anal. Chem.* **2003**, *75*, 5978-5983.

(248) Hawkridge, A. M.; Zhou, L.; Lee, M. L.; Muddiman, D. C. 'Analytical performance of a venturi device integrated into an electrospray ionization fourier transform ion cyclotron resonance mass spectrometer for analysis of nucleic acids',*Anal. Chem.* **2004**, *76*, 4118-4122.

(249) Wu, S.; Zhang, K.; Kaiser, N. K.; Bruce, J. E. 'Incorporation of a flared inlet capillary tube on a fourier transform ion cyclotron resonance mass spectrometer',*J.Am.Chem.Soc.Mass Spectrom.* **2006**, *17*, 772-779.

(250) Hampton, C. Y.; Forbes, T. P.; Varady, M. J.; Meacham, J. M.; Fedorov, A. G.; Degertekin, F. L.; Fernandez, F. M. 'Analytical performance of a venturi-assisted array of micromachined ultrasonic electrosprays coupled to ion trap mass spectrometry for the analysis of peptides and proteins',*Anal. Chem.* **2007**, *79*, 8154-8161.

(251) Dixon, R. B.; Muddiman, D. C. 'Quantitative comparison of a flared and a standard heated metal capillary inlet with a voltage-assisted air amplifier on an electrospray ionization linear ion trap mass spectrometer',*Rapid Commun.Mass Spectrom.* **2007**, *21*, 3207-3212.